Power Efficiency Improvements for Wireless Transmissions

A Thesis
Presented to
The Academic Faculty

by

Hua Qian

In Partial Fulfillment
of the Requirements for the Degree
Doctor of Philosophy

School of Electrical and Computer Engineering
Georgia Institute of Technology
August 2005

Power Efficiency Improvements for Wireless Transmissions

Approved by:

Professor G. Tong Zhou, Advisor
School of Electrical and Computer Engineering
Georgia Institute of Technology, Advisor

Professor Ye (Geoffrey) Li
School of Electrical and Computer Engineering
Georgia Institute of Technology

Professor Robert K. Feeney
School of Electrical and Computer Engineering
Georgia Institute of Technology

Professor Ronghua Pan
School of Mathematics
Georgia Institute of Technology

Professor J. Stevenson Kenney
School of Electrical and Computer Engineering
Georgia Institute of Technology

Date Approved: July 13, 2005

To my parents, and my wife Lin Sun.

ACKNOWLEDGEMENTS

I would like to express my gratitude to all whose direct and indirect support helped me complete my thesis.

First, I would like to thank my advisor, Prof. G. Tong Zhou who has continuously supported my work and ideas throughout my studies at Georgia Institute of Technology. I appreciate her close guidance and great efforts to prepare me to become a mature researcher.

Next, I would like to thank my thesis committee members: Dr. Robert K. Feeney, Dr. J. Stevenson Kenney, Dr. Ye Li and Dr. Ronghua Pan for helping to improve my dissertation with their thoughtful advice and suggestions. My special thanks also go to Dr. David V. Anderson, Dr. John R. Barry, Dr. Monson H. Hayes, Dr. Aaron D. Lanterman, and Dr. Marcus C. Spruill for the excellent classes they offered, which prepare me a lot for my research work.

I would like to thank my group members: Dr. Lei Ding, Dr. Raviv Raich, Ning Chen, Chunpeng Xiao, Chunming Zhao, Robert Baxley, Vincent Emanuele, and Thao Tran, for their willingness to help, our insightful discussions and fruitful collaborations.

My sincere thanks also go to my parents and my brother for their unconditional love, encouragement, and support.

Last but not least, I would like to express my deepest gratitude to my wife Lin Sun for her company during my graduate study. Without her love, patience, understanding, and support, I would not have been able to complete this work.

TABLE OF CONTENTS

LIST OF TABLES

LIST OF FIGURES

SUMMARY

Many signal formats, such as code division multiple access (CDMA) and orthogonal frequency division multiplexing (OFDM), are not power efficient because of their large peak-to-average power ratios (PARs). Moreover, in the presence of nonlinear devices such as power amplifiers (PAs) or mixers, the non-constant-modulus signals may generate both in-band distortion and out-of-band interference. Backing off the signal to the linear region of the device further reduces the system power efficiency. To improve the power efficiency of the communication system, one can pursue two approaches: i) linearize the PA, and / or ii) reduce the high PAR of the input signal.

In this dissertation, we first explore the optimal nonlinearity under the peak power constraint. The answer is a soft limiter with a specific gain calculated based on the peak power constraint, noise variance, and the probability density function of the input amplitude. The result is also extended to the fading channel case.

Next, we focus on digital baseband predistortion linearization for power amplifiers with memory effects. We describe a high-speed wireless testbed for carrying out digital baseband predistortion linearization experiments. We show measurement results and demonstrate that the memory polynomial predistorter is more effective than the memoryless one in linearizing PAs with memory effects.

To implement adaptive PA linearization in wireless handsets, we propose an adaptive digital predistortion linearization design that is especially suitable for the smaller, lower power wireless terminals. This new predistortion architecture utilizes existing components of the wireless transceiver to fulfill the adaptive predistorter training functionality.

In the third part of the thesis, we investigate the topic of PAR reduction for OFDM signals and forward link CDMA signals. Selected mapping (SLM) is a distortionless technique to reduce the PAR of OFDM signals. A drawback of SLM is its high computational requirement, which hinders its practical implementation. We propose a dynamic selected mapping

(DSLM) algorithm with a two-buffer structure to reduce the computational requirement of the SLM method without sacrificing the PAR reduction capability.

To reduce the PAR of the forward link CDMA signal, we propose to introduce a relative offset between the in-phase branch and the quadrature branch of the transmission system. Compared with existing PAR reduction algorithms, our proposed algorithm is distortionless, has a low computational complexity, and offers good PAR reduction capability with very little system modification.

CHAPTER I

INTRODUCTION

In modern wireless communication systems, many signal formats, such as code division multiple access (CDMA) and orthogonal frequency division multiplexing (OFDM), have been introduced for high speed data transmission. However, these non-constant-modulus signals are not power efficient because of their large peak-to-average power ratio (PAR), i.e., large fluctuations in the signal envelopes. Moreover, in the presence of nonlinear devices such as power amplifiers (PAs) or mixers, the non-constant-modulus signals may generate both in-band distortion and out-of-band interference. Backing off the signal to the linear region of the device further reduces the system power efficiency.

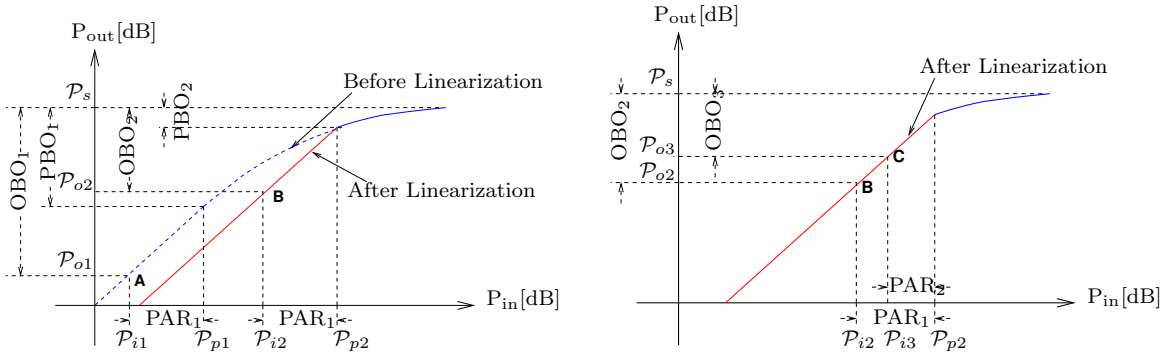

(a) Linearization. (b) PAR reduction.

Figure 1.1: Linearization and PAR reduction improve the power efficiency by reducing the PA output power back-off.

To improve the power efficiency of the communication system, one can pursue two approaches: i) linearize the PA, and / or ii) reduce the high PAR of the input signal [14]. Figure 1.1 shows the concept of linearization and PAR reduction. A linearized PA extends the linearity region close to the saturation point of the PA. Comparing with the conventional back-off approach, linearization allows a larger input range without causing distortion. PAR reduction diminishes or eliminates the occurrence of high peaks in the input signal.

Comparing with the original input, the signal after PAR reduction allows more average power to be transmitted under the same peak power constraint.

In this dissertation, we show our efforts in exploring both approaches. In this chapter, we first introduce nonlinear distortion performance metrics, and then give a brief review of PA linearization, and PAR reduction.

1.1 Performance Metrics of Nonlinear Distortions

Certain components in communication systems are nonlinear. For example, PAs are peak power limited in addition to being nonlinear. Denote by $x(t)$ a zero-mean complex baseband signal with variance σ_x^2 and by $v(t)$ a zero-mean additive noise process with variance σ_v^2. Let us consider the received signal modeled by

$$y(t) = h(x(t)) + v(t), \tag{1.1}$$

where $h(\cdot)$ is a memoryless nonlinear mapping.

Model (1.1) is of interest, for example, in transmission systems involving nonlinear components such as PAs or mixers [7,42,58], for nonlinear magnetic recording channels [117], or when companding [36, 108] or clipping [68, 69, 88, 92, 100] is involved for the purpose of peak-to-average power ratio (PAR) reduction.

A question can be asked: What undesirable effects are caused by the nonlinearity? In this section, we discuss performance metrics that quantify the nonlinear distortions.

1.1.1 AM/AM and AM/PM Conversion

Nonlinearity causes both amplitude and phase distortions to the input signal. Traditionally, the amplitude-to-amplitude (AM/AM) conversion is used to characterize the amplitude distortion, which is the relationship between the input power (amplitude) and the output power (amplitude) [42]. For a quasi-memoryless PA, phase deviation may also be present. The amplitude-to-phase (AM/PM) conversion is used to characterize the input amplitude dependency of the phase deviation.

However, memory effects may be present in a high power amplifier and / or when wideband input is used. In the presence of memory effects, the PA output depends not only

on its current input, but also on its past inputs. The AM/AM and AM/PM conversions may not fully describe the nonlinear relationship between the input and the output. We will discuss the PA memory effects in detail in Chapter 3.

1.1.2 Spectral Regrowth

In the frequency domain, nonlinearity produces both harmonics and intermodulations (IMDs). Comparing with the carrier frequency, the bandwidth of most communication signals can be considered as narrow. The harmonics are generally far away from the carrier frequency and can be easily removed by filtering. In comparison, the IMDs cause concerns since they are sufficiently close to the carrier frequency and thus may not be easily removed by filtering.

For a modulated signal, out-of-band IMDs cause adjacent channel interference as well as alternate channel interference. Adjacent channel power ratio (ACPR) is used to quantify the adjacent channel interference [13, 42]

$$ACPR = \frac{\int_{f_o-0.5B_{adj}}^{f_o+0.5B_{adj}} S(f)\ df}{\int_{-0.5B_{ch}}^{0.5B_{ch}} S(f)\ df}, \tag{1.2}$$

where $S(f)$ is the power spectral density function of the signal. The numerator in (1.2) is the interference power in a specified adjacent channel bandwidth B_{adj}, at a given frequency offset f_o from the carrier frequency. The denominator in (1.2) is the total main channel power in the specified channel bandwidth B_{ch} [43]. Please note that B_{adj} and B_{ch} may be different depending on the specification.

Table 1.1: Spurious Emission Limits for CDMA signal [97].

For frequency f with $\lvert f-$ Center Frequency$\rvert$	Greater than 780kHz	Greater than 1.98MHz
Spurious emission levels shall be less than either (a), or both (b) and (c)	(a) -42dBc/30kHz	(a) -54dBc/30kHz
	(b) -60dBc/30kHz (c) -54dBc/1.23MHz	
Spurious emission levels should be less than either (a), or both (b) and (c)	(a) -45dBc/30kHz	(a) -60dBc/30kHz
	(b) -66dBc/30kHz (c) -60dBc/1.23MHz	

Strict spectral emission limits are often imposed by the regulatory body. As an example, we show the spectral emission limits for IS-95 CDMA in Table 1.1 [97]. The ACPR is an

important performance metric to evaluate the signal quality. In measurement results shown in Chapter 3 and Chapter 4, we examine the power spectral density (PSD) of the input and the output signal to assess linearization performances.

1.1.3 Error Vector Magnitude

In-band IMD components degrade the BER. The error vector magnitude (EVM) is used to measure the difference between the reference waveform and the measured waveform. In general, both the reference signal and the measured transmitted signal go through the match filter and are mapped back to the signal constellation. This difference is called the error vector. EVM measures the normalized difference (expressed as a percentage) between the reference waveform and the measured waveform [96].

Denote by z the transmitted signal, by s the reference signal. The error vector is $e = z - s$, and the error vector magnitude is $|e|$. Specifically, the EVM is calculated according to

$$EVM = \sqrt{\frac{\sum_{n=0}^{N-1} |z(n) - s(n)|^2}{\sum_{n=0}^{N-1} |s(n)|^2}} \times 100\%. \tag{1.3}$$

Typical EVM figures are in the range of 5%-15% for mobile radio systems [42, pp. 210-211]. In [96], the EVM requirement is EVM < 17.5 %.

The EVM may also be used to assess the performance of PAR reduction algorithms with distortion. We use the EVM criterion when describing testbed results in Chapter 3.

The so-called *Rho*-factor defined as

$$\rho = \frac{\left(\sum_{n=0}^{N-1} |z(n)s(n)|\right)^2}{(\sum_{n=0}^{N-1} |s(n)|^2)(\sum_{n=0}^{N-1} |z(n)|^2)}, \tag{1.4}$$

is often used to assess CDMA system performance.

1.1.4 Signal-to-noise-and-distortion ratio

To evaluate the overall system performance degradation, we consider the signal-to-noise-and-distortion ratio (SNDR) [68, 69]. The SNDR concept is similar to the signal-to-noise ratio (SNR). The hope is to gain insight about the BER through the SNDR in the context of nonlinear systems.

The nonlinear mapping in (1.1) can be decomposed as

$$h(x(t)) = \alpha x(t) + d(t), \tag{1.5}$$

where $d(t)$ is the distortion created by $h(\cdot)$ and α is a constant, chosen such that $d(t)$ is uncorrelated with $x(t)$; i.e.,

$$E[x^*(t)d(t)] = 0. \tag{1.6}$$

Since $h(\cdot)$ is a memoryless system, we omit the t-dependence from now on for notational simplicity.

From (1.5), we obtain

$$E[x^*h(x)] = \alpha E[|x|^2] + E[x^*d] = \alpha E[|x|^2]. \tag{1.7}$$

Thus,

$$\alpha = \frac{E[x^*h(x)]}{E[|x|^2]} = \frac{E[x^*h(x)]}{\sigma_x^2}. \tag{1.8}$$

The distortion power is given by

$$\varepsilon_d = E[|d|^2] = E[|h(x)|^2] - |\alpha|^2\sigma_x^2. \tag{1.9}$$

The above decomposition ensures that d is uncorrelated with x. It makes sense to treat the distortion d as another source of additive noise. The SNDR is defined as [68, 69, 88]

$$\text{SNDR} = \frac{|\alpha|^2\sigma_x^2}{\varepsilon_d + \sigma_v^2} \tag{1.10}$$

$$= \frac{|E[x^*h(x)]|^2/\sigma_x^2}{E[|h(x)|^2] - |E[x^*h(x)]|^2/\sigma_x^2 + \sigma_v^2}. \tag{1.11}$$

We see from (1.11) that the SNDR depends on the distribution of x, the nonlinear mapping $h(\cdot)$, and the noise power σ_v^2.

The SNDR helps to evaluate the overall system performance degradation. We showed in [84] that the soft limiter with a specific gain maximizes the SNDR. We note however that the definition in (1.11) and the above result are for the AWGN channel case. In Chapter 2, we extend the SNDR definition and the optimal nonlinearity study to the fading channel case.

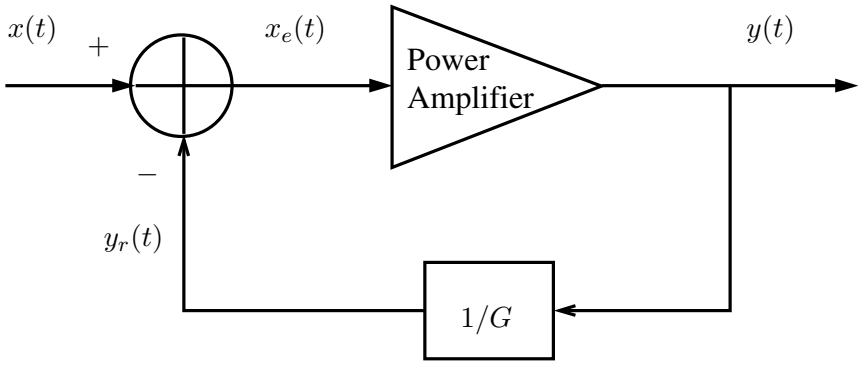

Figure 1.2: Feedback architecture for PA linearization.

1.2 Power Amplifier Linearization

As we explained earlier, non-constant envelope modulation schemes are sensitive to the PA nonlinearity. In these applications, PA linearization is often pursued to limit nonlinear distortions and to improve the efficiency of the PA. For mobile terminals, increased efficiency means reduced battery drain, reduced battery size and weight, and increased battery life. Power efficiency is also of prime importance for base station applications for the purposes of reducing the equipment cost, size, and network operating costs. According to a study described in [42, p. 13], application of PA linearization technologies can yield annual power savings of 164 million kilowatt hours for a surveyed network consisting of approximately 10,000 base sites.

1.2.1 Overview of PA Linearization Techniques

PA linearization has been investigated for decades. Available techniques include feedback, feedforward, predistortion approaches [21, 42, 95].

Feedback is widely used in control systems for error corrections. In Figure 1.2, we show a feedback system for PA linearization. A portion the output signal is demodulated and fed back for comparison with the desired input. However, the gain-bandwidth trade-off limits the feedback performance on RF PAs. Moreover, negative feedback also suffers from instability problems.

In theory, feedforward linearization can provide full IMD suppression. A feedforward linearization architecture is presented in Figure 1.3. An estimate of the distorted error

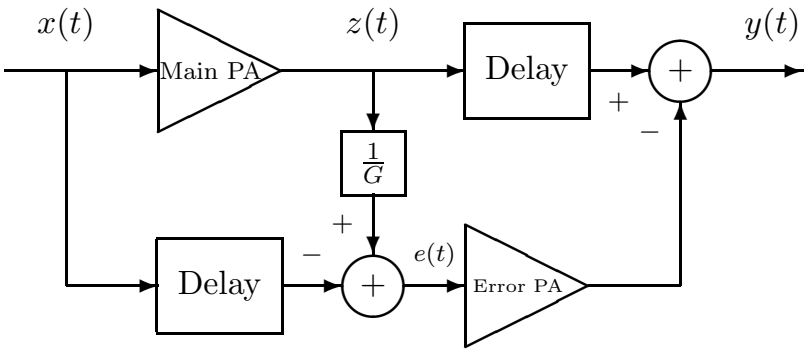

Figure 1.3: Feedforward architecture for PA linearization.

signal is generated and then subtracted from the PA output.

While ideally, this architecture is designed to perfectly linearize the PA, it is sensitive to changes in the parameters of the PA due to factors such as temperature, aging effects, and amplitude/phase matching, which require the gain G to continuously adapt [82]. In addition, a very linear error PA is required for the distortion products and the resulting system power efficiency degradation is significant.

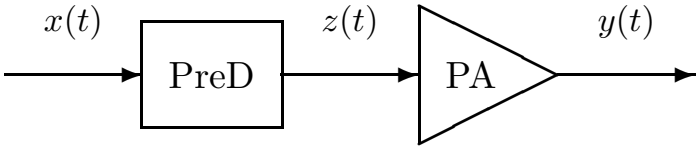

Figure 1.4: Predistortion for PA linearization.

A predistorter (PD), which (ideally) has the inverse characteristic of the PA, is used to compensate for the nonlinearity in the PA before the signal feeds into the PA. In Figure 1.4, we show the predistortion linearization architecture. We first pass the signal through a nonlinear block that is complementary to the PA response. The signal is distorted, but after subsequent distortion by the PA, a linearly amplified version of the original signal can be obtained.

Predistortion can be preformed in RF, IF, as well as in baseband. We are interested in

digital baseband predistortion techniques as they offer good compromise between complexity, cost, and linearization performance.

1.2.2 Memoryless and Memory Predistorter Models

If the PA under test is memoryless, a memoryless predistorter can be applied. The authors of Ref. [63] proposed an LUT based predistorter. Given a complex baseband input signal $x(t)$, the predistorter generates a complex correction signal $\Delta[x(t)]$ from a two-dimensional LUT indexed by the real and imaginary parts of $x(t)$. The predistorted signal $z(t)$ is then given by

$$z(t) \quad = \quad x(t) + \Delta[x(t)]. \tag{1.12}$$

Thus, the predistorter maps each complex input to its desired location. The drawback of this approach is the large LUT size since the LUT needs to be two-dimensional and cover a large number of input levels.

As for model based approaches, the polynomial model is a common choice due to its simplicity and ease of implementation [21, Sec. 3.3], [30]:

$$z(n) = \sum_{k=1}^{K} a_k \; |x(n)|^{k-1} x(n), \tag{1.13}$$

where $\{a_k\}_{k=1}^{K}$ are the predistorter coefficients and K is the highest polynomial order.

It is also possible to model the AM/AM and AM/PM characteristics of the desired predistorter using real-valued polynomials, as investigated in [95].

For high PAs or wideband applications, the memory effects in the PA can no longer be ignored. A full Volterra representation is needed to model the PA [8,85]. A $(2k+1)$th-order baseband Volterra model is given by

$$\begin{aligned} y(t) \quad = \quad & \sum_{k} \int \cdots \int h_{2k+1}(\boldsymbol{\tau}_{2k+1}) \\ & \prod_{i=1}^{k+1} x(t-\tau_i) \prod_{i=k+2}^{2k+1} x^*(t-\tau_i) d\boldsymbol{\tau}_{2k+1}, \end{aligned} \tag{1.14}$$

where $h_{2k+1}(\cdot)$ is the $(2k+1)$th-order Volterra kernel, $\boldsymbol{\tau}_{2k+1} = [\tau_1, \tau_3, \ldots, \tau_{2k+1}]^T$, and $d\boldsymbol{\tau}_{2k+1} = d\tau_1 d\tau_3 \cdots d\tau_{2k+1}$ [8,85].

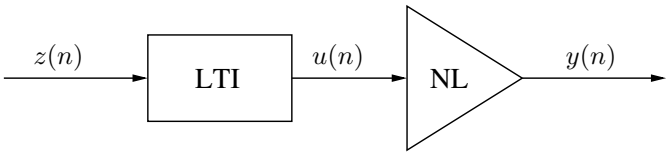

Figure 1.5: The Wiener Model.

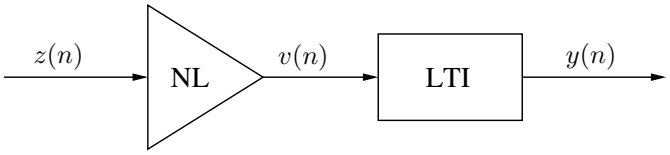

Figure 1.6: The Hammerstein Model.

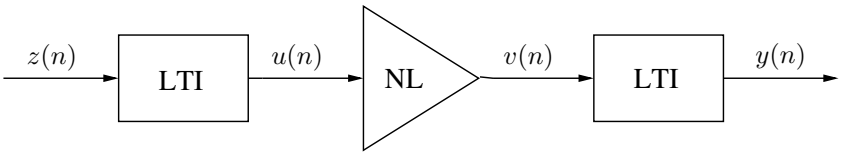

Figure 1.7: The Wiener-Hammerstein model.

Although the Volterra series is a general nonlinear model with memory [60, 89], its complexity is often prohibitive for real-time PD implementations. This drawback leads to the consideration of several special cases of the Volterra series; e.g., the Wiener model, the Hammerstein model, the Wiener-Hammerstein model, and the memory polynomial model.

The Wiener model is a linear time-invariant (LTI) system followed by a memoryless nonlinearity (NL) (see Figure 1.5). The LTI subsystem can be a finite impulse response (FIR) system given by

$$u(n) \;=\; \sum_{l=0}^{L-1} a_l \, z(n-l), \tag{1.15}$$

and the NL subsystem can be a polynomial nonlinearity given by

$$y(n) \;=\; \sum_{\substack{k=1 \\ k \text{ odd}}}^{K} b_k \, u(n)|u(n)|^{k-1}, \tag{1.16}$$

where a_l are the impulse response of the LTI block and b_k are the coefficients of the odd-order polynomial describing the memoryless nonlinearity. The Wiener model was used

by [15] to model the PA with memory effects, where improvements in modeling accuracy were observed by using the Wiener model instead of the memoryless polynomial model.

The Hammerstein model is a memoryless nonlinearity followed by an LTI system (see Figure 1.6). The pre-inverse of a Wiener system is a Hammerstein system. The Hammerstein model was used in [23] as a predistorter model, where improved predistortion performance was observed.

The Wiener-Hammerstein (W-H) model (see Figure 1.7) is an LTI system followed by a memoryless nonlinearity, which in turn is followed by another LTI system. Such a configuration is commonly used for satellite communication channels, where the PA at the satellite transponder is driven near saturation to exploit the maximum power efficiency [6].

The memory polynomial model was considered for modeling PAs with memory effects in [45]. It has been shown to be a robust pre-inverse for a variety of nonlinear systems with memory as well [25]. The memory polynomial model uses the diagonal kernels of the Volterra series and can be viewed as a generalization of the polynomial model:

$$z(n) = \sum_{k=1}^{K} \sum_{q=0}^{Q} a_{kq} \, |x(n-q)|^{k-1} x(n-q), \tag{1.17}$$

where K is the highest polynomial order and Q is the largest delay tap. To improve modeling accuracy, both even and odd order terms are included in (1.17) [24].

Time-delayed neural networks [57] and a frequency-dependent Saleh model [42, p. 79] are other notable alternatives for modeling nonlinear PAs with memory effects.

1.2.3 Orthogonal polynomials

For polynomial type of nonlinear models, high-order polynomials present a challenge. As pointed out in [83] and [86], in the process of solving for the model coefficients, a regressor matrix inversion is needed, which can cause a numerical instability problem if higher-order polynomial terms are included. The situation worsens if quantization errors are also present in the data.

To alleviate the numerical instability problem, we can replace the conventional polynomial basis function $\phi_k(x) = |x|^{k-1}x$ by the following set of orthogonal polynomial basis

functions:

$$\psi_k(x) = \sum_{l=1}^{k} (-1)^{l+k} \frac{(k+l)!}{(l-1)!(l+1)!(k-l)!} |x|^{l-1} x. \tag{1.18}$$

These functions are orthogonal in the sense that

$$E[\psi_k^*(x)\psi_l(x)] = 0, \qquad \forall\ k \neq l, \tag{1.19}$$

when $|x|$ is uniformly distributed in $[0, 1]$. The first seven orthogonal polynomial basis functions are listed in Table 1.2. The resulting orthogonal polynomial model coefficients can be extracted with much improved numerical stability.

Table 1.2: Orthogonal polynomial basis functions $\psi_k(x)$ for $1 \leq k \leq 7$.

$\psi_1(x) = x$
$\psi_2(x) = 4\|x\|x - 3x$
$\psi_3(x) = 15\|x\|^2x - 20\|x\|x + 6x$
$\psi_4(x) = 56\|x\|^3x - 105\|x\|^2x + 60\|x\|x - 10x$
$\psi_5(x) = 210\|x\|^4x - 504\|x\|^3x + 420\|x\|^2x - 140\|x\|x + 15x$
$\psi_6(x) = 792\|x\|^5x - 2310\|x\|^4x + 2520\|x\|^3x - 1260\|x\|^2x + 280\|x\|x - 21x$
$\psi_7(x) = 3003\|x\|^6x - 10296\|x\|^5x + 13860\|x\|^4x - 9240\|x\|^3x + 3150\|x\|x^2 - 504\|x\|x + 28x$

Although in reality, the uniform amplitude distribution assumption does not hold for communication signals. The above basis functions can still serve to lower the condition number of the regressor matrix. In practice, we do not require $|x|$ to be exactly in $[0, 1]$ in order for the orthogonal polynomial basis function $\psi_k(x)$ to be used. Details of the scaling operation can be found in [83].

For better numerical stability, the orthogonal polynomial basis functions in (1.18) can also be applied to the memory polynomial model; i.e.,

$$z(n) = \sum_{k=1}^{K} \sum_{q=0}^{Q} \alpha_{kq}\ \psi_k(x(n-q)), \tag{1.20}$$

and solve for the parameters $\{\alpha_{kq}\}$.

In Chapter 3, we describe a high-speed wireless testbed for carrying out digital baseband predistortion linearization experiments. We show measurement results of different predistorters. Superiority of the orthogonal polynomial model is demonstrated. In Chapter 4, we

propose an adaptive digital predistortion linearization design that is especially suitable for the smaller, lower power wireless terminals [81].

1.3 Peak-to-Average Power Ratio Reduction

Nonlinearity is not a problem for constant envelope signals. For a memoryless PA, the PA output signal envelope is constant if the input signal amplitude does not vary. The input signal only operates at a single point of the amplitude-to-amplitude (AM/AM) conversion curve, and the input signal *is* linearly amplified. This explains why nonlinear PAs are routinely used for constant envelope signals such as CW, FM, classical FSK, and GMSK (used in GSM) without causing performance degradations [82].

However, if the input signal has a large PAR, it is very sensitive to the system nonlinearity. To reduce the nonlinear effects, a large back-off is needed when the PAR is high, resulting in poor power efficiency. A large PAR also demands extra digits to provide enough dynamic range for digital signals, which may lead to extra computation and costs. PAR reduction is often necessary to reduce the cost and to improve the power efficiency of the transmission system.

Orthogonal Frequency Division Multiplexing (OFDM) is a popular transmission format that has been adopted by many standards including IEEE 802.11a/g/n, IEEE 802.16, HIPERLAN 2, Digital Audio Broadcast, and Digital Video Broadcast [41] [33, Sec. 1.2]. The Nyquist-rate sampled time-domain OFDM signal is given by [99]

$$x_n = \frac{1}{\sqrt{N}} \sum_{k=0}^{N-1} X_k \; e^{j\frac{2\pi kn}{N}}, 0 \leq n \leq N-1, \tag{1.21}$$

where N is the OFDM block length, and $\{X_k\}_{k=0}^{N-1}$ is the frequency domain OFDM signal belonging to a known constellation.

Denote by PAR_1 the PAR of the original OFDM signal,

$$\text{PAR}_1 = \text{PAR}\{x_n\} = \frac{\max\limits_{0 \leq n \leq N-1} |x_n|^2}{E[|x_n|^2]}, \tag{1.22}$$

where $E[\cdot]$ denotes statistical expectation.

If X_k has constant modulus, it can be shown that the worst case PAR of the OFDM signal x_n is N [99]. However, worst case PAR values rarely happen. Since PAR is a random

variable, an appropriate descriptor of the PAR is the complementary cumulative distribution function (CCDF), $Pr(\text{PAR}_1 > \gamma)$.

The CCDF of PAR_1 of the OFDM signal, i.e., the probability that PAR_1 exceeds a certain threshold γ, can be calculated as [3]:

$$Pr\{\text{PAR}_1 > \gamma\} = 1 - (1 - e^{-\gamma})^N. \tag{1.23}$$

Figure 1.8 shows the CCDF of the PAR of an OFDM signal where $N = 128$. In this example, there is a 1% chance that the OFDM block will have a PAR value ≥ 9.8 dB.

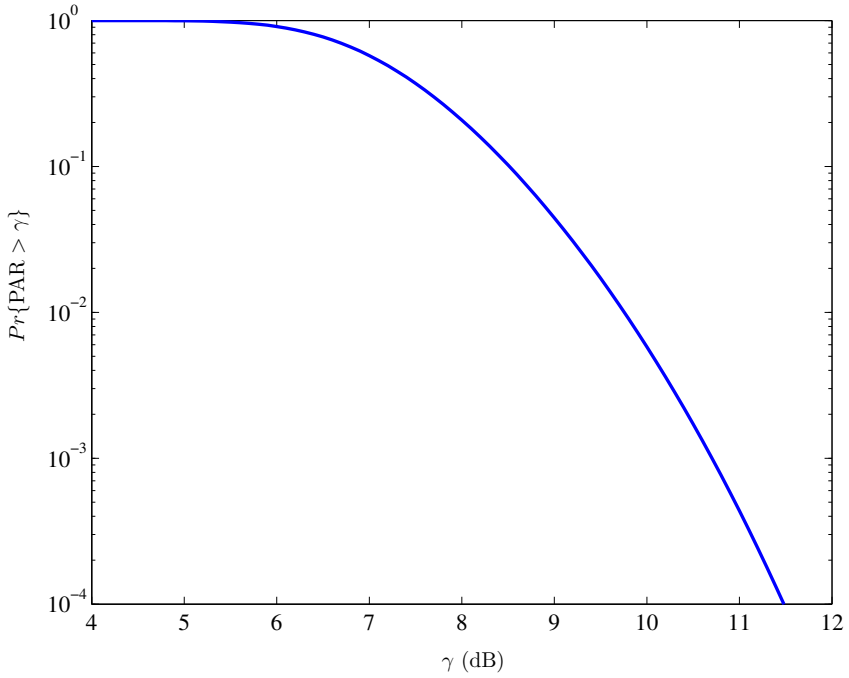

Figure 1.8: CCDF of the PAR of an OFDM signal with $N = 128$ subcarriers.

Another signal that has a large dynamic range is the forward link (i.e., base-station to mobile) Code Division Multiple Access (CDMA) signal [50, 53]. Figure 1.9 shows a block diagram of the forward link CDMA system [97], where a total of K users are active.

The summation of the Walsh coded multichannel symbols and the pulse shape filtering both contribute to the high PAR. To quantify the PAR, let us define the instantaneous-to-average power ratio (IAR) [52]

$$\text{IAR} = \frac{P(t)}{P_{av}}, \tag{1.24}$$

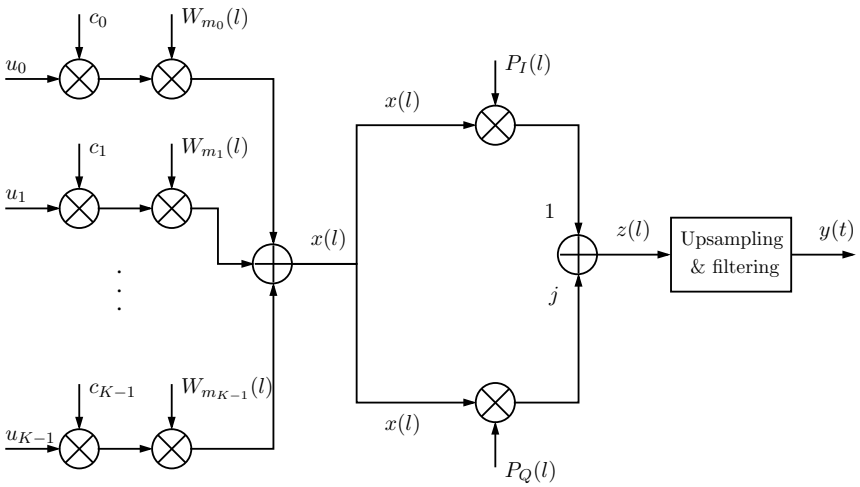

Figure 1.9: IS-95 CDMA forward link schematic for a given symbol period.

where $P(t)$ is the instantaneous power of the baseband signal and P_{av} is its average power. Since IAR is a random variable, its probabilistic distribution is of interest.

Figure 1.10 shows the CCDF of IAR of a 24-channel (3 overhead channels plus 21 traffic channels) forward link CDMA signal. We can see that with a 0.01% of chance, the signal will have IAR values in excess of 11.3 dB.

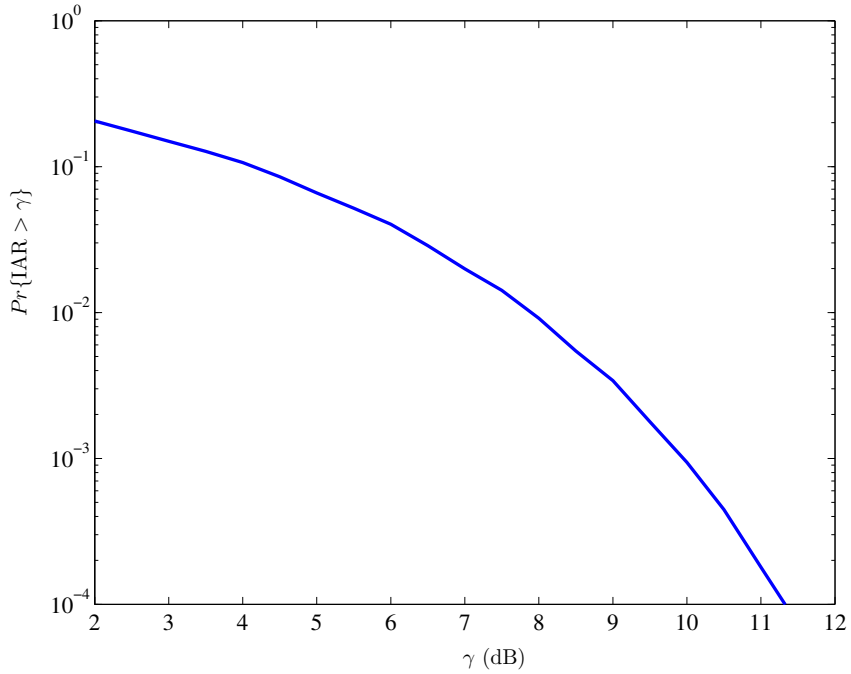

Figure 1.10: CCDF of the IAR of a forward link CDMA signal with 24 active channels.

1.3.1 PAR Reduction for OFDM Signal

There has been a great deal of research on PAR reduction for OFDM. One can pursue PAR reduction algorithms with distortion or without distortion.

Deliberate clipping [56], repeated clipping and filtering [55], and companding [109] are simple PAR reduction algorithms with distortion.

Amplitude clipping is a commonly used clipping method. The clipping function is a soft limiter, or

$$g(x) = \begin{cases} x, & |x| < A, \\ Ae^{j\angle x}, & |x| \geq A, \end{cases} \tag{1.25}$$

where A is the clipping threshold.

Clipping may effectively reduce the PAR, however, it introduces distortion as well. The distortion caused by clipping may fall both in-band and out-of-band. Out-of-band radiation reduces spectral efficiency and is usually unacceptable. Filtering after clipping, or repeated clipping-and-filtering [55], can reduce out-of-band radiation but may also cause peak regrowth.

These PAR reduction techniques with distortion generally require less computation. However, a trade-off must be made among PAR reduction capability, spectral regrowth, and symbol-error-rate (SER).

Distortionless PAR reduction algorithms include coding [39], selected mapping (SLM) [3], partial transmit sequence (PTS) [62], interleaving [37], active constellation extension (ACE) [47], tone injection and tone reservation [99], etc.

Next, we describe SLM which is an effective PAR reduction algorithm. The block diagram of the SLM method is shown in Fig. 1.11.

In SLM, we assume that the same phase table $\{\phi_k^{(d)}\}$, $0 \leq k \leq N-1$, $1 \leq d \leq D$, where $\phi_k^{(1)} = 0$, $\forall\ k$, is available to both the transmitter and the receiver. In SLM, we first rotate the phases of X_k as in

$$X_k^{(d)} = X_k\ e^{j\phi_k^{(d)}}, \tag{1.26}$$

and then take the IDFT to obtain $x_n^{(d)}$. Although $X_k^{(d)}$ and X_k contain the same information,

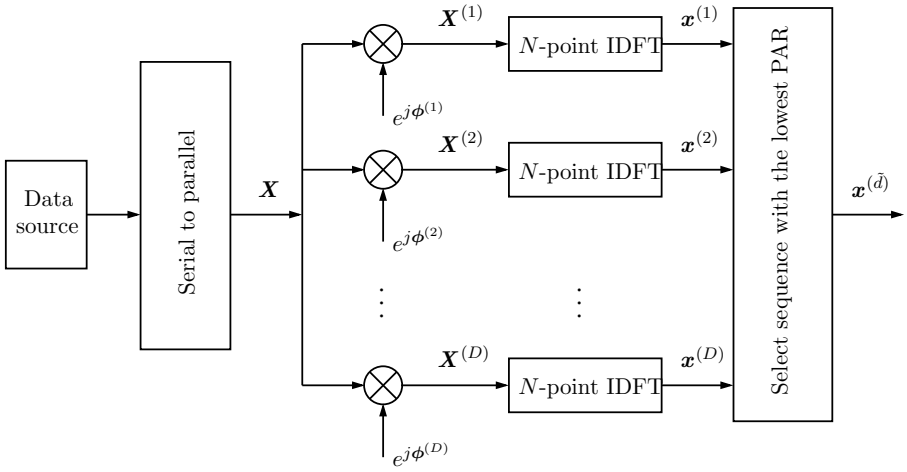

Figure 1.11: The block diagram of SLM method.

$x_n^{(d)}$ and x_n can have very different PAR values. In SLM, $x_n^{(\tilde{d})}$ which has the lowest PAR among the D equivalent sequences, is transmitted; i.e.,

$$\tilde{d} = \underset{1 \le d \le D}{\arg\min} \ \mathrm{PAR}\{x_n^{(d)}\}. \tag{1.27}$$

We denote the associated lowest PAR value by

$$\mathrm{PAR}_D = \min_{1 \le d \le D} \mathrm{PAR}\{x_n^{(d)}\}. \tag{1.28}$$

The CCDF of PAR_D is given by [3]

$$Pr\{\mathrm{PAR}_D > \gamma\} = (1 - (1 - e^{-\gamma})^N)^D. \tag{1.29}$$

The CCDF curve (1.29) lowers as D is increased, with $D = 1$ corresponding to the original OFDM signal. Under the same peak power constraint, the average power is increased when the PAR is decreased. Ref. [3] gives an example. For a 128-subcarrier OFDM signal, at the peak clipping probability level of 10^{-4}, SLM with $D = 4$ results in about 3 dB gain in the average power.

However, SLM, like other distortionless PAR reduction algorithms, requires a large amount of additional computations, which may hinder its practical use in high speed data transmissions. In Chapter 5, we propose the dynamic selected mapping (DSLM) algorithm to reduce the computational requirement of the SLM method without sacrificing the PAR reduction capability.

1.3.2 PAR Reduction for CDMA Signal

Many PAR reduction techniques have been proposed in the literature. Most published results deal with OFDM signals [99]. In comparison, the body of literature on PAR reduction for CDMA signals is rather small.

Similar to PAR reduction for OFDM signal, one can pursue PAR reduction techniques with distortion, such as clipping [104], windowing [104], repeated filtering and clipping [18].

For distortionless PAR reduction, a Walsh code selection algorithm [50, 51, 91] was proposed to reduce the PAR with the assumption that only some of the channels are active at any given time. Based on the same assumption, a PAR reduction algorithm was proposed in [105] by adding a signal that is orthogonal to all the active channel codes. In [53], the authors proposed to reduce the PAR of the forward link CDMA signal by changing the signs of half of the Walsh codes in one branch of the quadrature modulation. These distortionless PAR reduction techniques generally require more computation than the PAR reduction techniques with distortion.

In [53], the authors suggested to keep the in-phase branch of the CDMA signal unchanged and modify the signal sent into the quadrature branch by flipping the signs of the input signals from odd-numbered Walsh indices. With this modification, correlation between the in-phase and quadrature branches is reduced and PAR reduction of more than 1 dB can be achieved.

In Chapter 6, we introduce a relative offset between the in-phase branch and the quadrature branch of the forward link CDMA system. This simple modification leads to considerable PAR reduction with very little cost.

1.4 Organization of this Dissertation

The rest of this dissertation is organized as follows:

In Chapter 2 [74, 84], we explore the optimal nonlinearity that maximizes the SNDR under the peak power constraint. The answer is a soft limiter with a specific gain calculated based on the peak power constraint, noise variance, and the probability density function of the input amplitude. The result is also extended to the fading channel case.

In Chapter 3 [75, 116], we describe a high-speed wireless testbed for carrying out digital baseband predistortion linearization experiments. We show measurement results and demonstrate that the memory polynomial predistorter is more effective than the memoryless one in linearizing PAs with memory effects.

Adaptive PA linearization has been practiced mostly on the larger, higher power PAs. In Chapter 4 [81], we propose an adaptive digital predistortion linearization design that is especially suitable for the smaller, lower power wireless terminals. This new predistortion architecture utilizes existing components of the wireless transceiver to fulfill the adaptive predistorter training functionality. This predistortion architecture is cost effective and power efficient.

In Chapter 5 [76–78], we propose a dynamic selected mapping (DSLM) algorithm with a two-buffer structure. DSLM can greatly reduce the computational requirement of the SLM method without sacrificing the PAR reduction capability. In addition, the proposed algorithm reduces the amount of side information associated with the SLM algorithm.

In Chapter 6 [79, 80], we propose a new algorithm for PAR reduction of the forward link CDMA signal. It works by introducing a relative offset between the in-phase branch and the quadrature branch of the system. Compared with existing PAR reduction algorithms, our algorithm is distortionless, and offers good PAR reduction capability with very little system modification and low computational complexity.

Finally, in Chapter 7, we summarize this dissertation and suggest topics for future research.

For the reader's convenience, we have made an effort to keep every chapter as self contained as possible.

CHAPTER II

OPTIMIZATION OF SNDR IN THE PRESENCE OF AMPLITUDE LIMITED NONLINEARITY AND MULTIPATH FADING

Many physical devices, such as power amplifiers, are intrinsically nonlinear and thus introduce nonlinear distortions. Transmission systems with a peak power (or peak amplitude) constraint are considered here. To address the trade-off between maximizing the output power efficiency and minimizing the signal distortion, we consider two criteria: signal-to-noise-and-distortion ratio and symbol-error-rate. For multipath fading channels, we show that a soft limiter with a particular gain offers an optimal solution when the peak amplitude constraint is imposed at the transmitter. Numerical examples are provided to illustrate the concepts.

2.1 Introduction

Many physical devices in communication systems have a peak power (or peak amplitude) constraint. For example, power amplifiers or mixers [42, 58] are peak amplitude limited in addition to being nonlinear. In the presence of nonlinear devices with the peak power constraint, communication systems may experience increase in symbol-error-rate (SER) [42], expansion of spectrum [114], or reduction in channel capacity [90].

On the other hand, nonlinearities may also be judiciously introduced to improve the system performance. For example, companding [108] or clipping [68] can be applied to reduce the peak-to-average power ratio (PAR) of a signal. Following PAR reduction, we can re-scale the input signal to take full advantage of the amplitude limit of the physical device, thus increasing the average transmit power and improving the power efficiency [73].

To evaluate the impact of the nonlinearities on the system performance, one may use as

criterion, channel capacity [90,93], SER [42,92], signal-to-noise-and-distortion ratio (SNDR) [68, 99], or power spectrum [114]. In this chapter, we choose SNDR or SER as the system performance criterion.

It is possible to find the best nonlinearity according to a given system performance criterion. In [84], we showed that the soft limiter with a properly selected gain maximizes the SNDR among a class of peak amplitude limited memoryless nonlinearities. The results of [84], however, assume an AWGN channel.

Multipath fading is often present in mobile radio communication channels. In this chapter, we extend our work on the optimization of peak amplitude limited nonlinearities to multipath fading channels. We will show that similar to the AWGN channel case, the ideal linearizer (which is overall nonlinear) with a properly selected gain maximizes the SNDR. However, unlike the AWGN case, optimizing the SNDR does not necessarily optimize the SER for the multipath fading channel case. We will discuss the optimization of SER as well.

The organization of this chapter is as follows. In Section 2.2, we first present the system model, state our previous result on optimizing SNDR for the AWGN channel case, and then define the frequency dependent SNDR for the fading channel case. In Section 2.3, we consider optimizing SNDR for both flat fading and frequency selective fading channels. SER performance results are presented in Section 2.4. Finally, conclusions are drawn in Section 2.5.

2.2 System Setup

Let us consider a baseband equivalent communication system shown in Figure 2.1. Denote by $x(t)$ a baseband input signal with zero mean and variance σ_x^2, and by $v(t)$ an additive noise process with zero mean and variance σ_v^2. Let us consider the received signal $y(t)$ modeled by

$$y(t) = \tilde{g}(x(t)) \star h(t) + v(t), \tag{2.1}$$

where $\tilde{g}(\cdot)$ is a memoryless nonlinear mapping with a peak amplitude constraint $|\tilde{g}(x(t))| \leq A$, $h(t)$ is the impulse response of the channel, and $\star$ denotes linear convolution.

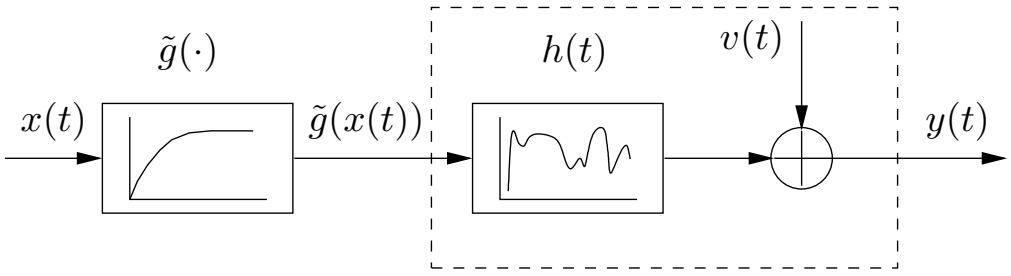

Figure 2.1: Baseband equivalent communication system: peak limited nonlinearity followed by a fading channel.

2.2.1 Optimization of SNDR for the AWGN Channel

The nonlinear mapping in (2.1) can be decomposed into a linear term αx plus a distortion term d [68]; i.e.,

$$\tilde{g}(x) = \alpha x + d. \tag{2.2}$$

We choose α such that d is uncorrelated with x; i.e., $E[x^* d] = 0$. This means that

$$E[x^* \tilde{g}(x)] = \alpha E[|x|^2] + E[x^* d] = \alpha E[|x|^2]. \tag{2.3}$$

Thus, the linear coefficient α can be calculated from

$$\alpha = \frac{E[x^* \tilde{g}(x)]}{E[|x|^2]} = \frac{E[x^* \tilde{g}(x)]}{\sigma_x^2}. \tag{2.4}$$

The distortion power is given by

$$\varepsilon_d = E[|d|^2] = E[|\tilde{g}(x)|^2] - |\alpha|^2 \sigma_x^2. \tag{2.5}$$

For the AWGN channel case, the signal-to-noise-and-distortion ratio (SNDR) is given by [84]:

$$\text{SNDR} = \frac{|\alpha|^2 \sigma_x^2}{\varepsilon_d + \sigma_v^2} \tag{2.6}$$

$$= \frac{|E[x^* \tilde{g}(x)]|^2 / \sigma_x^2}{E[|\tilde{g}(x)|^2] - |E[x^* \tilde{g}(x)]|^2 / \sigma_x^2 + \sigma_v^2}. \tag{2.7}$$

Assume that $\tilde{g}(\cdot)$ can be expressed as

$$\tilde{g}(x) = A g(\gamma) e^{j \angle x}, \tag{2.8}$$

where $0 \leq g(\cdot) \leq 1$, and $\gamma = |x|/\sigma_x$. Here, $g(\cdot)$ is the so-called amplitude-to-amplitude (AM/AM) conversion and $\angle g(\cdot)$ is the so-called amplitude-to-phase (AM/PM) conversion. Substituting (2.8) into (2.7), we obtain

$$\text{SNDR} = \frac{(E[\gamma g(\gamma)])^2}{E[g^2(\gamma)] - (E[\gamma g(\gamma)])^2 + \frac{\sigma_v^2}{A^2}}. \tag{2.9}$$

In [84], we showed within the class of $g(\cdot)$ satisfying $0 \leq g(\cdot) \leq 1$, the following $g(\cdot)$ maximizes the SNDR expression in (2.9):

$$g(\gamma) = \begin{cases} \frac{\gamma}{\eta^\star}, & 0 \leq \gamma < \eta^\star, \\ 1, & \gamma \geq \eta^\star, \end{cases} \tag{2.10}$$

where the threshold $\eta^\star$ is found from[1]

$$\eta^\star = T^{-1}(A^2/\sigma_v^2), \tag{2.11}$$

with

$$T(\eta) = \frac{\eta}{C_1(\eta) - \eta C_o(\eta)}, \tag{2.12}$$

$$C_o(\eta) = \int_\eta^\infty p(\gamma) d\gamma, \tag{2.13}$$

$$C_1(\eta) = \int_\eta^\infty \gamma p(\gamma) d\gamma, \tag{2.14}$$

and $p(\gamma)$ is the PDF of γ. The optimal SNDR is found as

$$\text{SNDR}^\star = \frac{1}{\frac{1}{R(\eta^\star)} - 1}, \tag{2.15}$$

where

$$R(\eta^\star) = \frac{C_1^2(\eta^\star)}{C_o(\eta^\star) + \frac{\sigma_v^2}{A^2}} + \bar{C}_2(\eta^\star), \tag{2.16}$$

and

$$\bar{C}_2(\eta) = \int_0^\eta \gamma^2 p(\gamma) d\gamma. \tag{2.17}$$

To illustrate the concepts of peak amplitude limited nonlinearities and the optimization of SNDR, consider the following example. Assume that x is i.i.d. complex Gaussian

[1] $T^{-1}(\cdot)$ denotes the inverse of $T(\cdot)$. We show in [84] that $T(\cdot)$ is a monotonically increasing function and thus $T^{-1}(\cdot)$ exists.

distributed with mean 0 and variance σ_x^2, and that the peak amplitude constraint of the device is $A = 2\sigma_x$. Assume that the channel is AWGN and the additive noise v has variance $\sigma_v^2 = 0.1A^2$. The following three nonlinear mappings all satisfy the peak amplitude constraint $\tilde{g}(\cdot) \leq A$:

$$\tilde{g}_1(x) = \begin{cases} x, & |x| \leq A, \\ Ae^{j\angle x}, & |x| > A, \end{cases} \tag{2.18}$$

$$\tilde{g}_2(x) = \begin{cases} \frac{A}{1.09\sigma_x}x, & |x| \leq 1.09\sigma_x, \\ Ae^{j\angle x}, & |x| > 1.09\sigma_x, \end{cases} \tag{2.19}$$

$$\tilde{g}_3(x) = \begin{cases} 2x - \frac{|x|x}{A}, & |x| \leq A, \\ Ae^{j\angle x}, & |x| > A. \end{cases} \tag{2.20}$$

Figure 2.2 (a), (b) and (c) illustrate $\tilde{g}_1(x)$, $\tilde{g}_2(x)$, and $\tilde{g}_3(x)$, respectively. Among the above three nonlinearities, $\tilde{g}_1(x)$ is a typical soft limiter; $\tilde{g}_2(x)$ is a soft limiter with gain calculated according to (2.11); $\tilde{g}_3(x)$ is a mapping that may be used to (approximately) describe the behavior of a memorlyess nonlinear power amplifier.

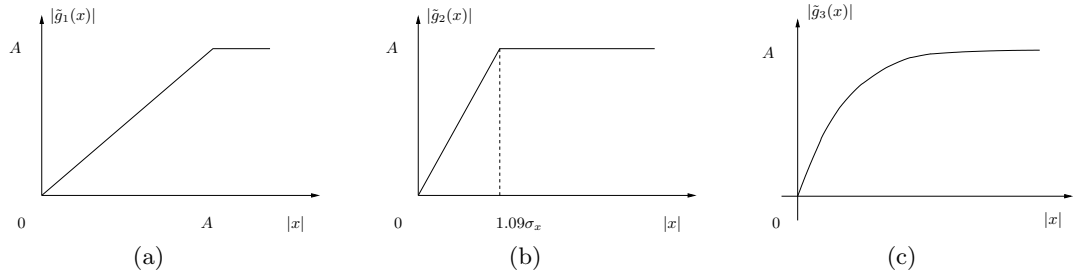

Figure 2.2: Nonlinear mappings with the peak amplitude constraint: (a) soft limiter; (b) soft limiter with gain $A/(1.09\sigma_x)$; (c) nonlinear mapping given by (2.20).

From (2.7), we find the SNDR of $\tilde{g}_1(x)$, $\tilde{g}_2(x)$, and $\tilde{g}_3(x)$ to be 3.87 (5.88 dB), 6.42 (8.08 dB), and 5.81 (7.64 dB) respectively. In this example, the nonlinearity in (2.19) gives the highest SNDR among the three nonlinearities. The result is consistent with (2.11).

2.2.2 SNDR Definition for the Fading Channel

If we substitute (2.2) into (2.1) and take the Fourier transform on both sides of (2.1), we obtain

$$Y(f) = (\alpha X(f) + D(f))\ H(f) + V(f), \tag{2.21}$$

where $Y(f)$, $X(f)$, $D(f)$, $H(f)$, and $V(f)$ are the Fourier transforms of $y(t)$, $x(t)$, $d(t)$, $h(t)$, and $v(t)$, respectively. The continuous-time Fourier transform is given by

$$X(\omega) = \mathcal{F}(x(t)) = \frac{1}{\sqrt{2\pi}} \int_{-\infty}^{\infty} x(t) e^{-j\omega t} dt. \tag{2.22}$$

We treat the channel $h(t)$ and thus $H(f)$ as random. Denote the variance of $H(f)$ by $\sigma_H^2(f)$, and write $H(f) = \beta(f) e^{j\theta(f)}$. For the AWGN channel, $\beta(f) = 1$ and $\theta(f) = 0$ within the band of interest. For a flat fading channel, $\beta(f)$ and $\theta(f)$ are constant for a given realization. For a frequency selective fading channel, $\beta(f)$ and $\theta(f)$ are frequency dependent.

If we assume that x is independent and identically distributed (i.i.d.), d is also i.i.d. due to the memoryless nature of the $\tilde{g}(\cdot)$ mapping. Furthermore, we assume that the noise v is white. Since the Fourier transform is a unitary transformation, we have

$$E[|X|^2] = E[|x|^2] = \sigma_x^2, \tag{2.23}$$

$$E[|D|^2] = E[|d|^2] = \varepsilon_d, \tag{2.24}$$

and

$$E[|V|^2] = E[|v|^2] = \sigma_v^2. \tag{2.25}$$

The received signal power is $|H(f)|^2 |\alpha|^2 E[|X(f)|^2] = \beta^2(f) |\alpha|^2 \sigma_x^2$. Similarly, the received distortion power is $|H(f)|^2 E[|D(f)|^2] = \beta^2(f)\ \varepsilon_d$. Therefore, at each frequency bin, the SNDR is

$$\mathrm{SNDR}(\beta(f)) = \frac{\beta^2(f) |\alpha|^2 \sigma_x^2}{\beta^2(f)\ \varepsilon_d + \sigma_v^2}, \tag{2.26}$$

which is a function of the channel magnitude response.

Substituting (2.4), (2.5), and (2.8) into (2.26), we obtain

$$\mathrm{SNDR}(\beta(f)) = \frac{(E[\gamma g(\gamma)])^2}{E[g^2(\gamma)] - (E[\gamma g(\gamma)])^2 + \frac{\sigma_v^2}{\beta^2(f) A^2}}. \tag{2.27}$$

Comparing (2.27) with (2.9), we see that in the fading channel case, A^2 is replaced by $\beta^2(f) A^2$. Next we treat flat fading and frequency selective fading channels separately.

Flat Fading Channel. For a flat fading channel, $\beta(f)$ is a constant β for all frequencies. Assuming that we have knowledge of the probability density function $q(\beta)$ of the channel gain β, the average SNDR can be obtained

$$\text{SNDR} = E_\beta[\text{SNDR}(\beta)] = \int \text{SNDR}(\beta)\ q(\beta)\ d\beta. \tag{2.28}$$

Consider as an example the Rayleigh flat fading case. The channel gain β is Rayleigh distributed

$$q(\beta) = \frac{2\beta}{\sigma_H^2} e^{-\frac{\beta^2}{\sigma_H^2}}. \tag{2.29}$$

The average SNDR can be obtained by substituting (2.27) and (2.29) into (2.28):

$$\begin{aligned} \text{SNDR} &= \int_0^\infty \text{SNDR}(\beta) \frac{2\beta}{\sigma_H^2} e^{-\frac{\beta^2}{\sigma_H^2}} d\beta & (2.30)\\ &= \frac{\sigma_H^2 A^2}{\sigma_v^2} (E[\gamma g(\gamma)])^2 \xi(\gamma) \left(1 - \xi(\gamma) e^{\xi(\gamma)} \text{E}_1(\xi(\gamma))\right), & (2.31) \end{aligned}$$

where

$$\xi(\gamma) = \frac{\sigma_v^2}{\sigma_H^2 A^2 \left(E[g^2(\gamma)] - (E[\gamma g(\gamma)])^2\right)}, \tag{2.32}$$

and

$$\text{E}_1(x) = \int_x^\infty \frac{e^{-t}}{t} dt. \tag{2.33}$$

To simplify (2.31), we introduce an approximation:

$$e^{\xi} \text{E}_1(\xi) \approx \frac{1}{1+\xi}, \tag{2.34}$$

which is a good approximation when ξ is large ($\xi > 1$).

Substituting (2.34) into (2.31), we obtain

$$E_\beta[\text{SNDR}(\beta)] \approx \frac{(E[\gamma g(\gamma)])^2}{E[g^2(\gamma)] - (E[\gamma g(\gamma)])^2 + \frac{\sigma_v^2}{\sigma_H^2 A^2}}. \tag{2.35}$$

Comparing (2.35) with (2.9), we infer that the average SNDR in the flat fading case with $\sigma_H^2 = 1$ can be approximated by the SNDR of the AWGN channel. Furthermore, we infer that (2.35) can be optimized w.r.t. $g(\cdot)$ using Theorem 1 of [84] with $\eta = T^{-1}(\frac{\sigma_H^2 A^2}{\sigma_v^2})$. If the

channel variance σ_H^2 is 1, (2.35) reduces to (2.9). In other words, as a first approximation, the results obtained for the AWGN channel case can be used for the flat fading channel case.

Frequency Selective Fading Channel. For a frequency selective fading channel, the channel gain $\beta(f)$ is not only frequency dependent, but also changes from realization to realization. Assume that we have knowledge of the probability density function $q(\beta(f))$ of the channel gain $\beta(f)$ at any frequency. The SNDR expression is

$$\begin{aligned} \text{SNDR} &= \int E_{\beta(f)}[\text{SNDR}(\beta)]\ df \qquad (2.36) \\ &= \int\int \text{SNDR}(\beta(f))\ q(\beta(f))\ d\beta(f)\ df. \qquad (2.37) \end{aligned}$$

If the channel is wide-sense-stationary and uncorrelated-scattered [5], [72], $q(\beta(f))$ does not depend on f. Equation (2.37) then reduces to (2.28).

2.3 Optimization of SNDR for the Fading Channel

Next, we consider the optimization of a *functional of the SNDR* with respect to the nonlinear function $g(\cdot)$:

$$\int E_{\beta(f)}[F(\text{SNDR}(\beta(f)))]\ df = \int\int F(\text{SNDR}(\beta(f)))\ q(\beta(f))\ d\beta(f)df, \qquad (2.38)$$

where $F(\cdot)$ is monotonic and differentiable with respect to $\text{SNDR}(\beta(f))$.

We will show that within the class of $g(\cdot)$ satisfying $0 \le g(\cdot) \le 1$, the soft-limiter with gain maximizes (as in the case of SNDR) or minimizes (as in the case of SER) the left hand side of (2.38).

Theorem 1. *Within the class of $g(\cdot)$ satisfying $0 \le g(\cdot) \le 1$, the following $g(\cdot)$ maximizes or minimizes the expression in (2.38):*

$$g(\gamma) = \begin{cases} \frac{\gamma}{\eta}, & 0 \le \gamma < \eta, \\ 1, & \gamma \ge \eta, \end{cases} \qquad (2.39)$$

where the threshold η is obtained from

$$\eta = \frac{\int E_{\beta(f)}[\frac{\partial F(\text{SNDR}(\beta(f)))}{\partial \text{SNDR}(\beta(f))} \frac{\kappa(\eta)}{\mu(\eta)}]\ df}{\int E_{\beta(f)}[\frac{\partial F(\text{SNDR}(\beta(f)))}{\partial \text{SNDR}(\beta(f))} \frac{\lambda(\eta)}{\mu(\eta)}]\ df}, \qquad (2.40)$$

where

$$\kappa(\eta) = C_1(\eta) + \frac{\bar{C}_2(\eta)}{\eta}, \tag{2.41}$$

$$\lambda(\eta) = C_o(\eta) + \frac{\bar{C}_2(\eta)}{\eta^2} + \frac{\sigma_v^2}{\beta^2(f)A^2}, \tag{2.42}$$

$$\mu(\eta) = \Big(\lambda(\eta) - \kappa^2(\eta)\Big)^2, \tag{2.43}$$

$$C_o(\eta) = \int_{\eta}^{\infty} p(\gamma)d\gamma, \tag{2.44}$$

$$C_1(\eta) = \int_{\eta}^{\infty} \gamma p(\gamma)d\gamma, \tag{2.45}$$

$$\bar{C}_2(\eta) = \int_{0}^{\eta} \gamma^2 p(\gamma)d\gamma, \tag{2.46}$$

and $p(\gamma)$ is the probability density function (PDF) of $\gamma = |x|/\sigma_x$.

Proof: See Section A.

The above theorem instructs us to first obtain the $C_o(\eta)$, $C_1(\eta)$, and $\bar{C}_2(\eta)$ expressions from the PDF of γ. We then obtain $\lambda(\eta)$, $\mu(\eta)$, and $\kappa(\eta)$. Since the latter three are functions of $\beta(f)$, the averaging operations on the right hand side (RHS) of (2.40) ensure that the RHS of (2.40) becomes a function of η only. Finally, equation (2.40) yields a numerical solution for η.

The optimal $g(\cdot)$ that maximizes the average SNDR can be obtained from Theorem 1 by setting the functional $F(a) = a$.

Figure 2.3 shows the optimal η versus PSNR $= \frac{\sigma_H^2 A^2}{\sigma_v^2}$ for the Rayleigh fading channel when different optimization criteria are used. The input signal x is assumed to be i.i.d. complex Gaussian distributed with mean 0 and variance σ_x^2. The dash-dotted line was obtained by optimizing (2.31); the solid line was obtained by optimizing (2.35); the dashed line was obtained by optimizing (2.48). In Figure 2.3, we observe that the dash-dotted line and the solid line are fairly close, indicating that the simplifying approximation used in (2.35) does not introduce much error.

2.4 Performance Comparisons

Next, we investigate the SER performance for the nonlinearity discussed in Theorem 1. Since OFDM is a popular transmission format for dispersive channels, we assume that

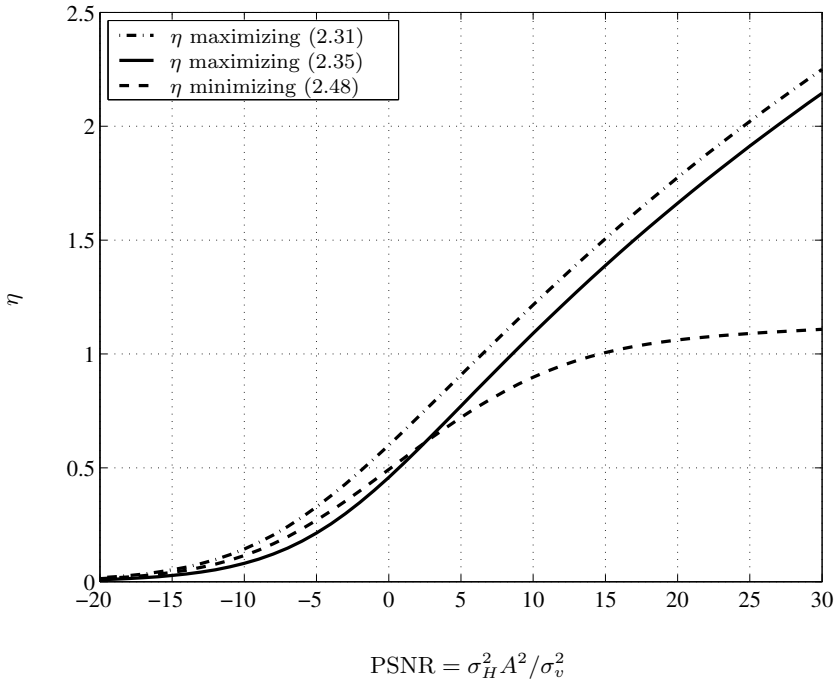

Figure 2.3: The value of η at a given PSNR for various optimization criteria. The dash-dotted line was obtained by optimizing (2.31); the solid line was obtained by optimizing (2.35); the dashed line was obtained by optimizing (2.48).

the symbols are drawn from a constellation in the frequency domain (i.e., $X(f)$ are the symbols), and we decode each frequency subcarrier separately. The conventional minimum distance receiver is applied. The SER can be evaluated by replacing SNR by the SNDR in the linear channel SER expression. For example, the SER of a binary phase shift keying (BPSK) signal [72] is given by

$$P_2 = \int E_{\beta(f)}[Q(\sqrt{\mathrm{SNDR}(\beta(f))})]\, df, \tag{2.47}$$

and the SER of a quadrature phase shift keying (QPSK) signal [72] is given by

$$P_4 = \int E_{\beta(f)}[Q(\sqrt{\mathrm{SNDR}(\beta(f))})(2 - Q(\sqrt{\mathrm{SNDR}(\beta(f))}))]\, df. \tag{2.48}$$

In Theorem 1, if we set $F(a) = Q(\sqrt{a})$ or $F(a) = Q(\sqrt{a})(2 - Q(\sqrt{a}))$, we infer that the soft limiter with a specific gain is also the optimal solution to (2.47) or (2.48). In the Rayleigh flat fading case, the optimal η, which minimizes (2.48), is calculated numerically and is shown in Figure 2.3 (the dashed line). We observe that when the PSNR is small, the dashed line and the solid line are very close; when the PSNR is large, the difference between the dashed line and the solid line becomes significant.

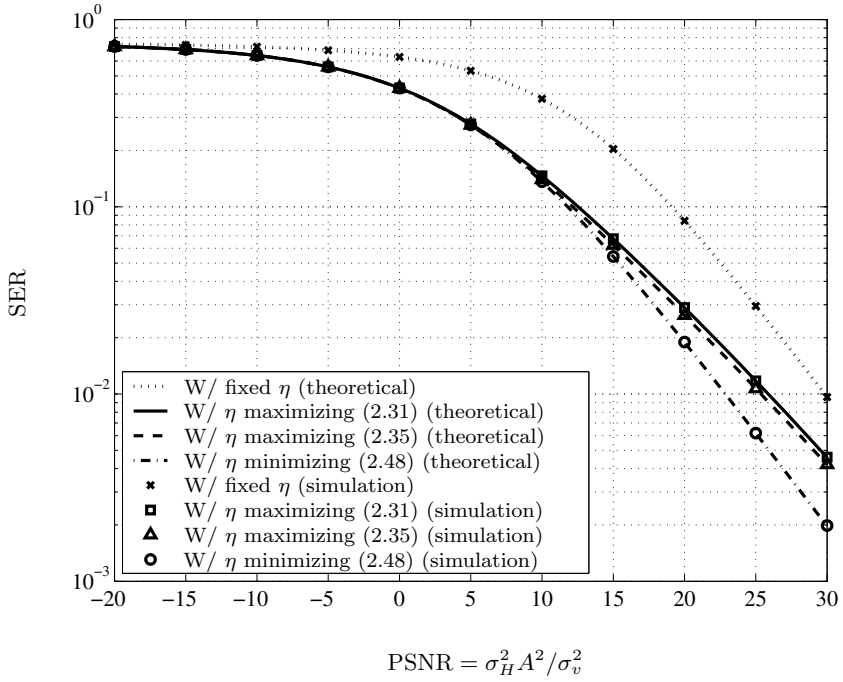

Figure 2.4: SER performance for a QPSK-OFDM input signal. The dotted line was obtained with $\eta = 3.29$; the solid line was obtained with the η that maximizes (2.31) at each PSNR; the dashed line was obtained with the η that maximizes (2.35) at each PSNR; the dash-dotted line was obtained with the η that minimizes (2.48) at each PSNR. The marked points were obtained by simulations. The channel variance was $\sigma_H^2 = 1$.

In the AWGN channel case, we know that the $g(\cdot)$ that maximizes the SNDR also minimizes the SER. In the fading channel case, however, the $g(\cdot)$ that maximizes the average SNDR may be different from the $g(\cdot)$ that minimizes the SER (2.48).

The SER performance of a QPSK-OFDM input signal in the presence of a Rayleigh flat fading channel is shown in Figure 2.4. Denote by $\{X(k)\}_{k=0}^{N-1}$ the frequency domain OFDM signal drawn from a QPSK constellation $\mathcal{C}$, and N is the number of sub-carriers. Nyquist-rate sampled time domain OFDM signal is represented as

$$x(n) = \frac{1}{\sqrt{N}} \sum_{k=0}^{N-1} X(k)\ e^{j\frac{2\pi kn}{N}}, \quad 0 \le n \le N-1. \tag{2.49}$$

The time domain OFDM signal $|x(n)|$ exhibits high peaks, especially for N large [99]. A proper nonlinearity, e.g., a soft limiter with a particular gain, may help to increase the average signal power and improve the SER performance.

At the receiver side, the received signal is first transformed into the frequency domain. Then the minimum-distance receiver is applied. In the simulations, $N = 128$. A total

of 10^6 blocks of data were used. Figure 2.4 shows the SER versus the PSNR for the QPSK-OFDM input signal in a flat fading environment with $\sigma_H^2 = 1$. The dotted line was obtained with $\eta = 3.29$ (the signal was practically "unclipped" [73, 99]); the solid line was obtained by selecting the η that maximizes (2.31); the dashed line was obtained by selecting the η that maximizes (2.35); the dash-dotted line was obtained by selecting the η that minimizes (2.48). The marked points were obtained by simulations (they agree well with the theoretical values). The channel variance was $\sigma_H^2 = 1$. We observe a similar performance when optimizing according to (2.31) and (2.35). A PSNR gain of 4 dB was obtained at SER $= 10^{-2}$. The performance for (2.31) was slightly worse than that for (2.35). If the channel variance equals 1, (2.35) reduces to (2.9). The optimal η obtained under the AWGN channel assumption also improves the SER performance for the fading channel case. The SER performance of the soft limiter with a gain obtained by minimizing (2.48) outperforms other methods yielding a PSNR gain of 7 dB at SER $= 10^{-2}$.

2.5 Conclusions

Many physical devices in communication systems are intrinsically nonlinear and thus introduce nonlinear distortions. To address the trade-off between maximizing the output power efficiency and minimizing the signal distortion, we consider the SNDR and the SER criteria.

In both AWGN channels and multipath fading channels, we showed that a soft limiter with a specified gain offers an optimal solution, in terms of the SNDR or the SER, when a peak amplitude constraint is presented at the transmitter. With the optimal nonlinearity, the SER performance can be significantly improved. We also showed that the optimal nonlinear function obtained under the AWGN channel assumption, which is a sub-optimal solution for the fading channel case, also improves (although not optimizes) the SER performance for the fading channel.

CHAPTER III

AN ADAPTIVE DIGITAL BASEBAND PREDISTORTION LINEARIZATION TESTBED FOR POWER AMPLIFIERS WITH MEMORY EFFECTS

Digital baseband predistortion is a cost effective approach to linearize modern RF/microwave power amplifiers (PAs). Traditionally, PAs are considered memoryless nonlinear devices. However, for wideband (such as WCDMA, or multicarrier) and/or high power (such as base station) applications, PAs exhibit memory effects. The so-called memory polynomial predistorter has a build-in memory structure and is a good candidate for linearizing PAs with memory effects. To improve the numerical stability of the memory polynomial predistorter, an orthogonal polynomial basis can be applied. In this chapter, we describe a high-speed wireless testbed for carrying out digital baseband predistortion linearization experiments. We show measurement results and demonstrate that the memory polynomial predistorter is more effective than the memoryless one in linearizing PAs with memory effects.

3.1 Introduction

The power amplifier (PA) is a major source of nonlinearity in a communication system. With the modern, more spectrally efficient transmission formats, such as Orthogonal Frequency Division Multiplexing (OFDM) or Code Division Multiple Access (CDMA), the signals tend to exhibit large peak-to-average power ratios (PAPRs) and are thus vulnerable to device nonlinearities. To increase the power efficiency, PAs are often driven into their nonlinear region, causing spectral regrowth (broadening) as well as in-band distortion. PA linearization is often necessary to suppress spectral regrowth, contain adjacent channel interference, and reduce bit error rate (BER).

Among all linearization techniques, digital baseband predistortion is one of the most

cost effective. Ideally, a digital baseband predistorter has the inverse characteristic of the PA. The baseband input signal passes through the predistorter before it is fed into the PA. Our hope is for the PA output to be an approximately scaled version of the predistorter input. To linearize a memoryless nonlinear PA, one can pursue lookup table (LUT) based or model based approaches. The LUT approach is easy to implement but may take a relatively long time to converge. Moreover, the piece-wise linear curve has a zig-zag appearance which may introduce additional nonlinearities that degrade the linearization performance [54]. As for model based approaches, the memoryless polynomial model is a common choice due to its simplicity and ease of implementation [21, Sec. 3.3], [30]. However, the memoryless polynomial may not be suitable for PAs with memory effects [106], which are known to be significant for high power amplifiers (HPAs) and/or for wideband signals [44]. Volterra series [28] and certain special cases of the Volterra series, for example, the Hammerstein model [23] and the memory polynomial model [25], have been proposed for predistorter designs that include memory effects.

Table 3.1: Digital baseband predistortion performances reported in the literature.

Reference	PA Size (PEP)	Predistorter	Test Signal (Bandwidth)	Performance
[49]	0.5 W	LUT	CDMA (1.25 MHz)	7 dB
[113]	0.5 W	LUT	2-tone (150 kHz)	20 dB
			2-tone (2.5 MHz)	< 20 dB
			modulated (300 kHz)	15 dB
			modulated (1.25 MHz)	10 dB
			modulated (5 MHz)	7.5 dB
[65]	1 W	LUT	$\pi/4$ DQPSK (0.6 MHz)	25 dB
[64]	1 W	NN	$\pi/4$ DQPSK (1.2 MHz)	25 dB
[113]	4 W	LUT	2-tone (150 kHz)	30 dB
			2-tone (2.5 MHz)	20 dB
			modulated (300 kHz)	12 dB
			modulated (1.25 MHz)	12 dB
			modulated (5 MHz)	10 dB
[48]	30 W	LUT	4-carrier WCDMA (20 MHz)	15 dB
			2-carrier WCDMA with 10 MHz separation (20 MHz)	15 dB
[9]	90 W	LUT	8-tone (2 MHz)	20 dB
			CDMA 2000 (3.75 MHz)	10 dB
[40]	300 W	Multiple LUTs	WCDMA (5 MHz)	12 dB

In Table 3.1, we summarize digital baseband predistortion linearization performances that have been reported in the literature. In this table, the size of the PA is indicated by its peak envelope power (PEP). NN stands for neural network predistorter. For modulated signals, the performance metric is improvement in the adjacent channel power ratio (ACPR) after predistortion. For 2-tone input signals, the performance metric is the amount of reduction in the 3rd-order intermodulation distortion (IMD_3). For 8-tone input signals, the performance metric is the amount of reduction in the IMD next to the main channel.

This chapter is organized as follows: In Sec. 3.2, we describe our high speed wireless testbed and show some measurement results that reveal memory effects in the PA. In Sec. 3.3, we reviewed the memory polynomial predistorter. In Sec. 3.4, the performance of the memoryless polynomial predistorter and that of the memory polynomial predistorter are demonstrated. Moreover, orthogonal polynomials are used to improve the numerical stability of the memory polynomial predistorter. Advantages of the memory polynomial predistorter over the memoryless polynomial predistorter for PAs with memory effects are demonstrated. Sec. 3.5 concludes this chapter.

3.2 Testbed Setup

3.2.1 Testbed Setup

We show in Figure 3.1 our testbed configuration. The high-speed digital I/O system has a 150 million samples per second (MSPS) 16-bit digital input/output capability. In the transmission mode, the digital I/O system first generates digital baseband data $x(n)$, predistorts it to yield $z(n)$, digitally up-converts $z(n)$ to an intermediate frequency (IF) of 30 MHz, and then sends out the 14-bit data stream to the digital-to-analog (D/A) converter at a sampling rate of 120 MSPS. In the acquisition mode, the digital I/O system acquires 12-bit digital IF data at the sampling rate of 120 MSPS from the analog-to-digital (A/D) converter. In the figure, $y(n)$ is obtained by converting the PA output to baseband and removing the time delay τ between the input and the output of the digital I/O system. Since the signal is modulated in the digital domain, any in-phase and quadrature imbalance problem in the quadrature modulator is obviated. Superheterodyne up-conversion and down-conversion

chains are adopted to convert the digital IF signal to and from the radio frequency (RF). We have designed the RF transmit and receive chains to have a linear response over a wide bandwidth and a large dynamic range.

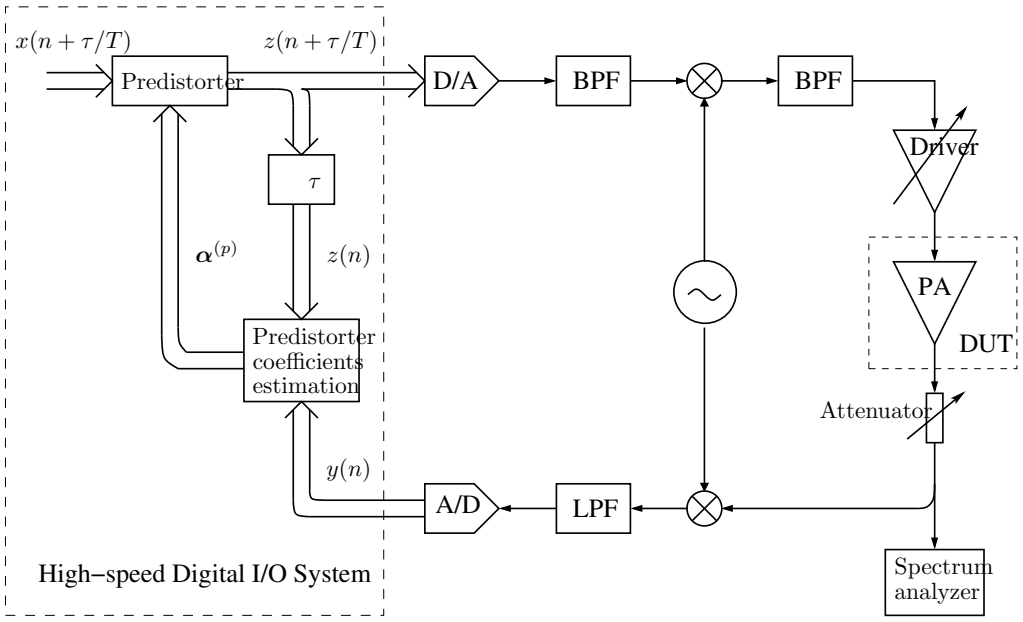

Figure 3.1: System diagram of the high-speed wireless testbed.

3.2.2 Measurement of Power Amplifiers with Memory Effects

For experiment validations, the device under test (DUT) is a Siemens CGY0819 1 W PA, shown in Figure 3.2, or an Ericsson 19D903800G1 45 W PA. shown in Figure 3.3. The Siemens PA is a dual band GaAs class-AB handset PA and operates at the cellular band with a center frequency of 836 MHz. The Ericsson PA is a silicon bipolar transistor based class-AB base-station PA and operates at the cellular band with a center frequency of 881 MHz.

Figure 3.4 shows the amplitude-to-amplitude (AM/AM) conversion of the Siemens 1 W PA. For comparison, Figure 3.5 shows the AM/AM response of the Ericsson 45 W PA. The input signal used in both cases is a two-tone signal with 1.0 MHz tone spacing. In Figure 3.4, the AM/AM response of the Siemens PA stays "focused" and forms a single curve. In contrast, the AM/AM response in Figure 3.5 reveals some hysteresis behavior and is no longer a single curve. In other words, for the same PA input, the PA output might be

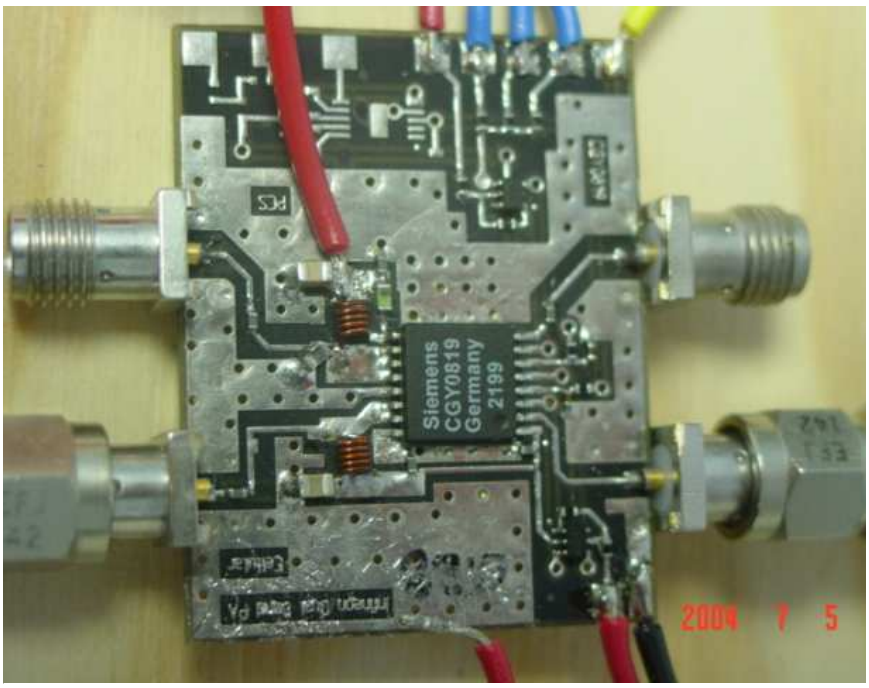

Figure 3.2: Siemens 1 W power amplifier.

Figure 3.3: Ericsson 45 W power amplifier.

different. This phenomenon is a sign of memory effect in the PA.

In order to further ascertain memory effects in the Ericsson 45 W PA, we conducted a two-tone experiment. In this experiment, we fixed the peak PA output power at 36.5

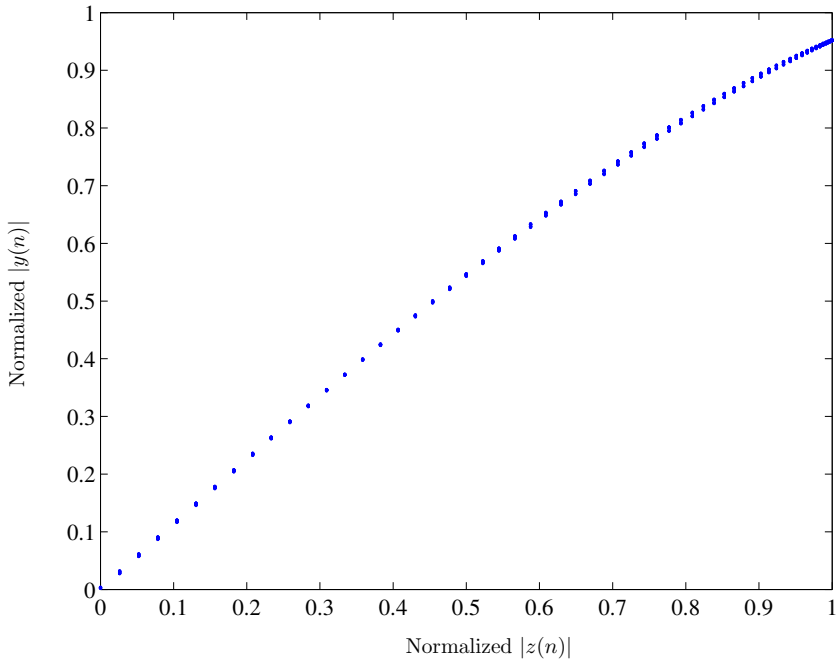

Figure 3.4: The AM/AM response of the Siemens 1W PA.

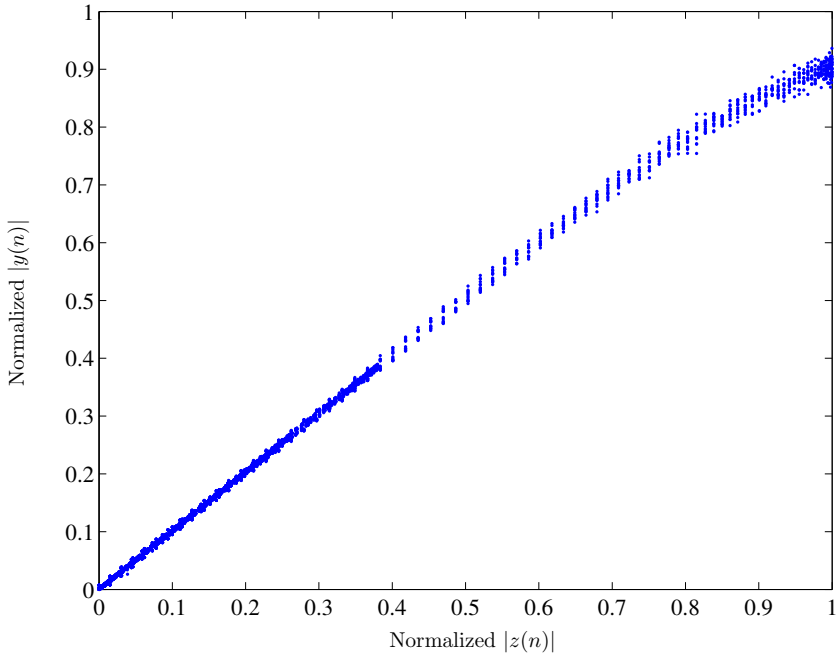

Figure 3.5: The AM/AM response of the Ericsson 45 W PA.

dBm but incrementally changed the tone spacing from 100KHz to 20MHz. Figure 3.6 shows the IMD_3 at the lower sideband of the main channel ($IMD_{3,L}$) and at the upper sideband of the main channel ($IMD_{3,U}$), as well as the $IMD_{5,L}$ and $IMD_{5,U}$, when the tone

spacing is changed. We observe that the IMD products vary significantly with changes in the tone-spacing, and appear asymmetric between the lower and upper sidebands. $\text{IMD}_{3,\text{L}}$ and $\text{IMD}_{3,\text{U}}$ differed by as much as 5 dB, whereas $\text{IMD}_{5,\text{L}}$ and $\text{IMD}_{5,\text{U}}$ differed by as much as 9 dB. These led us to believe that the Ericsson 45 W PA exhibits significant memory effects.

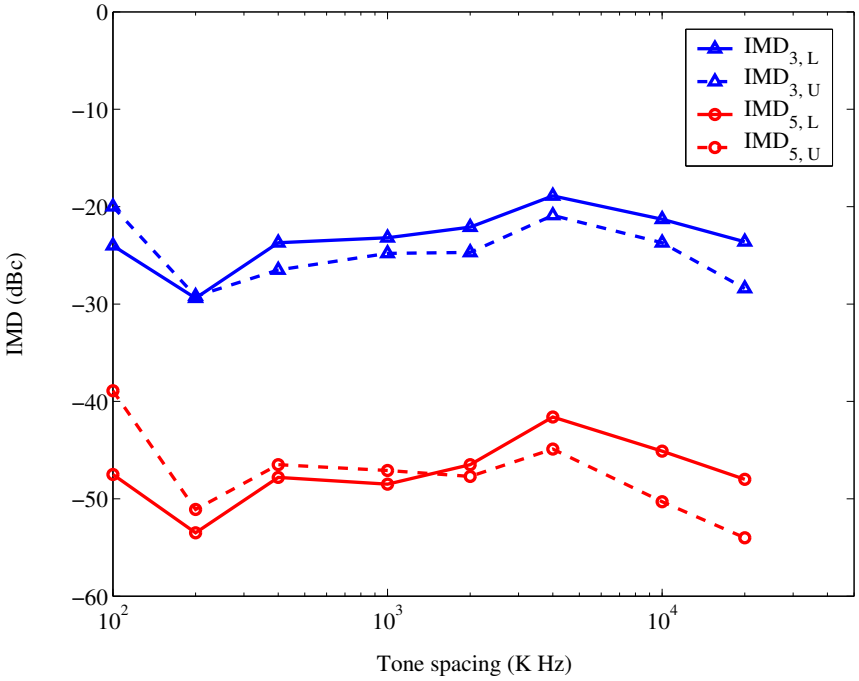

Figure 3.6: The IMD products vs. the tone spacing for the Ericsson 45W PA.

3.3 Digital Baseband Predistortion

3.3.1 Predistorter Models

Following the notations of Figure 3.1, a memoryless polynomial predistorter is given by [25]:

$$z(n) = \sum_{k=1}^{K} a_k \; |x(n)|^{k-1} x(n), \tag{3.1}$$

where $\{a_k\}_{k=1}^{K}$ are the predistorter coefficients and K is the highest polynomial order. Eq. (3.1) can be easily extended to a memory polynomial model [25]:

$$z(n) = \sum_{k=1}^{K} \sum_{q=0}^{Q} a_{kq} \; |x(n-q)|^{k-1} x(n-q), \tag{3.2}$$

where Q is the largest delay tap. To improve modeling accuracy, both even and odd order terms are used in (3.1) and (3.2) [24].

Ref. [25] demonstrated by *computer simulations* that the memory polynomial predistorter can suppress well the spectral regrowth generated by a nonlinear PA with memory effects. Numerical instability has been reported in [83] as a challenging problem for the polynomial predistorter when high order polynomials are used. This is because the regressor matrix used in solving for the predistorter coefficients is close to being singular when the polynomial order is high [83]. The so-called orthogonal polynomials can help to improve the numerical stability. Let us rewrite the memory polynomial model as

$$z(n) = \sum_{k=1}^{K} \sum_{q=0}^{Q} \alpha_{kq} \ \psi_k(x(n-q)), \tag{3.3}$$

where $\psi_k(x)$ is given by [83]

$$\psi_k(x) \quad = \quad \sum_{l=1}^{k} (-1)^{l+k} \frac{(k+l)!}{(l-1)!(l+1)!(k-l)!} |x|^{l-1} x. \tag{3.4}$$

$\psi_{k_1}(x(n-q_1))$ and $\psi_{k_2}(x(n-q_2))$ are strictly orthogonal to each other for $k_1 \neq k_2$ and $q_1 = q_2$ if $|x|$ is uniformly distributed in $[0, 1]$. For input signals with other distributions or when $q_1 \neq q_2$, $\psi_{k_1}(x(n-q_1))$ and $\psi_{k_2}(x(n-q_2))$ are generally not exactly orthogonal. However, the basis set (3.4) can still help to reduce the condition number of the regressor matrix and thus improve the numerical stability.

A matrix representation of (3.3) is

$$\mathbf{z} = \mathbf{\Psi} \ \boldsymbol{\alpha}, \tag{3.5}$$

where

$$\boldsymbol{\alpha} = [\alpha_{10}, \ldots, \alpha_{1Q}, \alpha_{20}, \ldots, \alpha_{KQ}]^T, \tag{3.6}$$

$$\mathbf{z} = [z(1), z(2), \ldots, z(N-Q)]^T, \tag{3.7}$$

$$\mathbf{\Psi} = [\boldsymbol{\psi}_1(\mathbf{x}(0)), \ldots, \boldsymbol{\psi}_1(\mathbf{x}(Q)), \boldsymbol{\psi}_2(\mathbf{x}(0)), \ldots, \boldsymbol{\psi}_K(\mathbf{x}(Q))], \tag{3.8}$$

and

$$\boldsymbol{\psi}_k(\mathbf{x}(q)) = [\psi_k(x(Q+1-q)), \psi_k(x(Q+2-q)), \ldots, \psi_k(x(N-q))]^T \tag{3.9}$$

for $0 \leq q \leq Q$, $1 \leq k \leq K$.

3.3.2 Predistorter Model Coefficients Calculation

We adopt the indirect learning architecture to obtain the predistorter model coefficients [27]. Let us denote the predistorter model by function $f(\cdot)$. An iterative block training approach can be implemented:

Step 1. Initialize the predistorter model with $f^{(0)}(x(n)) = x(n)$ and set the iteration number $p = 1$.

Step 2. For a given block of input data $\{x^{(p)}(n)\}_{n=1}^{N}$, where N is the total number of samples available, calculate the predistorted signal

$$z^{(p)}(n) = f^{(p-1)}(x^{(p)}(n)), \tag{3.10}$$

and measure the corresponding PA output $\{y^{(p)}(n)\}_{n=1}^{N}$.

Step 3. Now let $y(n)/G$ be the input, and $z(n)$ be the output of the model $f(\cdot)$. Estimate the p-th model parameters of $f^{(p)}(\cdot)$ based on the samples $\{z^{(p)}(n)\}_{n=1}^{N}$ and $\{y^{(p)}(n)\}_{n=1}^{N}$. For example, the predistorter coefficients in (3.5) can be obtained using least-squares:

$$\boldsymbol{\alpha}^{(p)} = \left(\boldsymbol{\Psi}^H \boldsymbol{\Psi}\right)^{-1} \boldsymbol{\Psi}^H \mathbf{z}, \tag{3.11}$$

by replacing $z(n)$ with $z^{(p)}(n)$, and $x(n)$ with $y^{(p)}(n)/G$ in (3.3).

Step 4. Increase p by one and go back to Step 2.

This iterative procedure ensures that the predistorter can adapt to slow changes in the PA characteristics due to biasing changes, ambient temperature variations, aging, etc.

The procedure described above is for the off-line training mode, in which case $x^{(p)}(n)$ can be the same block of data $x(n), \forall p$. For online updates, the algorithm cycles between steps 2 and 3.

3.4 Measurement Results

In this section, we show the measurement results when the memoryless polynomial predistorter and the memory polynomial predistorter are applied. The predistorter model coefficients are computed by a 32-bit floating point precision C program. In the experiments, the highest polynomial order was set to $K = 5$. For the memory polynomial predistorter, we chose $Q = 9$ when the input signal is a 2-tone or 8-tone signal, and $Q = 4$ when the input signal is a modulated signal (multi-carrier CDMA or WCDMA signal).

To quantitatively measure the predistorter performance, we used the ACPR and the normalized mean square error (NMSE) as performance metrics. For the 2-tone or 8-tone input signals, we considered the IMD product that is next to the main channel in the ACPR measurements.

The NMSE indicates the total distortion of the system, which can be calculated by [32]:

$$\text{NMSE} = \sqrt{\frac{\sum_{n=1}^{N} \|y(n) - G\ x(n)\|^2}{\sum_{n=1}^{N} \|y(n)\|^2}}, \tag{3.12}$$

where N is the total number of samples.

The ACPR is defined as the power contained in a defined adjacent band divided by the power contained in a defined band around the center frequency [42]. The ACPR is an indication of the amount of spectral regrowth in the adjacent channel, or the level of inter-channel interference. In this chapter, we measured the power spectral density (PSD) of the PA output using two 30 kHz bandwidth markers, one at the carrier frequency f_c, and the other one at the frequency $f_c \pm 0.8 f_s$, where f_s is the bandwidth of the input signal. Between the lower and upper adjacent channels, the one that has the higher marker reading is recorded. The difference (in dB) between the two marker readings can be viewed as an approximation to the ACPR if the bandwidth of the main channel and that of the adjacent channel are assumed equal in the ACPR calculation.

3.4.1 Conventional vs. Orthogonal Polynomials

We first compared the performance of the conventional memory polynomial predistorter with that of the orthogonal memory polynomial predistorter. In this experiment, the DUT

was the Siemens 1 W PA. The input signal was a 1.25 MHz bandwidth CDMA signal with a peak-to-average power ratio (PAPR) of 6 dB. The PEP of the PA output was 28 dBm.

We first examined the condition numbers of the matrices involved in the least-squares estimation ($(\mathbf{\Phi}^H\mathbf{\Phi}$ [83]) in the conventional polynomial case, and ($\mathbf{\Psi}^H\mathbf{\Psi}$) in the orthogonal polynomial case). The condition numbers for ($\mathbf{\Phi}^H\mathbf{\Phi}$) at iterations 3, 4 and 5 were 1.08×10^{13}, 0.98×10^{13}, and 0.90×10^{13}, respectively; while the condition numbers for ($\mathbf{\Psi}^H\mathbf{\Psi}$) at iterations 3, 4 and 5 were 2.58×10^6, 3.14×10^6, and 2.66×10^6, respectively. The orthogonal polynomials helped to reduce the condition numbers significantly, thus improving the numerical stability of the memory polynomial predistorter.

Figure 3.7 shows the performance of the conventional memory polynomial predistorter (3.2) and the orthogonal memory polynomial predistorter (3.3) in terms of the PSD of the PA output. In Figure 3.7, line (a) is the PA output PSD without predistortion; lines (b)-(d) are the PA output PSDs with conventional memory polynomial predistortion at iteration numbers 3, 4, and 5; lines (e)-(g) are the PA output PSDs with orthogonal memory polynomial predistortion at iteration numbers 3, 4, and 5. In this experiment, we observed that the conventional memory polynomial predistorter performance was not stable (the lines fluctuated up and down). In contrast, the orthogonal memory polynomial predistorter showed stability and effectiveness; it successfully suppressed the IMD in the adjacent channel by 22 dB. In the remaining experiments, the orthogonal polynomial basis (3.4) is adopted.

3.4.2 Memoryless Polynomial vs. Memory Polynomial

Next, we compared the performances of the memoryless and memory polynomial predistorters. We first used the Siemens 1 W PA as the DUT. The input signal was a 1.2 MHz bandwidth 8-tone signal with 150 kHz tone spacing. The PEP of the PA output was 28 dBm.

Figure 3.8 shows the performance of the memory polynomial predistorter and the memoryless polynomial predistorter in terms of PSD of the PA output. In Figure 3.8, line (a) is the PA output PSD with memory polynomial predistortion; line (b) is the PA output PSD with memoryless polynomial predistortion; line (c) is the PA output PSD without

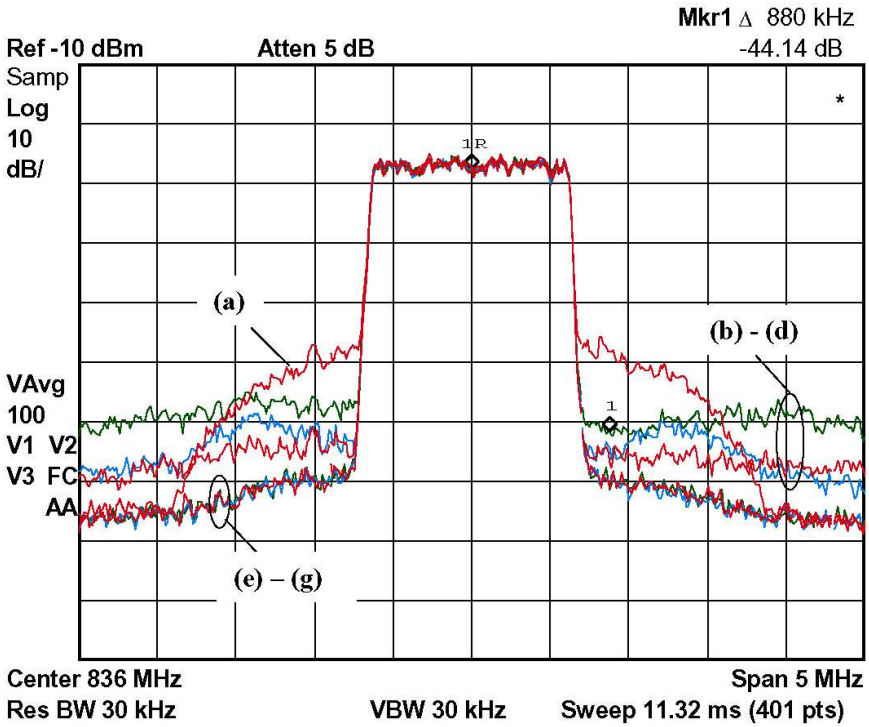

Figure 3.7: Measured PA output PSDs for the Siemens 1 W PA: (a) without predistortion; (b)-(d) with conventional memory polynomial predistortion at iteration numbers 3, 4, and 5; (e)-(g) with orthogonal memory polynomial predistortion at iteration numbers 3, 4, and 5. Both the conventional and the orthogonal polynomial predistorters used $K = 5$ and $Q = 4$.

predistortion. In this experiment, we observed that the memory polynomial predistorter suppressed almost all the spectral regrowth. In the adjacent channel, the memory polynomial predistorter suppressed the nearest IMD product by 33 dB, while the memoryless polynomial predistorter gave 23 dB of IMD reduction. The memory polynomial predistorter outperformed the memoryless predistorter by about 10 dB.

Next, we used the Ericsson 45 W PA as the DUT. The input signal was a 2.5 MHz bandwidth 2-carrier CDMA signal with a peak-to-average power ratio (PAPR) of 8.5 dB. The PEP of the PA output was 36.5 dBm.

Figure 3.9 shows the performances of the memory polynomial predistorter and the memoryless polynomial predistorter in terms of PSD of the PA output. In Figure 3.9, line (a) is the PA output PSD with memory polynomial predistortion; line (b) is the PA output PSD with memoryless polynomial predistortion; line (c) is the PA output PSD without

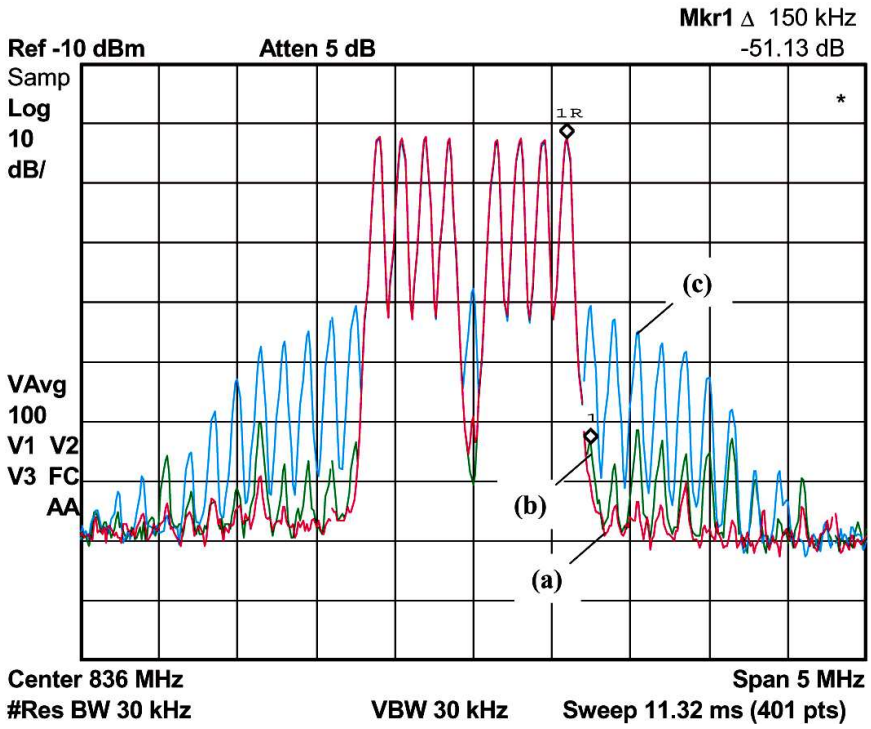

Figure 3.8: Measured PA output PSD for the Siemens 1 W PA: (a) with the $K = 5$, $Q = 9$ memory polynomial predistorter; (b) with the $K = 5$ memoryless predistorter; (c) without predistortion.

predistortion. In this experiment, we observed that the memory polynomial predistorter suppressed the IMD in the adjacent channel by 15 dB, whereas the memoryless polynomial predistorter only gave 8 dB of IMD reduction. The results showed that the memory polynomial predistorter had a significant advantage over the memoryless polynomial predistorter for the PA with memory effects.

To further explore the predistorter performance when the input power of the PA changes, we repeated the above experiment when the PEP of the PA output swept from 27.5 to 38.5 dBm. Figure 3.10 shows the ACPR improvement results of the memoryless polynomial predistorter and the memory polynomial predistorter when the PA output power level changes. In Figure 3.10, the solid line is the ACPR performance for the PA with the memory polynomial predistorter; the dashed line is the ACPR performance for the PA with the memoryless polynomial predistorter; the dash-dotted line is the ACPR performance for the PA output without predistortion linearization. From Figure 3.10, we can determine the PEP of the PA input for a given spectral mask requirement. For example, if the desired

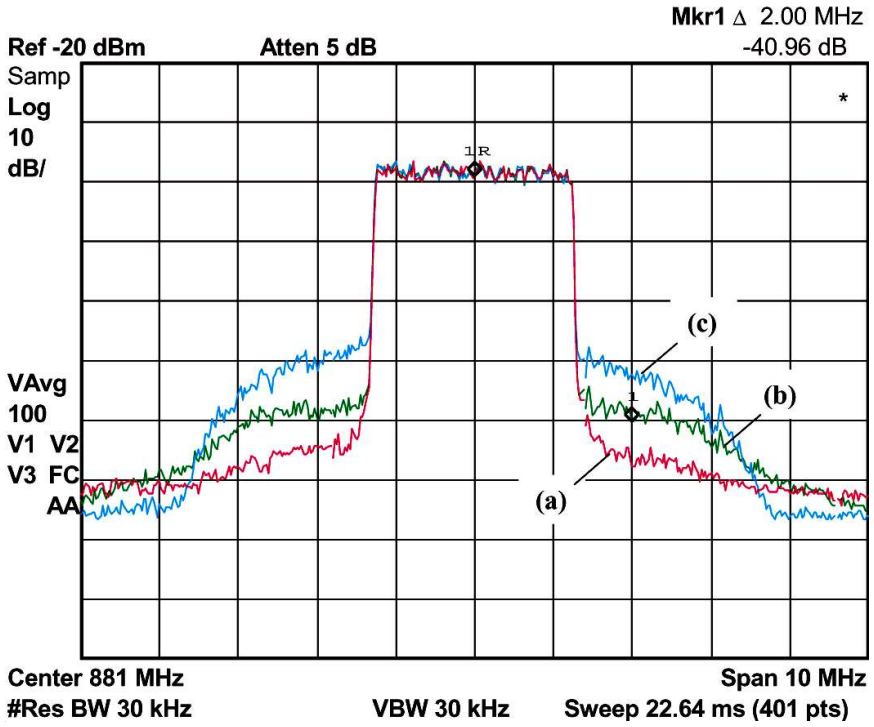

Figure 3.9: Measured PA output PSD for the Ericsson 45 W PA: (a) with the $K = 5$, $Q = 4$ memory polynomial predistorter; (b) with the $K = 5$ memoryless predistorter; (c) without predistortion.

ACPR is 45 dB, the maximum PEP of the output from the PA without predistorter is approximately 29.5 dBm, while the maximum PEP of the output from the PA with the memory polynomial predistorter is approximately 36.5 dBm. An average power gain of 7 dB is achieved when the memory polynomial predistorter is used.

3.4.3 Performance on the Siemens 1 W PA vs. Performance on the Ericsson 45 W PA

The following experiments summarize the predistorter performances on both the Siemens 1 W PA and the Ericsson 45 W PA for various input signals with different bandwidths. For the Siemens PA, the PEP of the PA output was set at 28 dBm. For the Ericsson PA, the PEP of the PA output was set at 36.5 dBm.

Table 3.2 summarizes the ACPR improvement results (ΔACPR) and the NMSE results on the Siemens 1 W PA that we have achieved; PD stands for predistorter.

Table 3.3 summarizes the ACPR improvement results (ΔACPR) and the NMSE results

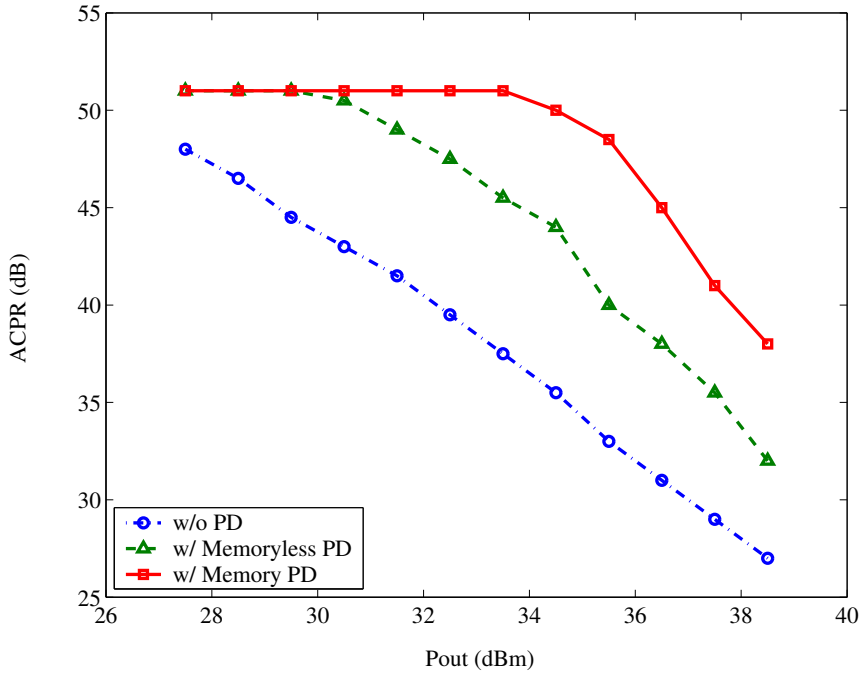

Figure 3.10: Measured ACPR results for the Ericsson 45 W PA when the PA input power changes: the solid line is with the $K = 5$, $Q = 4$ memory polynomial predistorter; the dashed line is with the $K = 5$ memoryless predistorter; the dash-dotted line is without predistortion.

on the Ericsson 45 W PA that we have achieved.

From Table 3.2, we observe that for the Siemens 1 W PA, the ACPR improvement and the NMSE result for the PA with the memory polynomial predistorter were always better than those with the memoryless polynomial predistorter. The results imply that the Siemens 1 W handset PA also had some memory effects, which may be due to the frequency dependency of the matching circuits or the bias networks. The predistorter performance gain decreases when the signal bandwidth increases; this may be attributed to frequency dependent memory effects that cannot be modeled accurately by the memory polynomial model. We also observed that the memoryless polynomial predistorter, which is a special case of the memory polynomial predistorter, is fairly effective when the signal bandwidth is small.

From Table 3.3, we observe that for the Ericsson 45 W PA, the ACPR improvement and the NMSE result for the PA with the memory polynomial predistorter were always better than when the memoryless polynomial predistorter is utilized. The ACPR improvement for

Table 3.2: Memoryless and memory polynomial predistortion results on the Siemens 1 W PA.

Input Signal		Memoryless polynomial PD		Memory polynomial PD	
Format	Bandwidth	ΔACPR	NMSE (%)	ΔACPR	NMSE (%)
2-tone signal	0.2 MHz	21 dB	1.05	34 dB	1.03
2-tone signal	1.0 MHz	21 dB	0.73	29 dB	0.24
8-tone signal	1.2 MHz	23 dB	0.96	33 dB	0.41
CDMA	1.25 MHz	21 dB	2.97	22 dB	2.50
2-carrier CDMA	2.5 MHz	15 dB	6.11	18 dB	4.83
WCDMA	3.84 MHz	11 dB	9.38	14 dB	7.65
4-carrier CDMA	5.0 MHz	8 dB	11.91	10 dB	9.62

Table 3.3: Memoryless and memory polynomial predistortion results on the Ericsson 45 W PA.

Input Signal		Memoryless polynomial PD		Memory polynomial PD	
Format	Bandwidth	ΔACPR	NMSE (%)	ΔACPR	NMSE (%)
2-tone signal	0.2 MHz	16 dB	1.46	24 dB	1.13
2-tone signal	1.0 MHz	10 dB	2.41	24 dB	1.39
8-tone signal	1.2 MHz	9 dB	1.66	14 dB	0.95
CDMA	1.25 MHz	8 dB	6.15	15 dB	5.72
2-carrier CDMA	2.5 MHz	8 dB	6.22	15 dB	5.45
WCDMA	3.84 MHz	5 dB	7.63	9 dB	6.48
4-carrier CDMA	5.0 MHz	7 dB	8.68	9 dB	6.57

the memory polynomial predistorter was significantly better than that for the memoryless polynomial predistorter. This may be due to the strong memory effects that the Ericsson 45 W PA exhibits which render the memoryless polynomial predistorter not very effective.

3.5 Conclusions

Digital baseband predistortion is a cost effective approach to linearize modern RF PAs. In this chapter, we constructed a testbed that allows us to measure behaviors of power amplifiers as well as to evaluate the performance of various predistorter models. For the Siemens 1 W PA with narrowband inputs, the PA can be regarded as memoryless, and the memoryless predistorter can be fairly effective. However, when the signal bandwidth increases and/or the size of the PA increases, the memory effects become significant. The memoryless predistorter provides diminishing returns, whereas the memory polynomial predistorter can be effective over a broad range of conditions. To alleviate the numerical instability problem

associated with the memory polynomials when the polynomial order is high, an orthogonal polynomial basis is utilized. We showed that the orthogonal polynomials can greatly reduce the condition number of the regressor matrix, thus improving the numerical stability of the memory polynomial predistorter. To the best of our knowledge, our measurement results are comparable to or better than the results published in the literature.

CHAPTER IV

A LOW COST PREDISTORTION LINEARIZATION ARCHITECTURE FOR PORTABLE WIRELESS DEVICES[0]

For a mobile wireless device, power efficiency of the power amplifier (PA) in the transmitter is an important issue since the PA consumes a great deal of power and directly impacts the battery life of the device. PA linearization is often sought for achieving good efficiency while maintaining good linearity of the PA. However, adaptive PA linearization has been practiced mostly on the larger, higher power PAs. In this article, we propose an adaptive digital predistortion linearization design that is especially suitable for the smaller, lower power wireless terminals. This new predistortion architecture utilizes existing components of the wireless transceiver to fulfill the adaptive predistorter training functionality; it is cost effective and power efficient. Potential applications include cellular phones and wireless sensor units.

4.1 Introduction

In a mobile wireless device, power efficiency of the power amplifier (PA) in the transmitter is an important design metric [26]. High efficiency is desired as it means low battery drain, long talk time and/or light weight for the device. However, high efficiency PAs are usually nonlinear. The nonlinearity leads to spectral regrowth (broadening) as well as in-band distortion. PA linearization is often necessary in order to achieve good efficiency while maintaining good linearity of the PA.

Among all linearization techniques, digital baseband predistortion is one of the most cost effective [11, 22, 25, 31, 61, 110]. A predistorter (PD), which has approximately the inverse

[0]Protected by U.S. provisional patent [81], Sept. 2004.

characteristic of the PA, is used to compensate for the nonlinearity of the PA. Ideally, the output of the PD-PA cascade is a scalar version of the original input signal up to the saturation point.

In the past decade, numerous PA linearization techniques for the mobile terminal have been proposed. In [34, 35], the authors proposed a circuit level predistorter design. A predistorter was integrated in the PA design itself. A 10 dB adjacent-channel-power-ratio (ACPR) improvement was achieved over a 3.84 MHz bandwidth for a handset PA with a hybrid phase shift keying modulated input. In [46], the authors applied a Schottky diode as the predistorter in a 2 watt PA design. The ACPR was improved by 7.25 dB over a 1.25 MHz bandwidth with a CDMA 900 MHz input signal. In [66], the authors used an active feedback network to linearize the PA. The ACPR was improved by about 10 dB over a 5 MHz bandwidth for a WCDMA input signal. The techniques proposed in [34,35,46,66], however, do not adapt to changes in the PA characteristics. The predistorter can be calibrated when the device is manufactured but may become less effective when the PA operating conditions change. In [49], the authors applied an RF predistorter to the cellular handset PA. The performance of the predistorter, however, was limited because of inaccuracy of the analog components in the correction loop.

Digital baseband predistortion has been applied to linearize the PA for the wireless device. In [2, 59, 94], the authors utilized a feedback path from the PA output. Ref. [59] presents a handset architecture that gets feedback from the PA output and allowed baseband predistortion. Ref. [94] uses the look-up-table (LUT) based predistortion algorithm to linearize the PA. Ref. [2] proposes a nonlinear optimization predistortion algorithm. The technologies in [2,59,94] require a separate down conversion chain to implement the adaptive predistorter training functionality, which can increase both the cost and power consumption of the wireless unit. In [12], the authors implemented a LUT based predistortion algorithm in the field programmable gate array (FPGA). It does not require a feedback path; however, a major drawback of this method is that the LUT entries are determined based on the characteristics of the PA obtained off-line (e.g., during factory calibration), and hence are non-adaptive. Ref. [111] proposed to use LUTs to implement the predistorter gain function,

but did not consider the timing issue in the feedback loop.

In this chapter, we propose a new predistorter architecture to linearize the PA for the wireless transmitter. The key idea is to utilize existing components of the transceiver to implement the down-conversion process, thus reducing the cost and power consumption in the predistorter training loop.

4.2 Adaptive Digital Baseband Predistortion Linearization Architecture

In order to implement an *adaptive* predistortion algorithm, a feedback path from the PA output is necessary in order to learn about the current characteristics of the PA. Changes in the PA characteristics can be due to temperature variations, aging, biasing changes, etc and usually have slow time constants. The challenge in the predistortion architecture design for portable devices is to incur as low cost as possible with as low power consumption as possible.

4.2.1 Conventional Predistortion Architecture

Figure 4.1 shows a commonly employed adaptive digital baseband predistortion linearization architecture [42]. A separate down-conversion chain is employed (the top portion of Figure 4.1). The purpose of this feedback path is to facilitate learning of the current behavior of the PA. A coupler, an attenuator, an RF mixer, a bandpass filter (BPF2), two IF mixers, two low pass filters (LPF3, LPF4) and two ADCs (ADC1, ADC2) are added to the original transmitter (the bottom portion of Figure 4.1). These components not only add to the cost but also the power consumption of the transmitter.

This architecture is well suited for base station or other large PA linearization applications since the cost and power consumption of the feedback path are small as compared to the overall cost and power consumption of the large (and expensive) PA. For consumer applications (such as the cellular phone) however, the architecture in Figure 4.1 is less appealing, because the added cost can be a significant portion of the overall design budget. For this reason, *adaptive* predistortion linearization has not been widely applied to handheld devices.

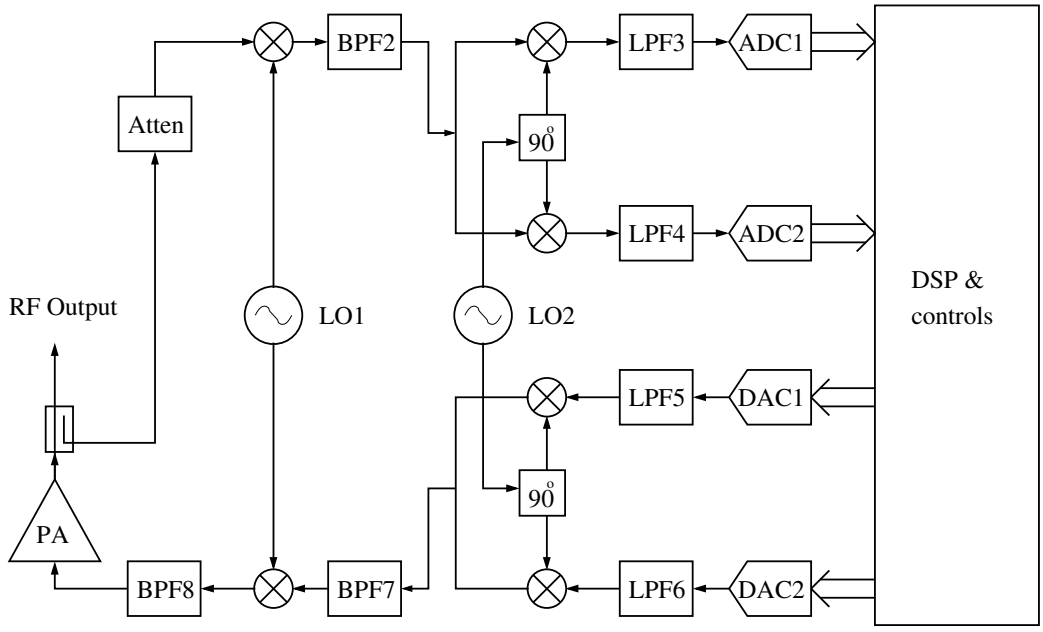

Figure 4.1: A conventional adaptive digital baseband predistortion linearization architecture for the transmitter.

Next, we review the commonly employed transceiver architectures to appreciate the similarities between the adaptive predistorter and the transceiver.

4.2.2 Existing Transceiver Architectures

Currently, there are three main architectures for the radio frequency (RF) transceiver design [87]:

1. Superheterodyne. This is the conventional architecture for transceivers. Main advantages are high selectivity and high sensitivity. Main disadvantages are image rejection problems, high power consumption, and high cost. Figure 4.2 shows the RF part of the conventional superheterodyne transceiver. When the transceiver operates at the frequency duplex model, the switch attached to the antenna is not necessary. When the transceiver operates at the time duplex model, local oscillators LO1 and LO3 can be the same.

2. Direct conversion / zero IF. This is a rather new technique. Main advantages are high integration, low power consumption, low cost and no image rejection problem. Main disadvantages are I/Q matching problems and DC offset.

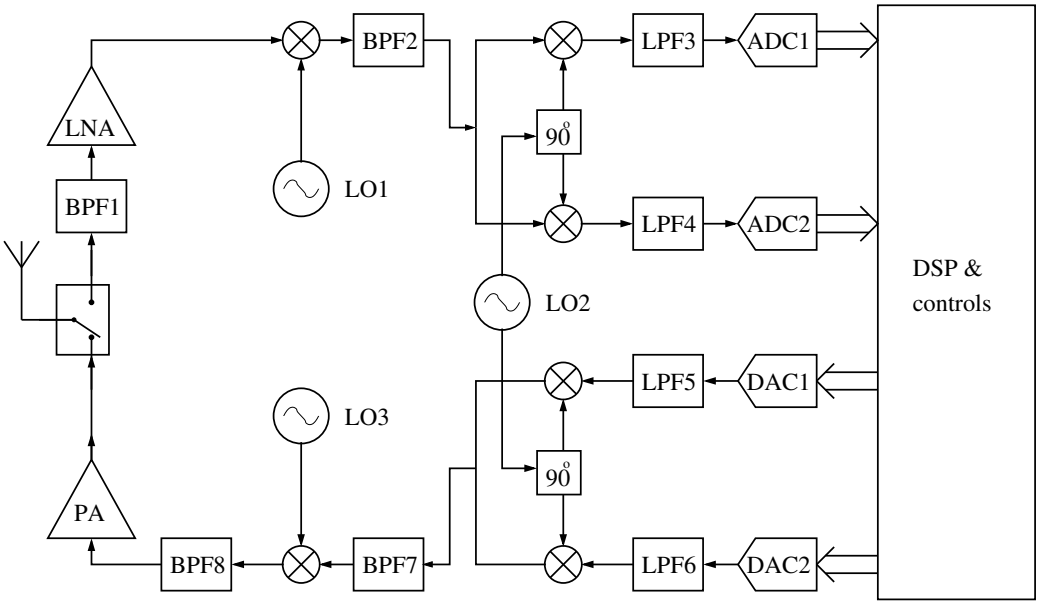

Figure 4.2: Conventional superheterodyne transceiver architecture.

3. Low IF. Main advantages are high integration and freedom from DC offset problems. Main disadvantages are I/Q matching problems, image signal suppression problems and stringent ADC dynamic range requirements.

Next, we will explain how the transceiver architecture in Figure 4.2 can be modified to achieve adaptive predistortion linearization similar to Figure 4.1. We would like to point out that the proposed structure can be modified to work with the direct conversion and low IF transceiver architectures as well.

4.2.3 Proposed Digital Baseband Predistortion Transceiver Architecture

The top part of Figure 4.2 is the receiver portion of the transceiver which converts the received RF signal to baseband. It has the same functionality as the feedback path in the adaptive predistortion architecture (top portion of Figure 4.1). It thus makes sense to reuse this down-conversion chain to implement the feedback path for the predistorter.

Our proposed digital baseband predistortion transceiver architecture is shown in Figure 4.3. As compared with Figure 4.2, a coupler at the output of the PA and a soft switch after the low-noise amplifier (LNA) are the only hardware components added to the conventional transceiver. Comparing to the transmitter in Figure 4.1, the proposed digital baseband

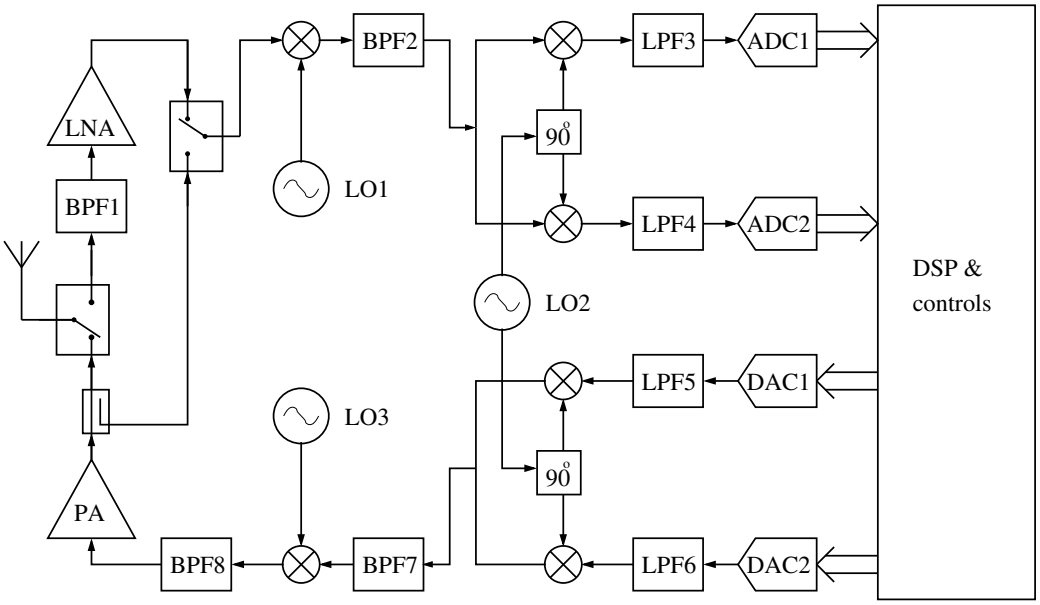

Figure 4.3: Modified superheterodyne transceiver architecture suitable for adaptive digital baseband predistortion linearization.

predistortion transceiver architecture has just one added components in the transmitter, the coupler. With careful design, the insertion loss of the coupler can be very small, usually less than 0.1 dB. The coupler returns a fraction of the PA output signal to the feedback (receiver) path. It also adjusts the signal to the desired power level.

Comparing to the receiver in Figure 4.2, the proposed digital baseband predistortion transceiver architecture added a soft switch to bypass the received signal from the antenna. The soft switch connects to the coupler in the predistorter training mode or connects to the LNA in the receiving mode. The power consumption of the added soft switch is not significant since the added switch is in the receiver path.

Comparing to the predistortion architecture in Figure 4.1, our design is much simplified without compromising the performance. The coupler and the switch are analog components and can be easily integrated on board, whereas the conventional predistorter feedback path requires several additional stand-alone chips.

In the conventional predistortion architecture (c.f. Figure 4.1), the transmission path and the feedback path have the same carrier frequency (i.e., they share the same LO1), but the existing transceiver (c.f. Figure 4.2) can have different transmit and receive frequencies

if the transceiver operates at the frequency duplex mode (e.g., in cellular phones). Thus, simply "borrowing" the receiver chain for the purpose of predistorter training may not seem feasible. For example, for the mobile unit, the U.S. cellular band uses 825 - 849 MHz for the mobile transmitter but 869 - 894 MHz for the mobile receiver. During the predistorter training mode, the coupler provides a signal in the 825 - 849 MHz range. This signal cannot be converted to the baseband correctly if the frequency of the local oscillator (LO1) of the receiver still targets the 869 - 894 MHz signal.

Fortunately, the frequency of the local oscillator can be reconfigured and locked to a different frequency because the voltage controlled oscillator (VCO), which may operate over a large frequency range, is often used as the signal generator. The VCO can be tuned to a different frequency [102, 112] that is specified by the phase lock loop (PLL). In the predistorter training mode, we can instruct the PLL to lock the VCO to the same frequency as that used in the VCO of the transmitter (i.e., LO1 and LO3 have the same frequency during predistorter training). This is all done in software and no additional hardware modifications are necessary.

The proposed predistortion transceiver architecture in Figure 4.3 subsumes the functionalities of both Figure 4.1 and Figure 4.2. It is suitable for many wireless communication applications that require a linearized PA, such as cellular phones, cordless phones [16, 17], low power sensor radios [1], 802.11 wireless transmissions [118], etc.

In some applications (e.g., some half duplex systems), the transmit and receive frequencies are the same. In that case, LO1 = LO3 in Figure 4.2 and Figure 4.3, thus switching from the receive mode to the predistortion training mode is even easier.

4.2.4 Sampling Rate Requirement

One may ask whether the ADC1 and ADC2 in the conventional receiver can meet the sampling rate requirement in the predistorter training mode. In the conventional predistortion architecture shown in Figure 4.1, the analog to digital converters (ADC1, ADC2) for the feedback path usually have high sampling rate requirements. This is because the PA output signal can experience K times spectral regrowth if Kth-order ($K = 3, 5, 7, \ldots$) nonlinearity

is present in the PA. Suppose that the PA input signal bandwidth is B_x. If the highest-order nonlinearity in the PA is K, then the PA output signal bandwidth becomes KB_x (assuming K is odd). Therefore, sampling requirements for the ADC1 and ADC2 in Figure 4.1 are generally much higher than those in Figure 4.2 to prevent aliasing in the PA output signal samples. We explain below that this is not an issue for memoryless nonlinear PAs, however.

Consider a memoryless nonlinear device with continuous-time input $x(t)$, continuous-time output $y(t)$, and the relationship

$$y(t) = f(x(t)), \tag{4.1}$$

where $f(\cdot)$ is a memoryless nonlinear mapping from x to y. Denote the samples of $x(t)$ and $y(t)$ by

$$x[n] = x(t) \mid_{t=nT_s}, \tag{4.2}$$

$$y[n] = y(t) \mid_{t=nT_s}, \tag{4.3}$$

respectively, where T_s is the sampling interval and n is an integer. Substituting $t = nT_s$ in (4.1) and utilizing (4.2)-(4.3), we infer that

$$y[n] = f(x[n]). \tag{4.4}$$

Therefore, the same memoryless nonlinear mapping $f(\cdot)$ can be inferred from the discrete time samples $x[n]$ and $y[n]$ as indicated by (4.4). Lower than Nyquist rate sampling is possible, provided that the samples can ensure the identifiability of $f(\cdot)$. Even if $x[n]$ is an aliased version of $x(t)$ and $y[n]$ is an aliased version of $y(t)$, the same $f(\cdot)$ relationship still governs the $x[n]$ and $y[n]$ samples. If $f(\cdot)$ is parameterized by M parameters, then in theory, we can recover $f(\cdot)$ with a minimum of M sets of $\{x[n], y[n]\}$ samples. In reality however, we still would like to use $\gg M$ samples in order to reduce the effects of modeling error and noise.

The proceeding arguments justify that for memoryless predistortion linearization, no special provisions for the ADC1 and ADC2 in Figure 4.3 beyond the usual requirements for the receiver, are necessary.

4.2.5 Special Considerations of Power Savings

Predistortion itself is a relatively simple algorithm that operates in the "DSP & control" block of Figure 4.1 or Figure 4.3. As we have seen, the challenge is in adaptively acquiring new predistorter parameters or LUT entries to account for changes in the PA characteristics.

In order to save power, we can run the predistorter training algorithm infrequently; e.g, once every 30 minutes, or when temperature changes dramatically. Moreover, when the automatic gain control is applied and the PA is not running at the full power mode (has large back-off), we may shut down the predistorter in the DSP since the PA is fairly linear when the back-off is large. The savings in the DSP cycles also reduce the power consumption.

Obviously, with the architecture in Figure 4.3, we cannot both receive signal and update the predistorter. Fortunately, predistorter training only needs to occur once in a while, and the duration of receiving the transmitter signal is very short. Assume that we need to receive 1000 samples which is sampled at 10 MSPS. The duration of receiving the transmitter signal only lasts 0.1 ms, which is tolerable in wireless communication systems. We can also take advantage of the communication idle period to update the predistorter coefficients using a stored predistorter training sequence. Alternatively, we can train and update the predistorter before each new connection as part of the start up procedure.

The objective of PA linearization is to ultimately save power. With predistortion, we will be able to increase the efficiency of the transmit PA. Since the power efficiency $\eta = P_{\mathrm{RF}}/P_{\mathrm{DC}}$, where P_{RF} is the average PA output power and P_{DC} is the power drawn from the DC source (e.g., the battery), for a given η, the savings in P_{DC} is proportional to P_{RF}. Since predistorter training and predistortion itself require DSP resources and consume power as well, adaptive predistortion for very small PAs (say in mW range or less) may not be worthwhile.

4.2.6 Compare to Existing Patents

In [59], the authors proposed a mobile wireless unit architecture that gets feedback from the PA output and allows baseband predistortion. However, it requires a complete down

conversion chain, which adds more cost and power consumption to the mobile wireless unit. A variable amplifier, which could be very expensive, two mixers, one local oscillator (LO), two analog-to-digital converters (ADCs), and one LO phase shifting network is required in this design. While we propose to reuse almost all the components in the existing receiver chain, thus reducing the cost and power consumption of the predistorter. In [59], the authors just gave a feedback path. They did not propose any predistorter schemes to use. While we justify the choice of memoryless (polynomial) predistorter.

In [111], the authors proposed to use LUTs to implement the predistorter gain function. The LUT values are driven by a scaled version of the error signal. It has been known that the LUT based predistorter may take a relatively long time to converge. Moreover, the piece-wise linear curve has a zig-zag appearance which may introduce additional nonlinearities that degrade the linearization performance [54]. We propose a model based approach with memoryless polynomial predistorter that is easy to implement; has no convergence problem and is free of the zig-zag nonlinearities. In [111], the author only implemented gain LUTs. The predistorted signal needs to be calculated with additional multipliers and that might cause numerical instability problem. While we propose to get the predistorter output value directly, not just the gain value. Moreover, in [111], the authors did not consider the timing issue in the feedback loop and they did not consider that the center frequencies of the uplink and the downlink may be different in the mobile wireless unit.

4.3 Digital Predistortion Linearization Algorithm

In this section, we recommend predistortion algorithms that can be used with the proposed architecture in Figure 4.3 to linearize PAs used in wireless devices.

First, we need to decide whether memory nonlinear effects need to be compensated for. Memory effects typically occur in high power amplifiers (HPAs) or for wideband applications (e.g., multicarrier PAs or MCPAs for basestation applications). Since our concern here is the wireless device, the power level is relatively low (typically 0.1 - 4W [1,17,29,46,67,70,103]), so the thermal memory effect is of little concern. Depending on the bandwidth of the transmitted signal (some examples are given in Table 4.1), the frequency dependent memory

effect may (e.g. in WCDMA) or may not (e.g., in AMPS, CDMA) cause concern. Since the wireless device typically only accommodates one user, the signal bandwidth is generally not as wide as in MCPA applications.

Table 4.1: Bandwidth of various communication signals.

Communication Standard	Bandwidth
AMPS	30 kHz
N.A. TDMA	30 kHz
GSM / DCS 1800	200 kHz
IS-95 CDMA	1.25 MHz
3G standard	5 MHz

If the nonlinear PA does exhibit memory effects, the predistorter needs to include nonlinear terms with memory as well. Volterra series is a general nonlinear model with memory [89], which has been used in PA modeling as well as predistorter design [28]. Certain special cases of the Volterra series, for example, the Hammerstein model [23] and the memory polynomial model [25], have been proposed for predistorter design that includes memory effects.

Our experience with low power PAs (2W or less) is that memory predistortion algorithms offer incremental improvements over memoryless predistortion algorithms, but the former require more computational resources. Such performance - cost tradeoff motivates us to focus on memoryless predistortion algorithms for low power devices.

For predistorter training, we advocate the use of the indirect learning architecture [27] as shown in Figure 4.4.

The baseband predistorter input is denoted by $x(t)$, the predistorter output / baseband PA input is denoted by $z(t)$, and the baseband PA output is denoted by $y(t)$. The feedback path labeled "Predistorter Training Branch" (block A) has $y(t)/G$ as its input, where G is the intended gain of the PA, and $\hat{z}(t)$ is its output. The actual predistorter (copy of A) is an exact copy of the predistorter training branch. Since when $y(t) = Gx(t)$, the error $e(t) = z(t) - \hat{z}(t)$ is 0, the predistorter parameters can be found by minimizing $\|e(t)\|^2$. The benefit of the indirect learning architecture is that, instead of assuming a model for the PA, estimating the PA parameters and then constructing its inverse, we can go directly after

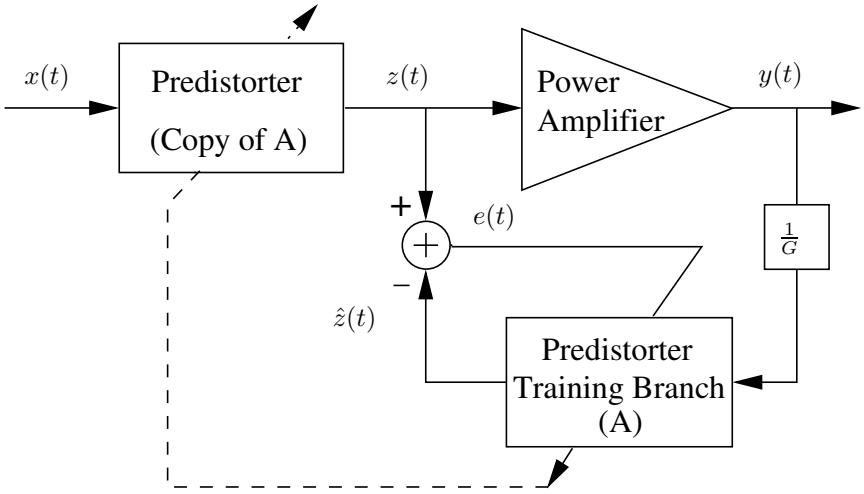

Figure 4.4: The indirect learning architecture. The signals $x(t)$, $y(t)$, $z(t)$, $\hat{z}(t)$ are all baseband equivalent quantities.

the predistorter[1].

We recommend to use the following baseband polynomial model [24] for the predistorter,

$$\hat{z}(t) = \sum_{k=1}^{K} a_k \left| \frac{y(t)}{G} \right|^{k-1} \frac{y(t)}{G}. \tag{4.5}$$

Based on a set of PA input $\{z(t_n)\}_{n=1}^{N}$ and output $\{y(t_n)\}_{n=1}^{N}$ measurements, a least-squares solution can be obtained for the predistorter coefficients, $\mathbf{a} = [a_1, \ldots, a_K]^T$, with $y(t)/G$ as its input, and $z(t)$ as its output. Once the coefficients $\{a_k\}$ are found, they are plugged into the predistorter in the forward branch to generate

$$z(t) = \sum_{k=1}^{K} a_k \ |x(t)|^{k-1} x(t) \tag{4.6}$$

as input to the PA.

This procedure can be repeated; one benefit of the iterations being that more diverse values of $z(t)$ and $y(t)$ are possible and are helpful for obtaining more accurate model parameter estimates. To initialize, $\mathbf{a} = [1\ 0\ \ldots\ 0]^T$ can be used. Such recursive procedure enables the predistorter to linearize even a (slowly) time-varying PA.

To increase the transmission speed, the predistorter can be implemented using LUTs. The LUT entries are calculated from (4.6) and indexed by the amplitude of the input

[1]The term "indirect learning" seems counter-intuitive here, since the predistorter is learned directly; it is the PA characteristics that are learned indirectly.

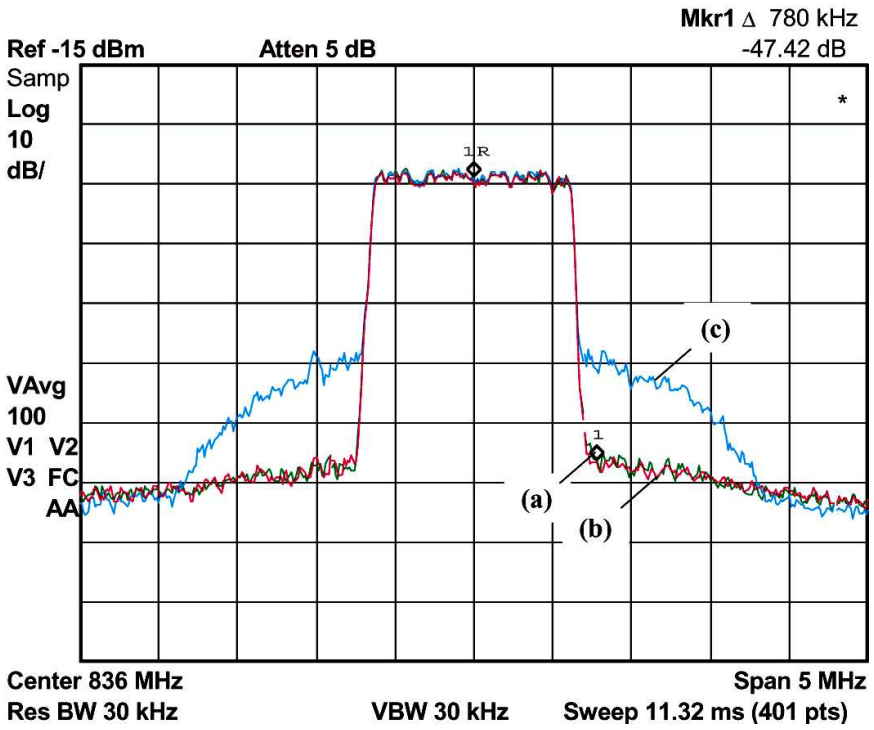

Figure 4.5: The performance of memoryless polynomial predistorters for a handset PA. Line (a): PA output PSD when the predistorter is acquired with the 120 MSPS sampling rate. Line (b): PA output PSD when the predistorter is acquired with the 1.2 MSPS sampling rate. Lines (a) and (b) almost coincide. Line (c): PA output PSD without predistortion.

signal [12].

4.4 Experimental Results

In this section, we show some testbed results to demonstrate the predistortion linearization algorithm discussed in Section 4.3. The baseband signal is first modulated to the IF in the digital domain. A Celerity high-speed digital I/O system is used to generate and process the IF signals at the sampling rate of 120 million samples per second (MSPS). A two stage superheterodyne transceiver architecture converts the signal to the desired RF frequency. The digital predistorter training algorithm and the predistorter itself are implemented in the Celerity system.

In this experiment, the device under test (DUT) is a Siemens CGY0819 handset PA operating at the cellular band (824-849 MHz). The input is a 1.25 MHz bandwidth CDMA

signal centered at 836 MHz. The PA is operated near the 1 dB compression point, so a significant amount of nonlinearity is present. The memoryless polynomial predistorter model (4.6) with highest nonlinear order $K = 5$ is applied to linearize the PA. Predistorter A was trained using 400 $\{y[n], z[n]\}$ measurements sampled at the rate of 120 MSPS. Predistorter B was trained with 400 $\{y[n], z[n]\}$ measurements sampled at the rate of 1.2 MSPS (1/100 of the previous sampling rate and below the Nyquist sampling rate of the input signal). Figure 4.5 shows the PA output power spectral density (PSD) measured by a spectrum analyzer. Line (a) is the PA output PSD when predistorter A is applied. In this case, an ACPR of 47 dB was achieved. Line (b) is the PA output PSD when predistorter B is applied. Lines (a) and (b) almost coincide. For comparison, line (c) is the PA output PSD without predistortion and shows significant amount of spectral regrowth (broadening). Approximately 15 dB of ACPR improvement was achieved with either predistorter.

This experiment demonstrates the effectiveness of the memoryless polynomial predistorter on a handset PA. It also verifies that below Nyquist rate sampling is feasible for memoryless predistortion training and can help to reduce the computational cost.

4.5 Conclusions

In a mobile wireless unit, power efficiency of the transmit power amplifier (PA) is an important design metric since it represents a large portion of the device's power budget. PA linearization is often desired to achieve good efficiency while maintaining good linearity of the PA. In this chapter, we proposed a new adaptive baseband predistortion linearization architecture that is especially suitable for the low cost, low power devices. It re-uses components of the existing receiver to implement the adaptive predistorter training functionality. We suggested a practical memoryless predistortion linearization algorithm and demonstrated its performance on a handset PA using our wireless testbed. We also argued that for the purpose of identifying the memoryless nonlinear PA or its predistorter, it is theoretically justifiable to sample the PA input and output signals below the Nyquist rate. Subsampling offers another mechanism to reduce the computational and power costs of adaptive predistorter training.

CHAPTER V

PEAK-TO-AVERAGE POWER RATIO REDUCTION FOR OFDM USING DYNAMIC SELECTED MAPPING[0]

Orthogonal frequency division multiplexing (OFDM) transmission systems generally have low power efficiency, due to the large peak-to-average power ratio (PAR) of the OFDM signal. Selected mapping (SLM) is a distortionless technique to reduce the PAR of OFDM. A drawback of SLM is its high computational requirement, which hinders its practical implementation. In this chapter, we propose a dynamic SLM method with a two-buffer structure to reduce the computational requirement without sacrificing the PAR reduction capability. Performance analysis of the proposed technique is carried out and computer simulations results are provided to illustrate the concepts.

5.1 Introduction

Orthogonal frequency division multiplexing (OFDM) is a promising technique for high speed data transmission and has been adopted by many standards, such as IEEE 802.11a/g, asymmetric digital subscriber line (ADSL) in the US, and digital audio broadcasting (DAB), digital video broadcasting (DVB), HiperLAN/2 in Europe [41], [33, Sec. 1.2]. However, one serious drawback of OFDM is its large peak-to-average power ratio (PAR), which causes problems when the OFDM signal passes through nonlinear components such as power amplifiers and mixers in the transmitter. When the PAR is high, a large back-off of the PA is needed in order to avoid nonlinear distortions, thus resulting in poor power efficiency. To provide enough dynamic range for the digital signal, a large PAR also demands extra digits, which may lead to extra computations. PAR reduction is often necessary to reduce the cost and improve the power efficiency of the transmission system.

There has been a great deal of research on PAR reduction for OFDM. One can pursue

[0]Protected by U.S. provisional patent [78], March 2005.

PAR reduction algorithms with distortion or without distortion. Deliberate clipping [56], repeated clipping and filtering [55], and companding [109] are simple PAR reduction algorithms with distortion. These methods, however, cause increase in the symbol-error-rate (SER) and/or spectral regrowth. Distortionless PAR reduction algorithms such as selected mapping (SLM) [3], partial transmit sequence (PTS) [62], active constellation extension (ACE) [47], tone injection and tone reservation [99], etc., have appeared in the literature. Among all distortionless PAR reduction techniques, SLM is one of the most promising. SLM chooses one signal representation with the lowest PAR from a set of "equivalent" signal representations which are related in the frequency domain by a series of phase rotations. However, SLM, like other distortionless PAR reduction algorithms, requires additional inverse discrete Fourier Transform (IDFT) computations, which may hinder its practical use in high speed data transmissions.

To reduce the computational requirement of SLM, a simple approximation of the IDFT was proposed in [107], but the price paid is degradation in PAR reduction performance. In this chapter, we propose a dynamic SLM (DSLM) algorithm with a two-buffer structure that can greatly reduce the computational requirement of the SLM method without sacrificing the PAR reduction capability. In addition, the proposed algorithm reduces the amount of side information associated with the SLM algorithm.

This chapter is organized as follows: In Section 5.2, we describe the SLM method and discuss its computational requirement. In Section 5.3, we discuss in detail the proposed DSLM algorithm. In Section 5.4, we point out that the proposed DSLM algorithm is also capable of reducing the side information associated with the SLM algorithm. Section 5.5 concludes this chapter.

5.2 PAR Reduction and SLM

In OFDM, N frequency-domain sub-symbols $\{X_k\}_{k=0}^{N-1}$ are transformed into the time-domain by the inverse discrete Fourier transform (IDFT). If the signal is sampled at the

Nyquist rate, the discrete time-domain OFDM signal $\{x_n\}_{n=0}^{N-1}$ is given by [99]

$$x_n = \frac{1}{\sqrt{N}} \sum_{k=0}^{N-1} X_k \; e^{j(2\pi k/N)n}. \tag{5.1}$$

Denote by PAR_1 the PAR of the original OFDM signal,

$$\mathrm{PAR}_1 = \mathrm{PAR}\{x_n\} = \frac{\max\limits_{0 \le n \le N-1} |x_n|^2}{E[|x_n|^2]}, \tag{5.2}$$

where $E[\cdot]$ denotes statistical expectation. From (5.2), we know that the PAR of the OFDM signal is a random variable.

Assume that $\{X_k\}_{k=0}^{N-1}$ is stationary with variance σ_x^2 and that X_k and X_l are uncorrelated for $k \neq l$. Based on the Central Limit Theorem, $\{x_n\}_{n=0}^{N-1}$ is approximately independently and identically distributed (i.i.d.) complex Gaussian when N is large [99]. The complementary cumulative distribution function (CCDF) of PAR_1; i.e.,the probability that PAR_1 exceeds a certain threshold γ, can be calculated as [3]:

$$Pr\{\mathrm{PAR}_1 > \gamma\} = 1 - (1 - e^{-\gamma})^N. \tag{5.3}$$

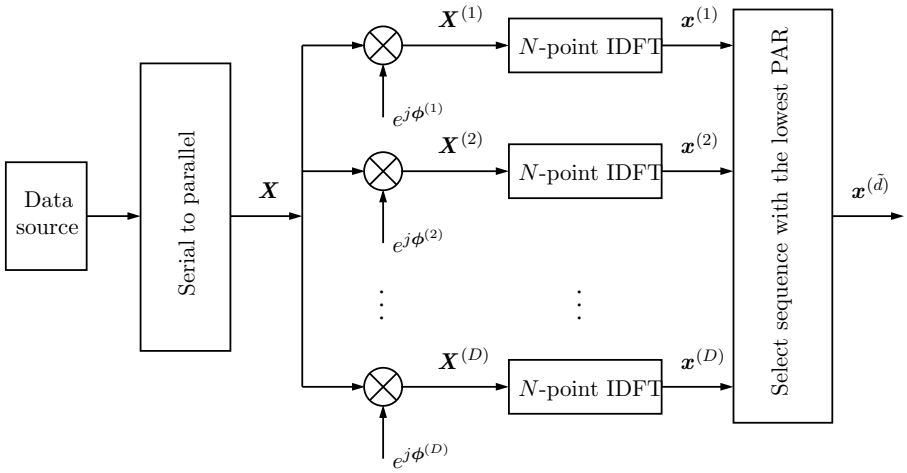

Figure 5.1: The block diagram of SLM method.

SLM was first proposed in [3] to reduce the PAR of the OFDM signal. The block diagram of the SLM method is shown in Figure 5.1. We assume that a random phase table $\{\phi_k^{(d)}\}$, $0 \le k \le N-1$, $1 \le d \le D$, where $\phi_k^{(1)} = 0$, $\forall\ k$, is generated and is available to both the transmitter and the receiver. In SLM, we first rotate the phases of X_k as in

$$X_k^{(d)} = X_k \; e^{j\phi_k^{(d)}}, \tag{5.4}$$

and then take the IDFT to obtain $x_n^{(d)}$. Although $X_k^{(d)}$ and X_k contain the same information, $x_n^{(d)}$ and x_n can have very different PAR values. Among the D equivalent sequences, $x_n^{(\tilde{d})}$, which has the lowest PAR , is selected and transmitted; i.e.,

$$\tilde{d} = \arg\min_{1 \le d \le D} \text{PAR}\{x_n^{(d)}\}. \tag{5.5}$$

We denote the associated lowest PAR value by

$$\text{PAR}_D = \min_{1 \le d \le D} \text{PAR}\{x_n^{(d)}\}. \tag{5.6}$$

With the assumption that the D equivalent sequences are statistically independent, the CCDF of PAR_D is given by [3, 115]

$$Pr\{\text{PAR}_D > \gamma\} = (1 - (1 - e^{-\gamma})^N)^D. \tag{5.7}$$

The concept of SLM and the performance as indicated in (5.7) is quite good. However, there are a few points to consider:

(i) There is a power cost associated with the $D - 1$ extra sets of computations involved in implementing SLM: mostly IDFTs and PAR calculations. It was shown in [4] that the amount of power that can be saved by SLM well exceeds the amount of power required for its implementation.

(ii) The receiver needs to know the optimal phase sequence index $\tilde{d}$ in order to decode. The transmission of the index information also takes bandwidth and power. Blind SLM methods that avoid the transmission of such side information have been investigated; see [38], [10].

(iii) In SLM, a fixed number of D mappings are performed at the transmitter, which consume approximately D times the computational resources as compared to simple OFDM. For simplicity, let us approximate the computational overhead of SLM by the amount of computation needed for the IDFTs. For example, an N-point IDFT can be implemented very efficiently on commercial DSPs which requires a total of $(2N+16)\log_2 N+25$ clock cycles according to [101]. When $D = 16$ and $N = 128$, the required number of DSP clock cycles is 30864, which implies that the sampling rate cannot exceed $128 \times 150 \times 10^6/30864 = 622$ thousand-samples-per-second at a 150 MHz clock rate, and thus the signal bandwidth cannot exceed 311 kHz, which is very limiting for modern communications applications. High

computational complexity caused by the SLM limits the throughput rate of the OFDM system. A larger bandwidth can be accommodated by lowering D, at the cost of less PAR reduction in SLM.

The objective of this chapter is to build upon the SLM framework, devise a PAR reduction method that has similar performance as SLM, but that requires much less computational resources requirement than SLM. In addition, the proposed algorithm reduces the amount of side information needed to code phase sequence indices.

5.3 Dynamic SLM Scheme for PAR Reduction

The basic idea of SLM is to find among D equivalent signal representations, the one that has the lowest PAR, to transmit. Since physical devises (such as ADCs, PAs) have a finite dynamic range, there is a practical limit γ for the PAR. From (5.7), for finite N and D values, there is always a non-zero probability that even after D mappings, SLM will not be able to reach a given PAR reduction threshold, and thus the peak of the OFDM block will have to be clipped. Often times in practice, the goal is to meet a certain threshold on the PAR with a high probability (e.g., 0.9999), therefore, minimizing the PAR for each OFDM block is not necessary. In that spirit, the PAR reduction problem can be stated as: Given a PAR threshold γ and a low probability ϵ, devise an efficient PAR reduction scheme with low computational overhead to ensure $Pr\{\text{PAR} > \gamma\} \leq \epsilon$.

For a given OFDM sequence $\{X_k\}$, each mapping used in the SLM algorithm can be regarded as a Bernoulli trial; the probability of "success", i.e., reducing the PAR of the mapped sequence to below the threshold γ in each trial is $(1 - e^{-\gamma})^N$ (c.f. (5.3)). Denote by Z the random variable corresponding to the first successful trial that realizes the goal PAR $< \gamma$. Clearly, Z has a Geometric distribution; i.e.,

$$Pr\{Z = d\} = a(1-a)^{d-1}, \tag{5.8}$$

where

$$a = (1 - e^{-\gamma})^N, \tag{5.9}$$

and $d = 1, 2, \ldots$.

Let us consider an example, where $N = 128$ and $\gamma = 7$ dB (i.e., $\gamma = 5.012$). We find from (5.7) that $Pr\{\text{PAR}_1 \leq \gamma\} = 0.4252$, $Pr\{\text{PAR}_2 \leq \gamma\} = 0.6696$, ... , $Pr\{\text{PAR}_{16} \leq \gamma\} = 0.9999$. Base on the above calculations, we know that there is a 43% chance that a given OFDM block already has a low enough PAR and thus PAR reduction is not necessary. There is a 67% chance that SLM with $D = 2$ is sufficient in meeting the PAR goal. If we want $Pr\{\text{PAR}_D > \gamma\} \leq 10^{-4}$ in the above example, the required D is 16. However, as we have seen, $D = 16$ mappings are not necessary for all of the OFDM blocks. In fact, the average number of mappings needed to achieve the first successful trial that realizes the goal PAR $< \gamma$ can be calculated as follows [4]

$$E[Z] = \sum_{d=1}^{\infty} d \times a \times (1-a)^{d-1} = \frac{1}{a} = \frac{1}{(1-e^{-\gamma})^N}. \tag{5.10}$$

For $N = 128$, we infer from (5.10) that $E[Z] = 2.35$ mappings are required on average to satisfy PAR ≤ 7 dB.

A simple, modified SLM algorithm can be considered: If a given OFDM block has $\text{PAR}_1 \leq \gamma$, transmit it as is; otherwise, try an increasing number of mappings until $\text{PAR}_d \leq \gamma$ is realized. If after the maximum allowed D number of mappings, PAR_D is still $> \gamma$, stop trying and transmit the signal representation with the lowest PAR. This method reduces the computational load, but causes a delay jitter (variable latency) problem that is undesirable.

Our goal in this chapter is to improve upon SLM, to reduce the computational demand without introducing delay jitter and without sacrificing the PAR reduction performance. We shall achieve this by employing input and output buffers and a dynamic SLM mechanism.

5.3.1 Queuing Model of DSLM

A DSLM scheme with two buffers is shown in Figure 5.2. The input buffer contains OFDM blocks to be processed (for PAR reduction). The output buffer contains OFDM blocks that have been processed and are ready to be transmitted. In the SLM processing unit, the task is to successively try new mappings until a representation with a PAR that is less than γ is found. This processed OFDM block will then be transferred to the output buffer. If the input buffer is not empty, the next available OFDM block in the input buffer will be retrieved by the SLM processing unit.

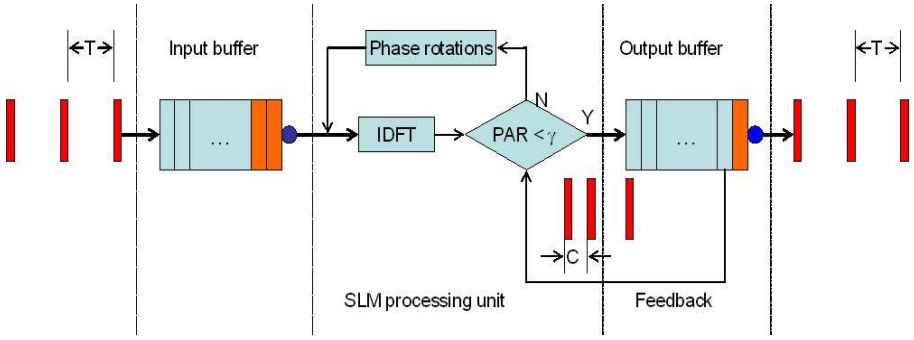

Figure 5.2: Queuing model for the proposed dynamic SLM scheme.

Assuming the input buffer and the output buffer are infinitely long (the phase table size is also infinity), we can reduce the PAR of the OFDM signal with N sub-symbols below the threshold γ with probability 1. The average number of mappings needed for each OFDM block is given by $1/(1-e^{-\gamma})^N$ as in (5.10).

The infinite buffer length assumption, however, is not suitable for practical transmission since the time interval between adjacent OFDM blocks and the total throughput delay cannot be infinite. We consider a DSLM model with finite buffer length. Let us denote by T the OFDM block arrival interval at the input buffer. Denote by C the processing time needed for one mapping (phase rotations, IDFT, and PAR calculation). Denote by M the input and the output buffer size. Set the total number of OFDM blocks in the two buffers and in the SLM processing unit is M. Then $M \times T$ is the total amount of delay between an OFDM block's arrival at the input buffer and its departure from the output buffer. For ease of discussion, we assume that $L = T/C$ is an integer.

To describe the queuing behavior of the input and output buffers, we introduce the following notations: $t_h = (hT)$, $t_h^- = (hT) - \delta$, $t_h^+ = (hT) + \delta$, where δ is a positive but infinitesimally small number. t_h^- and t_h^+ stand for the time instants immediately before and after t_h, respectively. We assume that at t_h^+, one OFDM block arrives at the input buffer and one OFDM block departs from the output buffer. If one OFDM block is retrieved by the SLM processing unit from the input buffer at t_h^+, and d phase rotations are carried out for PAR reduction, then this block will arrive at the output buffer at time instant $(t_h + dC)^-$. The queue lengths of both buffers are measured at time instants t_h, $h = 1, 2, \ldots$.

The arrival process at the input buffer is a deterministic process with a fixed interval T, which is equal to the symbol period. The service time of the SLM processing unit is the time it takes to find a qualified representation to meet the PAR threshold. The departure process of the input buffer and the arrival process of the output buffer have the same statistical behavior; their rates are determined by the number of mappings needed to meet the PAR threshold. To avoid any delay jitter, it is necessary to require that the departure process at the output buffer be a deterministic process with the same fixed interval T as well. This fixed departure rate requires that the output buffer cannot be empty at any time instant $t_h, h = 1, 2, \ldots$.

There are three modes for this DSLM model. In general, the SLM processing unit tries different mappings until one mapping has a PAR that is less than γ. The resulting OFDM block is then fed into the output buffer. However, the output buffer may underflow when there is only one OFDM block in the output buffer and the SLM processing unit cannot find a successful trial at the time when the OFDM block in the output buffer departs. To avoid delay jitter in the departure process of the output buffer, a feedback path from the output buffer to the SLM processing unit is added. When the output buffer underflow occurs, the selection in the SLM processing unit is terminated. From all existing candidates, the OFDM block with the lowest PAR is selected, even though its PAR is higher than γ, and is fed into the output buffer. The third possible mode occurs when the input buffer underflow. Assume that the output buffer contains $M - 1$ OFDM blocks and the SLM processing unit finds a successful trial before one OFDM block in the output buffer departs. At this time, the input buffer is empty since the next incoming OFDM block has not arrived yet. The SLM processing unit idles until one OFDM block arrives at the input buffer.

5.3.2 PAR Performance Analysis of DSLM

As in SLM, DSLM can only guarantee that the resulting PAR is smaller than γ with a certain probability. When the output buffer underflows and feedback is called for, DSLM fails to reduce PAR to be lower than γ. To analyze the PAR performance of the DSLM, we introduce a Markov model. Assume that the OFDM blocks are mutually independent

and that the phase rotation sequences are mutually independent. The state of the Markov model is chosen to be the queue length of the output buffer at time instant t_h, $h = 1, 2, \ldots$.

During one sample interval T, L mappings can be performed. Denote by random variable Y the number of OFDM blocks that can be processed by the SLM processing unit in the hth sample interval between time instants t_h and t_{h+1}. Then Y is the number of successes in L trials, which is Binomial distributed if there is no underflow in either the output buffer or the input buffer:

$$Pr\{Y = y\} = B_a(y|L) = \binom{L}{y}(1-a)^{L-y}\ a^y, \tag{5.11}$$

for $y = 0, 1, 2, ..., L$.

Denote by random variable S the queue length of the output buffer at time instant t_h. Therefore, the number of OFDM blocks in the input buffer and the SLM processing unit is $M - S$ at time instant t_h. Because one new OFDM block arrives at the input buffer at time instant t_h^+, $M - S + 1$ is the upper bound for Y. If $M - S + 1 \geq L$, the probability mass function of Y is also given by (5.11). On the other hand, if $M - S + 1 < L$, the probability mass function of Y is:

$$Pr\{Y = y\} = \begin{cases} B_a(y|L), & \text{if } y = 0, 1, \ldots, M-S, \\ \sum_{i=y}^{L} B_a(i|L), & \text{if } y = M - S + 1. \end{cases} \tag{5.12}$$

The output buffer underflows when $Y = 0$ happens S times consecutively. If at time instant t_h, there is only one OFDM block left in the output buffer ($S = 1$), and the SLM algorithm cannot find a suitable mapping to reduce the PAR to γ for the given data between time instants t_h and t_{h+1}, the SLM processing unit will be forced to produce an output to be pushed to the output buffer at t_{h+1}^- even though its PAR is higher than γ. For the case with $S = 1$ and $M \geq L$, the probability mass function of Y including the feedback is:

$$Pr\{Y = y\} = \begin{cases} B_a(0|L) + B_a(1|L), & \text{if } y = 1, \\ B_a(y|L), & \text{if } 2 \leq y \leq L. \end{cases} \tag{5.13}$$

For the case with $S = 1$ and $M < L$, the probability mass function of Y including the

feedback is:

$$Pr\{Y=y\}=\begin{cases} B_a(0|L)+B_a(1|L), & \text{if } y=1, \\ B_a(y|L), & \text{if } 2\le y\le M-1, \\ \sum_{i=y}^{L} B_a(i|L), & \text{if } y=M. \end{cases} \tag{5.14}$$

For the case with $S>1$, (5.11) holds for $M-S+1\ge L$, and (5.12) holds for $M-S+1<L$.

Denote by $R(\gamma)$ the probability that the DSLM fails to reduce PAR to be lower than γ. The failure only happens when $S=1$ at t_h and the Bernoulli trial fails L times between time instants t_h and t_{h+1}. Therefore, we have

$$R(\gamma)=Pr\{\text{PAR}>\gamma\}=Pr\{S=1\}B_a(0|L). \tag{5.15}$$

For given L and M values, $R(\gamma)$ is proportional to $Pr\{S=1\}$, the probability that there is only one OFDM block in the output buffer at time instant t_h.

The state transition matrix of this Markov model can be written as

$$\mathbf{P}=[P_{il}]_{M\times M}, \tag{5.16}$$

where P_{il} is the probability that $S=i$ at time instant t_{h+1} conditioned on $S=l$ at time instant t_h. That means $Y=i-l+1$ OFDM blocks arrive at the output buffer and one OFDM block departs from the output buffer between time instants t_h and t_{h+1}.

Due to the feedback from the output buffer to the input buffer, $P_{11}=B_a(0|L)+B_a(1|L)$, which is $Pr\{Y=1\}$ in (5.13). If $M-L+1\le l\le M$, the input buffer has a certain probability to underflow, so that $P_{Ml}=\sum_{y=M-l+1}^{L} B_a(y|L)$, which is $Pr\{y=M-S+1\}$ in (5.12). For the case without feedback and underflow, $P_{il}=B_a(i-l+1|L)$, which is $Pr\{Y=y\}$ in (5.11). In summary, the value of P_{il} can be expressed as:

$$P_{il}=\begin{cases} \sum_{y=0}^{2-l} B_a(y|L), & i=1, \text{ and } 1\le l\le 2, \\ B_a(i-l+1|L), & 2\le i\le M-1, \text{and} \\ & \max(1,i+1-L)\le l\le i+1, \\ \sum_{y=M-l+1}^{L} B_a(y|L), & i=M, \text{and} \\ & \max(1,M-L+1)\le l\le M, \\ 0, & \text{otherwise.} \end{cases} \tag{5.17}$$

By definition, the Markov chain described by (5.17) is irreducible and aperiodic with finite state, which guarantees ergodicity of the Markov chain. By Ergodicity Theorem [19], a unique steady state distribution exists, independent of the initial state.

Denote $\boldsymbol{\pi} = [\pi_1, \pi_2, \ldots, \pi_M]^T$ the steady state vector of the Markov chain, and $\sum_{k=1}^{M} \pi_k = 1$. The element π_i represents the probability that i blocks are in the output buffer at time t_h. $\boldsymbol{\pi}$ is the eigen vector of the probability transition matrix $\mathbf{P}$ corresponding to the eigen value 1. Then the probability that PAR $> \gamma$ is given by

$$R(\gamma) = \pi_1 B_a(0|L), \tag{5.18}$$

which happens when the SLM algorithm fails to reduce the PAR to below γ between time instants t_h and t_{h+1} for $S=1$.

SLM can be viewed as a special case of DSLM with $L = D$ and $M = 1$, for which $\pi_1 = 1$. Therefore, (5.18) reduces to

$$R(\gamma) = 1 \times B_a(0|L) = (1-a)^D, \tag{5.19}$$

which agrees with (5.7).

5.3.3 Example

In this example, we assume that the OFDM signal has $N = 128$ sub-carriers, the information symbol is randomly picked from a QPSK signal constellation $X_k \in \{\sigma_x e^{\pm j\pi/4}, \sigma_x e^{\pm j3\pi/4}\}$, and we assume the dynamic SLM uses $L = 4$, and $M = 5$. The corresponding Markov model has 5 states. The state diagram is shown in Figure 5.3 and the transition probability matrix is:

$$\mathbf{P} = \begin{bmatrix} \sum_{i=0}^{1} B_a(i|4) & B_a(0|4) & 0 & 0 & 0 \\ B_a(2|4) & B_a(1|4) & B_a(0|4) & 0 & 0 \\ B_a(3|4) & B_a(2|4) & B_a(1|4) & B_a(0|4) & 0 \\ B_a(4|4) & B_a(3|4) & B_a(2|4) & B_a(1|4) & B_a(0|4) \\ 0 & B_a(4|4) & \sum_{i=3}^{4} B_a(i|4) & \sum_{i=2}^{4} B_a(i|4) & \sum_{i=1}^{4} B_a(i|4) \end{bmatrix}. \tag{5.20}$$

The closed form expression of the steady state vector $\boldsymbol{\pi}$ is not straightforward to obtain. The steady state vector $\boldsymbol{\pi}$ can be solved numerically by substituting N and γ into (5.20) and setting $\mathbf{P}\boldsymbol{\pi} = \boldsymbol{\pi}$.

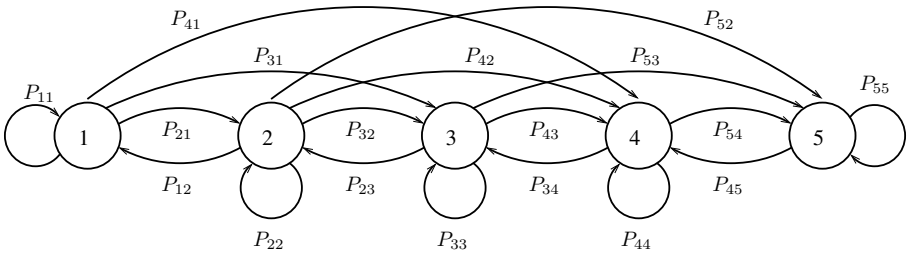

Figure 5.3: State diagram for the Markov Chain.

We tried to verify the theoretical result with 10^6 OFDM blocks for each marked point in Figure 5.4. Figure 5.4 shows the theoretical $R(\gamma)$ as a solid line for $L = 4$, $M = 5$ as well as the empirical $R(\gamma)$ values as marked points. For comparison, the CCDFs of the PAR using conventional SLM (c.f. (5.7)) with $D = 1,\ 4,\ 16,\ 20$, are also included. In Figure 5.4, we observe that the dynamic SLM scheme with $L = 4$, $M = 5$ outperformed the SLM method with $D = 4$ (note that they have the same computational requirement). On the other hand, the dynamic SLM scheme did not outperform the SLM method with $D = 20$, which has 5 times the computational load as compared to the dynamic SLM scheme. In general, the performance of SLM with $D = L$ and the performance of SLM with $D = LM$ form respectively, an upper bound and a lower bound for the dynamic SLM algorithm. The reason is that the number of mapping choices for each OFDM block in the dynamic SLM scheme is lower bounded by L (when underflow of the input buffer happens) or upper bounded by LM (when the output buffer is originally full but causes underflow in the end). In Figure 5.4, we also observe that for low PAR thresholds, the performance of the dynamic SLM scheme with $L = 4$, $M = 5$ is close to that of the SLM with $D = 4$. From (5.10), we know that when the PAR threshold γ is low, the average number of mappings required to obtain the first PAR that satisfies PAR $< \gamma$ becomes large. Within a fixed time interval LT, the SLM processing unit may not succeed in finding a suitable mapping. The queue of the output buffer is likely to be empty and the dynamic SLM tends to behave like SLM with $D = L$. Similarly, when the PAR threshold γ is high, the average number of mappings required to obtain the first PAR that satisfies PAR $< \gamma$ becomes small. The queue of the output buffer is likely to be full and the dynamic SLM tends to behave like SLM with $D = LM$.

At the 10^{-4} probability level, the DSLM algorithm with $L = 4$, $M = 5$ reduces the PAR to 7 dB. The PAR reduction capability is about the same at the SLM algorithm with $D = 16$. In this example, the result shows that the proposed DSLM algorithm reduces the computational load required for each OFDM block. When considering the computational load, approximately $E[Z]$ mappings are required on average for dynamic SLM. In comparison, a total of $D = LM$ mappings are required for SLM. In this example, the DSLM with $L = 4$, $M = 5$ produces the same PAR reduction as the SLM with $D = 16$. However, the average computational load for DSLM is only 2.35 (computed from B.10), which is only $2.35/16 = 15\%$ of that for SLM. Moreover, with DSLM, the throughput rate of the OFDM system is $\frac{1}{LT}$, which is 3 times faster than the throughput rate of the OFDM system when SLM with $D = 16$ is used.

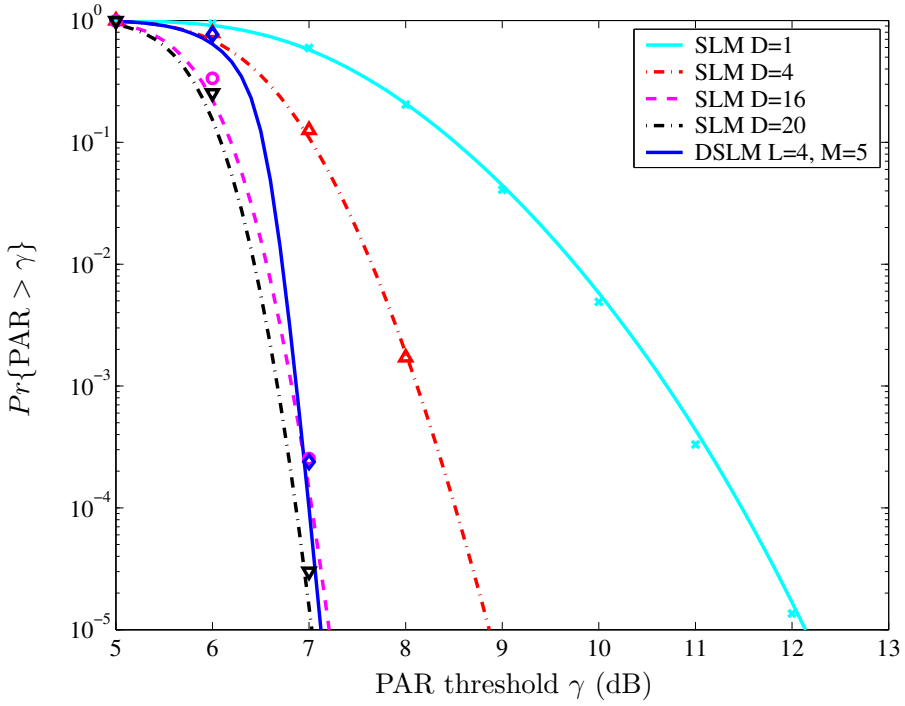

Figure 5.4: CCDFs of the PAR of the OFDM signals using SLM or DSLM. $N = 128$. At the 10^{-2} probability level, from right to left: SLM $D = 1$, SLM $D = 4$, DSLM $L = 4$, $M = 5$, SLM $D = 16$, SLM $D = 20$.

We recommend the following guidelines for selecting L and M for dynamic SLM. First, determine the PAR requirement (threshold) at a given probability level. Next, calculate $E[Z]$ using (5.10); L should be larger than $E[Z]$. Finally, determine the total number

of mappings D needed for SLM to achieve the PAR requirement and choose M such that $LM \geq D$. Fine tune L and M in the end if necessary. In general, to improve the throughput rate of the OFDM system, we pick L to be the smallest integer that is larger than $E[Z]$. At low probability levels, the performance of dynamic SLM is close to the lower bound. We pick M to be the smallest integer that satisfies $LM \geq D$.

5.3.4 DSLM for Band Limited OFDM

Our discussion about SLM and DSLM is based on the assumption that the OFDM signal is Nyquist-rate sampled. In specific applications, the OFDM signal may be upsampled filtered, which may impact the PAR of the signal [82]. Nevertheless, the SLM or the DSLM may still work under this circumstance. We may still rotate the phase of the OFDM subsymbols, apply filtering or upsampling, convert the signal to time-domain, compare the PAR of different equivalent sequences, then select one that has the lowest PAR to transmit.

We illustrate the effectiveness of the SLM and DSLM using a simulation example. In this example, we assume that $N = 128$ and the upsampling rate is $U = 8$. Every point was simulated using 10^7 blocks of OFDM signal. In Figure 5.5, we show the failure rate of the DSLM at different threshold level (solid line). For comparison, the CCDFs of the PAR for the upsampled OFDM signal using SLM with $D = 1,\ 12,\ 82,\ 156$, are also included. In this figure, we observed that statistically, upsampled OFDM has larger PAR than the Nyquist-rate sampled OFDM. SLM can still effectively reduce PAR. In order to reduce the PAR to a target threshold 7 dB with probability $1 - 10^{-4}$, a total of $D = 82$ mappings is needed. While the DSLM algorithm with $L = 12$, $M = 13$ gives similar performance. In this simulation, DSLM requires average number mappings of 9.32, which is $(80-9.32)/80 = 88\%$ less than that in the SLM. The throughput rate of the DSLM is $1/15C$, which is $80/15 = 5.3$ times faster than that in the SLM.

5.4 Side Information Reduction of DSLM

In SLM, the optimal phase sequence index as the side information, needs to be transmitted to the receiver. DSLM can help to reduce the amount of side information. In SLM, the optimal phase sequence is chosen to be the one that gives the lowest PAR among all D

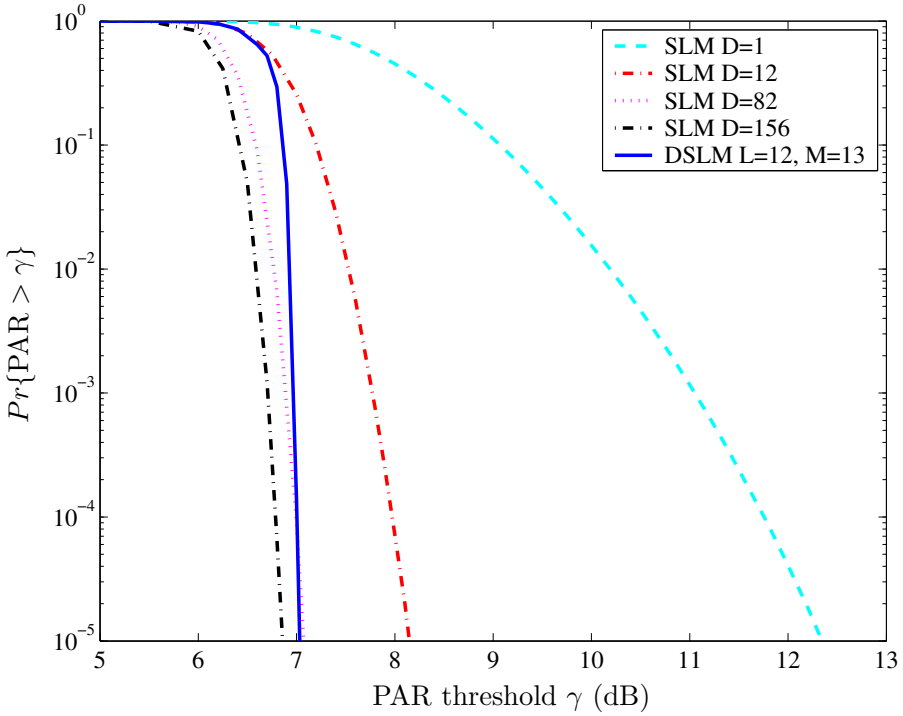

Figure 5.5: CCDFs of the PAR of the upsampled OFDM signals using SLM or DSLM. $N = 128$, $U = 8$. At the 10^{-2} probability level, from right to left: SLM $D = 1$, SLM $D = 12$, DSLM $L = 12$, $M = 13$, SLM $D = 82$, SLM $D = 156$.

representations. All D representations have equal probability. The total information, or the entropy that exists in the index, is $-\sum_{i=1}^{D} p_i \log_2 p_i = \log_2 D$ [20], where p_i is the probability that index $I = i$ is chosen.

In DSLM, in order to achieve the same PAR reduction performance, the size of phase table generally is slightly larger than that in SLM. However, the information contained in the index may be smaller than that in the SLM case. DSLM tests the phase table sequentially and stops at the phase sequence that reduces PAR to below a given threshold. The probability of occurrence of one index may be different from another. Considering as an example, when $N = 128$ and $\gamma = 7$ dB, we apply a DSLM algorithm with infinite buffer length. There is a 43% chance that a given OFDM block already has a low enough PAR and thus PAR reduction is not necessary. The probability of choosing the first row of the phase table is 43%. Similarly, The probability of choosing the second row of the phase table is 24%, etc. The larger index is less likely to be chosen. With the prior knowledge of the probability distribution of the index, we can compute the entropy of the index of DSLM. If

the DSLM algorithm has infinite buffer length, the probability that index $I = i$ is chosen can be computed as $p_i = a(1-a)^{i-1}$, where a is defined in (5.9). The entropy of the index is given by

$$\begin{aligned} H_\infty(I) &= -\sum_{i=1}^{\infty} p_i \log_2 p_i \\ &= -\sum_{i=1}^{\infty} a(1-a)^{i-1} \log_2(a(1-a)^{i-1}) \\ &= -\log_2 a - \frac{1-a}{a} \log_2(1-a). \end{aligned} \tag{5.21}$$

In the above example, $a = (1-e^{-\gamma})^N = 0.4252$. From (5.21), we know that the entropy of the index is 2.3136.

For DSLM with finite buffer length, the probability that index i is chosen is not simply $p_i = a(1-a)^{i-1}$. In Appendix B, we analyze in detail the probability distribution of the occurrence of index i, p_i. Moreover, we show in Appendix C that (5.21) is an upper bound for any DSLM with the same parameter a.

With the prior probability knowledge of p_i, the entropy of the index is given by

$$H_{L,M}(I) = -\sum_{i=1}^{LM} p_i \log_2 p_i. \tag{5.22}$$

Example. Substituting $N = 128$, $\gamma = 7$ dB, $L = 4$, and $M = 5$ into (B.5), the steady state vector is obtained by solving $\mathbf{P}\boldsymbol{\pi} = \boldsymbol{\pi}$. The steady state vector is given in Table 5.1.

Table 5.1: Steady state vector for the DSLM with $N = 128$, $\gamma = 7$ dB, $L = 4$, and $M = 5$.

State	Probability	State	Probability
4	0.000174	13	0.004790
5	0.000129	14	0.007350
6	0.000224	15	0.011290
7	0.000389	16	0.017334
8	0.000549	17	0.026615
9	0.000860	18	0.040867
10	0.001330	19	0.062748
11	0.002026	20	0.820206
12	0.003119		

Substituting the steady state vector into (B.8), we obtain the probability p_i of occurrence of each index $I = i$, as shown in Table 5.2. With Haffman coding, we obtain an optimal

Table 5.2: Probability of occurrence of each index.

Index (i)	Probability (p_i)	Codeword length	Index (i)	Probability (p_i)	Codeword length
1	0.425229	1	11	0.001672	11
2	0.244409	2	12	0.000960	12
3	0.140479	3	13	0.000552	13
4	0.080763	4	14	0.000317	14
5	0.046409	5	15	0.000182	15
6	0.026675	6	16	0.000104	16
7	0.015332	7	17	0.000060	17
8	0.008811	8	18	0.000034	18
9	0.005064	9	19	0.000019	19
10	0.002910	10	20	0.000022	19

(shortest expected codeword length) prefix code [20]. The codeword length for each indices is also listed in Table 5.2. The expected codeword length is 2.3514 bits, which is about 41% shorter than the codeword length of 4 bits in SLM with $D = 16$.

5.5 Conclusions

PAR reduction is often necessary in order to improve the power efficiency of an OFDM system. SLM is one of the most promising PAR reduction methods. However, it requires a large computation which hinders its use in high-speed data transmissions. In this chapter, we proposed a two-buffer, dynamic SLM scheme to reduce the computational requirement of SLM. Once the prescribed PAR threshold is met, the algorithm stops striving for lower PAR values. The number of mappings to try by the SLM processing unit is dynamically assigned. The proposed algorithm reduces the computational requirement without sacrificing the PAR reduction capability and without creating any throughput jitter. The proposed algorithm also increases the throughput rate of the OFDM system and reduces the amount of side information.

CHAPTER VI

LOW COMPLEXITY CREST FACTOR REDUCTION FOR FORWARD LINK CDMA USING IQ OFFSET[0]

Forward link code division multiple access (CDMA) signals generally have large crest factors, giving rise to low power efficiency of the transmission system. Crest factor reduction (CFR) for forward link CDMA is called for to improve the system power efficiency. In this chapter, we propose a CFR algorithm that reduces the probability of simultaneous occurrences of high peaks between the in-phase and the quadrature branches. Comparing with existing CFR approaches, our algorithm is distortionless, offers good CFR capability with very little modification to the existing system and has low computational complexity. Simulation results are provided to demonstrate the performance of the proposed CFR technique.

6.1 Introduction

Code division multiple access (CDMA) [97, 98] is a widely employed technique in modern wireless communication systems. In the forward link (base station to mobile unit) CDMA system, the signal envelope exhibits large variations due to the superposition of different channels as well as the baseband filtering [50, 51, 53]. Peak-to-average power ratio (PAR), or crest factor (which is the square root of the PAR) [42], has been used to quantify the variability of a signal. Since crest factor and PAR have the same value in dB, we do not distinguish the two in this chapter. A large crest factor signal presents the following challenges: (i) extra bits are generally required to represent the signal in digital form; (ii) the RF portion of the transmitter has to be oversized to handle the occasional large peaks; (iii) DC to RF power efficiency decreases and equipment cost increases when high PAR signals are transmitted. Therefore, crest factor reduction (CFR) is often necessary.

Many CFR techniques have been proposed in the literature. Most published results deal

[0]Protected by U.S. provisional patent [80], June 2005.

with orthogonal frequency division multiplexing (OFDM) signals [99]. In comparison, the body of literature on CFR for CDMA signals is rather small. CFR algorithms with distortion, such as clipping [104], windowing [104], repeated filtering and clipping [18] generally require less computation. However, the distortion introduced by these CFR algorithms can cause serious system performance degradations in terms of bit error rate (BER) and spectral regrowth. For distortionless CFR, a Walsh code selection algorithm [50, 51, 91] was proposed to reduce the crest factor with the assumption that only some of the channels are active at any given time. Based on the same assumption, a CFR algorithm was proposed in [105] by adding a signal that is orthogonal to all the active channel codes. In [53], the authors proposed to reduce the crest factor of the forward link CDMA signal by changing the signs of half of the Walsh codes (except for the pilot channel and the paging channel) in one branch of the quadrature modulation. These distortionless CFR algorithms all require more computation than the CFR techniques with distortion.

In this chapter, we propose a new CFR algorithm for the forward link CDMA system by introducing a relative offset between the in-phase (I) branch and the quadrature (Q) branch. Note that the concept of IQ offset has been exploited in the CDMA *reverse* link (mobile unit to base station) for the purpose of avoiding zero-crossing of the QPSK constellation. The so-called offset QPSK (OQPSK) is employed and the relative delay between the I and Q branches is 1/2 chip. However, in our research, we are interested in the *forward* link (not the reverse link) of the CDMA system; we tackle the CFR problem (not the zero-crossing problem); and we consider more general IQ offset scenarios (not just a 1/2 chip delay).

This chapter is organized as follows: In Section 6.2, we describe the forward link CDMA signal and its crest factor. In Section 6.3, we develop the CFR algorithm and provide a theoretical analysis. Simulation and comparison results are provided in Section 6.4. Finally, conclusions are drawn in Section 6.5.

6.2 System Setup

Figure 6.1 shows a block diagram of the forward link CDMA system [97], where a total number of K ($1 \leq K \leq 64$) channels can be active at any given time. In Figure 6.1, we

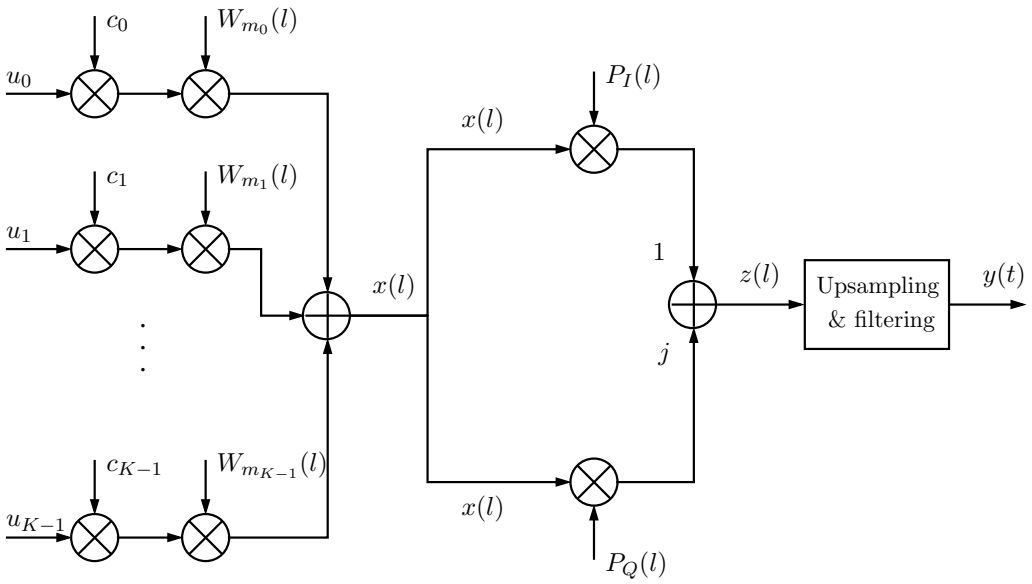

Figure 6.1: IS-95 CDMA forward link schematic for a given symbol period.

denote by u_k the kth user's data over the given symbol period, by c_k the corresponding power control coefficient, and by $W_{m_k}(l)$ the m_kth spreading code ($m_k = 0, 1, \ldots, 63$), which is the $(m_k + 1)$th column of the 64×64 Walsh-Hadamard matrix. The chip index $1 \leq l \leq L$; $L = 64$ is the number of chips contained in one CDMA symbol. For each user, the source data are encoded, interleaved, scrambled, and then mapped from unipolar to bipolar. The resulting u_k is randomized and can be modeled as a binary phase shift keying (BPSK) signal; thus, u_k has zero mean. We further assume that different user data are mutually independent; i.e., u_k and $u_{k'}$ are mutually independent, $\forall\ k \neq k'$. Without loss of generality, we assume that $\sum_{k=0}^{K-1} |c_k|^2 = 1$, where $|c_k|^2$ is the fraction of the total power that is allocated to the kth channel. Each u_k is spread into $L = 64$ chips; the resulting user data are then added together using the Walsh-Hadamard matrix. The lth chip of the given forward link CDMA symbol can be written as:

$$x(l) = \sum_{k=0}^{K-1} u_k\ c_k\ W_{m_k}(l). \tag{6.1}$$

The summation (over k) of the Walsh coded multichannel symbols contributes to the high crest factor encountered in the forward link CDMA signal. The above $x(l)$ is then duplicated into the I and Q branches and multiplied with the corresponding short PN sequences $P_I(l)$ and $P_Q(l)$ consisting of pseudo-random ± 1's generated by 15th-order characteristic

polynomials described in [97] [52, pp. 616]. In Figure 6.1, the forward link CDMA signal before the upsampling and pulse shaping filtering block can be written as:

$$z(l) \quad = \quad x(l)\ \big(P_I(l) + jP_Q(l)\big), \tag{6.2}$$

where $j = \sqrt{-1}$. We emphasize that because u_k is BPSK, $x(l)$ in (6.1) is real-valued. Afterwards, $z(l)$ is up-sampled and pulse shaped to yield the baseband signal $y(t)$.

To quantify the crest factor, let us first define the instantaneous-to-average power ratio (IAR) [52]

$$\text{IAR} = \frac{P(t)}{P_{av}}, \tag{6.3}$$

where $P(t)$ is the instantaneous power of a signal and P_{av} is its average power. Since IAR is a random variable, its probabilistic distribution is of interest.

In this chapter, we define the crest factor as the value γ corresponding to[1]

$$\Pr(\text{IAR} > \gamma) = 10^{-4}. \tag{6.4}$$

The objective of CFR is to reduce the γ defined above.

6.3 IQ offset in IS-95 forward link

From Figure 6.1, we see that the same $x(l)$ is applied to the I branch and the Q branch of the IS-95 forward link CDMA system. Such "coherence" between the I and Q branch data can lead to a large crest factor in $z(l)$ since peaks occur at the same time in both branches and thus add constructively.

Intuitively, if we can weaken the correlation between the I and Q branch data, we may be able to reduce the crest factor. For the CDMA forward link, the authors of [53] proposed to change the signs of the odd-numbered Walsh indices when generating the Q branch signal. When the number of active channels modulated by the odd-numbered Walsh indices is roughly half of the total number of active channels, correlation between the I and Q branches can be reduced using the method of [53].

[1]The complementary cumulative density function (CCDF) level of 10^{-4} is often used to assess CFR algorithm performances although other levels such as 10^{-3}, 10^{-5}, etc. can also be used.

In this chapter, we propose to introduce a timing offset between the I and Q branch data in order to reduce their correlation. The delay element can be placed in either the I branch or the Q branch. Without loss of generality, we place the timing offset unit D in the Q branch as shown in Figure 6.2.

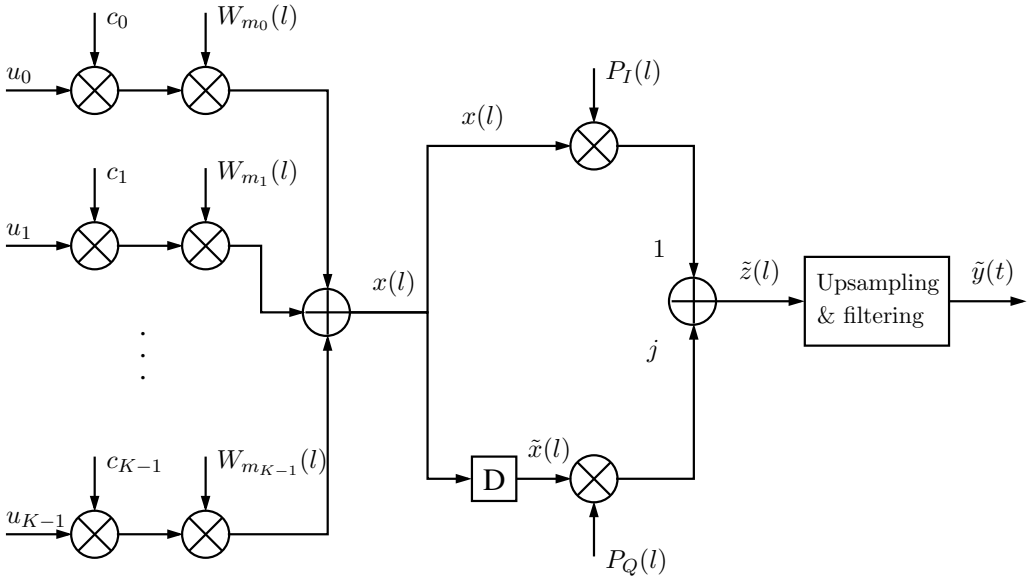

Figure 6.2: Modified IS-95 CDMA forward link structure for a given symbol period.

Next, we will examine the autocorrelation property of $x(l)$ within the symbol period.

6.3.1 Autocorrelation Analysis

Since $x(l)$ of (6.1) has zero mean, the autocorrelation function of $x(l)$ at lag d is given by

$$\begin{aligned} C_{2x}(d) &= E[x^*(l)x(l+d)] \\ &= \sum_{k=0}^{K-1}\sum_{k'=0}^{K-1} E[u_k^*\ c_k^*\ W_{m_k}^*(l)\ u_{k'}\ c_{k'}\ W_{m_{k'}}(l+d)] \\ &= \sum_{k=0}^{K-1}\sum_{k'=0}^{K-1} c_k^* c_{k'}\ E[u_k^* u_{k'}]\ E[W_{m_k}^*(l) W_{m_{k'}}(l+d)]. \end{aligned} \tag{6.5}$$

Since u_k and $u_{k'}$ have zero-mean and are mutually independent, we obtain

$$E[u_k^* u_{k'}] = \begin{cases} E[|u_k|^2] = 1, & k = k', \\ 0, & k \neq k'. \end{cases} \tag{6.6}$$

Table 6.1: Base station test model for $K = 9$ channels [98].

Channel	K	$\lvert c_k\rvert^2$	m_k
Pilot	1	0.2000	0
Sync	1	0.0471	32
Paging	1	0.1882	1
Traffic	6	0.09412	5, 9, 12, 36, 50, 57

Substituting (6.6) into (6.5), we can reduce the double summation into a single summation by setting $k = k'$:

$$\begin{aligned} C_{2x}(d) &= \sum_{k=0}^{K-1} |c_k|^2 \; E[W^*_{m_k}(l) W_{m_k}(l+d)] \\ &= \sum_{k=0}^{K-1} |c_k|^2 \; C_{2W_{m_k}}(d). \end{aligned} \tag{6.7}$$

Recall that $\sum_{k=0}^{K-1} |c_k|^2 = 1$. At $d = 0$, we obtain

$$\begin{aligned} C_{2x}(0) &= \sum_{k=0}^{K-1} |c_k|^2 \; C_{2W_{m_k}}(0) \\ &= \sum_{k=0}^{K-1} |c_k|^2 \; 1 = 1. \end{aligned} \tag{6.8}$$

When $d \neq 0$, the value of $C_{2x}(d)$ is not straightforward to obtain for an arbitrary K. However, when all 64 channels are active ($K = 64$) and the c_k's are the same, i.e., $c_k = 1/8$, we find

$$C_{2x}(d) = \sum_{k=0}^{63} \; (\frac{1}{8})^2 C_{2W_{m_k}}(d) = \begin{cases} 1, & d = 0 \\ 0, & d = 1, 2, \cdots, 63 \end{cases} . \tag{6.9}$$

We infer that $x(l)$ and $x(l+d)$ are uncorrelated $\forall\; d \neq 0$ in this scenario. Next, we illustrate $C_{2x}(d)$ for the following example cases:

Case 1: $K = 9$ channels are active. The parameters are given in Table 6.1 [98].

Case 2: $K = 24$ channels are active. The parameters are given in Table 6.2 [98].

Case 3: $K = 24$ channels are active. The active channels are $m_k = 0,\ 1,\ 2,\ 4,\ 6,\ 13,\ 15,\ 20,\ 24,\ 27,\ 28,\ 32,\ 35,\ 36,\ 37,\ 38,\ 41,\ 42,\ 45,\ 46,\ 47,\ 49,\ 54,\ 58$, and $c_k = \sqrt{1/24}\ \forall k$.

We plot $|C_{2x}(d)|$ in Figure 6.3. We observe that $|C_{2x}(d)|$ at $d \neq 0$ is considerably smaller than $C_{2x}(0)$.

Table 6.2: Base station test model for $K = 24$ channels [98].

Channel	K	$\lvert c_k \rvert^2$	m_k
Pilot	1	0.2000	0
Sync	1	0.01633	32
Paging	2	0.06531	$1, 2$
Traffic	20	0.03265	3, 4, 7, 10, 12, 14, 15, $26-28$, 31, 33, 34, 43, 45, 49, 51, 53, 55, 57, 62

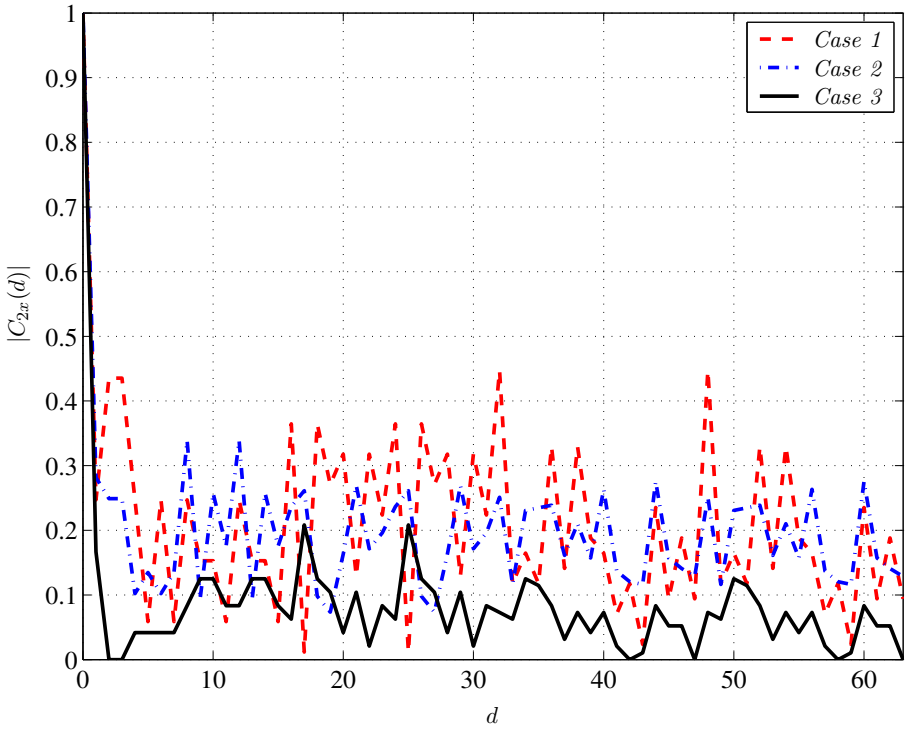

Figure 6.3: $|C_{2x}(d)|$ for cases $1-3$.

6.3.2 Crest Factor Analysis

Since the correlation between $x(l)$ and $x(l+d)$ is significantly reduced when $d \neq 0$, we can reduce the correlation between the I and Q branches by introducing a relative offset $D \neq 0$. Next, we relate the correlation reduction to crest factor reduction.

If the number of users K is large, then by the Central Limit Theorem, the composite signal $x(l)$ is approximately Gaussian distributed. Denote the variance of $x(l)$ by σ^2 and assume that u_k is i.i.d..

Since P_I and P_Q are ± 1 PN sequences, the baseband signal $z(l)$ in Figure 6.1 can be written as

$$z(l) = \pm x(l) \pm jx(l), \tag{6.10}$$

In (6.10), the $\pm$ signs before the I branch and the Q branch are determined by those of the short PN sequences that identify a specific base station.

Denote by R the IAR of $z(l)$. We have

$$R = \frac{x^2(l) + x^2(l)}{\sigma^2 + \sigma^2} = \frac{x^2(l)}{\sigma^2}. \tag{6.11}$$

Therefore, the IAR of $z(l)$ and the IAR of $x(l)$ are the same. Under the Gaussian assumption of $x(l)$ (when K is large), both IARs are χ^2-distributed with one degree of freedom; i.e., their probability density function (PDF) is [71]:

$$f_R(r) \;=\; \frac{1}{\sqrt{2\pi r}}\, e^{-\frac{r}{2}}, \qquad r \geq 0. \tag{6.12}$$

The corresponding CCDF is

$$Pr(R > r) = 2 - 2\ \Phi(\sqrt{r}), \tag{6.13}$$

where $\Phi(\cdot)$ is the CDF of the standard Gaussian distribution.

For the proposed IQ offset structure in Figure 6.2, let us denote $\tilde{x}(l) = x(l-D)$. Suppose that for a properly selected D, $x(l)$ and $x(l-D)$ are approximately uncorrelated. Under the assumption that $x(l)$ is approximately Gaussian distributed, $x(l)$ and $\tilde{x}(l)$ are approximately independent. In Figure 6.2, the baseband signal $\tilde{z}(l)$ can be written as

$$\tilde{z}(l) = \pm x(l) \pm j\tilde{x}(l), \tag{6.14}$$

which is approximately complex Gaussian distributed with variance $2\sigma^2$. Denote by S the IAR of $\tilde{z}(l)$

$$S = \frac{x^2(l)}{2\sigma^2} + \frac{\tilde{x}^2(l)}{2\sigma^2}. \tag{6.15}$$

It follows that $2S$ is χ^2-distributed with two degrees of freedom. In other words, S is exponentially distributed with mean $= 1$ [71]:

$$f_S(s) = e^{-s}, \qquad s \geq 0. \tag{6.16}$$

The corresponding CCDF is

$$Pr(S > s) = e^{-s}, \qquad s \geq 0 \tag{6.17}$$

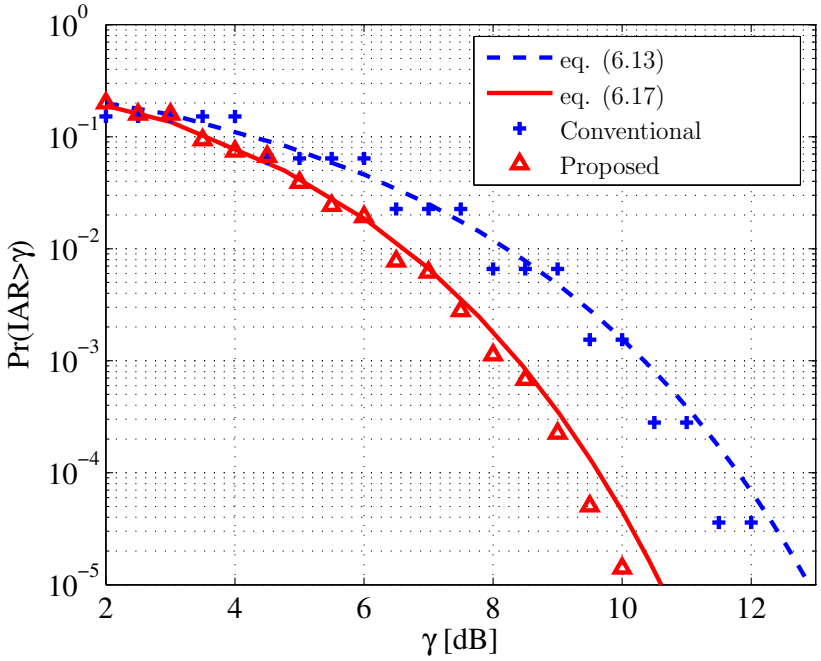

Figure 6.4: CCDF of the IAR of $z(l)$ and the IAR of $\tilde{z}(l)$ ($K = 24$).

In Figure 6.4, we plot the "theoretical" CCDFs given in (6.13) and (6.17), as well as empirical CCDFs for the actual CDMA cases. In the simulations, we assumed that $K = 24$, $c_k = \sqrt{1/24}$, $\forall k$. A total of 10^6 symbols were generated for each user (each k). In Figure 6.4, the dashed line corresponds to eq. (6.13); the discrete points with the plus sign correspond to the empirical CCDF of R (c.f. (6.11)); the solid line corresponds to (6.17); the

discrete points with the triangle sign correspond to the empirical CCDF of S (c.f. (6.15)). The simulated results agreed with the theoretical expressions (6.13) and (6.17) fairly well. Solving (6.13) and (6.17) at the 10^{-4} CCDF level, we find that the two theoretical CCDF curves differ by 2.1 dB, which implies that $\tilde{z}(l)$ has a crest factor that is 2.1 dB smaller than that of $z(l)$.

6.4 Simulations

In the above discussions, we have only considered signals $z(l)$ and $\tilde{z}(l)$ before up-sampling and the pulse shaping filtering. In reality, what matters is the crest factor of the signal after up-sampling and the pulse shaping filtering. It is difficult to theoretically analyze the IAR when filtering is involved; thus we will rely on computer simulations to demonstrate the CFR performance of the proposed algorithm.

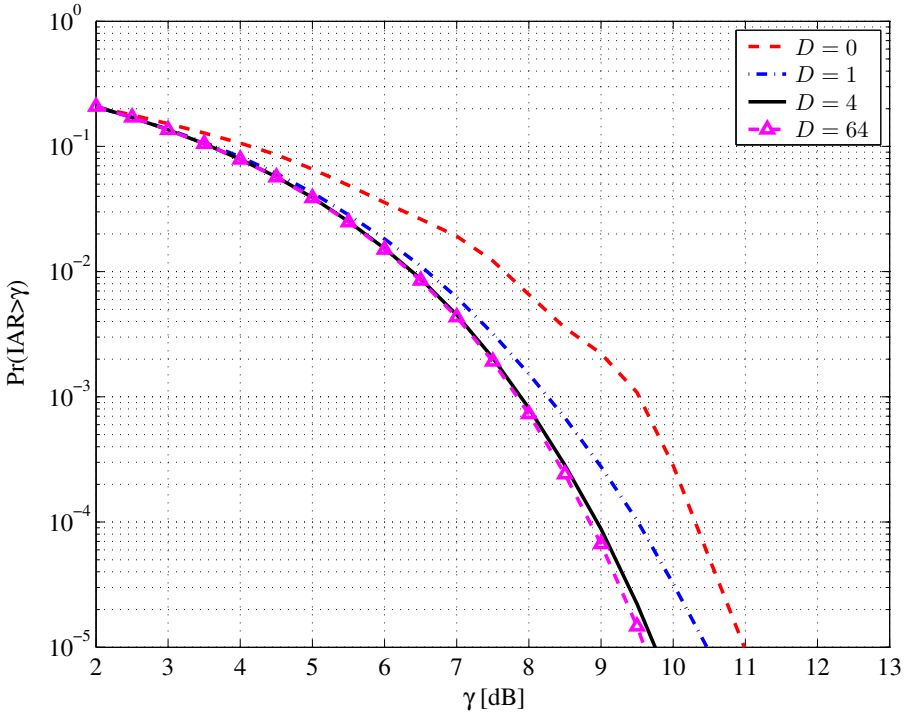

Figure 6.5: CCDF of the IAR of $\tilde{y}(t)$ for various offsets D. When $D = 0$, $\tilde{y}(t) = y(t)$ (conventional CDMA system). $K = 9$.

In Figure 6.5, we show CCDF curves of the IAR of the forward link CDMA signal after filtering. In this simulation, we assume the same $K = 9$ channel test model described

in Table 6.1. The pulse shaping filter is the same as the filter suggested in the IS-95 specification [97] with an up-sampling factor of 4. For our proposed method, we tried delay D equal to 1 chip, 4 chips, and 1 symbol, respectively. A total of 10^6 symbols were simulated.

In Figure 6.5, the dashed line is the empirical CCDF curve of the IAR of $y(t)$ for the conventional CDMA system describe in Figure 6.1; the dash-dotted line is the empirical CCDF curve of the IAR of $\tilde{y}(t)$ for the proposed modification described in Figure 6.2, when $D = 1$ chip; the solid line corresponds to $\tilde{y}(t)$ with $D = 4$ chips; and the dashed line with the $\triangle$ sign corresponds to $\tilde{y}(t)$ with $D = 1$ symbol (64 chips).

From Figure 6.5, we can see that delaying the Q branch by 1 chip does not perform as well as delaying it by 4 chips or by 1 symbol. The CFR performance with $D = 4$ chips was comparable to that with $D = 64$ chips (1 symbol). When the delay is 1 symbol, the I and Q branch data become independent, and the corresponding CCDF establishes a lower bound for the proposed system. From Figure 6.5, CFR of 1.5 dB was achieved for the 1 symbol offset case and 1.4 dB for the 4 chips offset case.

The same simulation settings as for Figure 6.4 were used for Figure 6.6 except that IAR of $\tilde{y}(t)$ instead of $\tilde{z}(l)$ is calculated. With $D = 4$ chips offset, 2.1 dB CFR was achieved.

Comparing Figure 6.5 with Figure 6.6, we observe that the CFR capability of the proposed algorithm is more evident when the number of users K is larger. In both examples, $D = 1$ chip offset does not perform as well as $D = 4$ chips offset, possibly due to the additional correlation introduced by the pulse shaping filter. $D = 4$ chips offset performed similarly to $D = 1$ symbol offset. Therefore in practice, we recommend to apply $D = 4$ chips offset to reach a compromise between the CFR performance and the processing delay.

The success of the proposed algorithm lies in reducing the correlation between the I branch and the Q branch data. In this section, we compare the proposed algorithm with the method described in [53].

In [53], the authors suggested to modify the signal fed to the Q branch by flipping the signs of user data with odd-numbered Walsh indices. With this modification, the signal in the I branch and the signal in the Q branch have reduced correlations if K is large and the

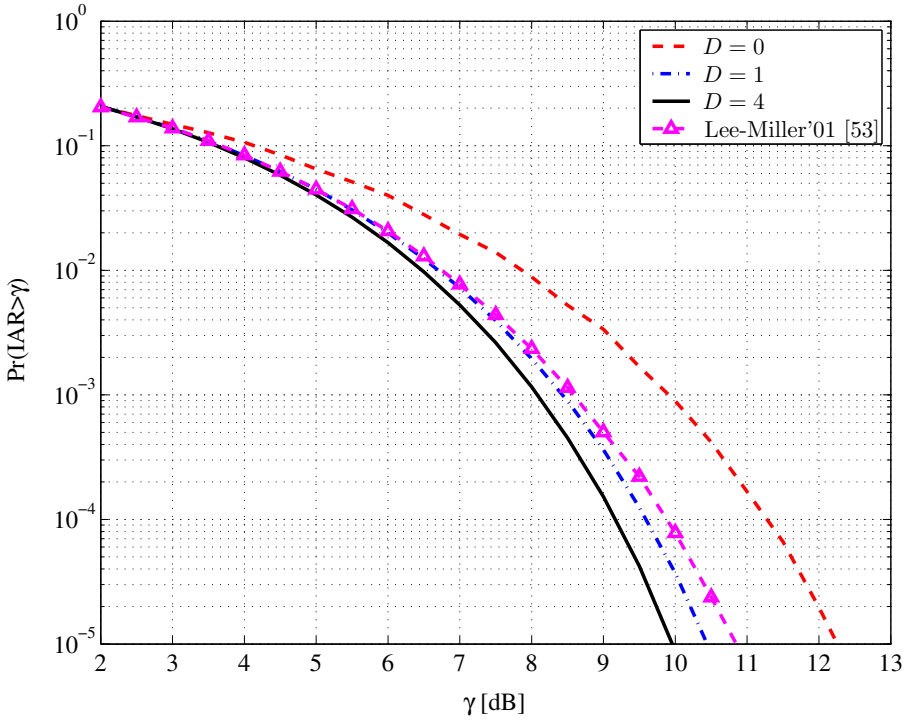

Figure 6.6: CCDF of the IAR of $\tilde{y}(t)$ for various offsets D. When $D = 0$, $\tilde{y}(t) = y(t)$ (conventional CDMA system). Comparison with the Lee-Miller method [53] is also included. $K = 24$.

number of active channels that occupy the odd-numbered Walsh indices is roughly $K/2$. Denote by $x_I(l)$ the signal sent into the I branch, then

$$x_I(l) = \sum_{i=even} S_i(l) + \sum_{k=odd} S_k(l) = S_e + S_o \tag{6.18}$$

where $S_i(l)$'s are Walsh coded signal using the even-numbered indices and their sum is called S_e. $S_k(l)$'s are Walsh coded signal using the odd-numbered indices and their sum is S_o.

The signal sent into the Q branch, $x_Q(l)$, can also be expressed using $S_i(l)$ and $S_k(l)$ as:

$$x_Q(l) = \sum_{i=even} S_i(l) - \sum_{k=odd} S_k(l) = S_e - S_o \tag{6.19}$$

Since $S_i(l)$ and $S_k(l)$ are mutually independent, the covariance between $x_I(l)$ and $x_Q(l)$ is $Cov(x_I(l), x_Q(l)) = Var\{S_e\} - Var\{S_o\}$. When the number of even terms equals the number of odd terms and the power is equally allocated, $Var\{S_e\} = Var\{S_o\}$. Therefore $x_I(l)$ and $x_Q(l)$ become uncorrelated. However, in reality, the signal in the pilot channel and

in the paging channel cannot be modified as such. Furthermore, it is difficult to control the active channels so that the even and the odd numbered Walsh indices have equal opportunity of being activated at any time. Thus, the CFR performance of the algorithm in [53] may not perform as well as our proposed algorithm.

Comparison between the CFR algorithm in [53] and our proposed CFR algorithm is also included in Figure 6.6. The dashed line with the $\triangle$ sign is the empirical CCDF curve of the IAR of $y(t)$ using the method of [53]. In this example, the algorithm in [53] gave a CFR performance of 1.4 dB, whereas our proposed algorithm achieved a CFR performance of 2.1 dB. When compared with other distortionless CFR algorithms, our algorithm is advantageous in that it requires very little hardware modification and it has little computational overhead. Besides, we do not rely on the existence of inactive codes or the knowledge of Walsh code indices of the active channels as in [50, 51, 91, 105].

The IQ offset architecture can be implemented using a shift register or a buffer for a fixed offset; e.g., $D = 4$ chips. At the receiver side, the I and Q branch data can be re-aligned after equalization. There is no degradation to the system performance.

6.5 Conclusions

The forward link CDMA signal has a large crest factor, which negatively impacts the transmission system power efficiency. In this chapter, a simple modification is proposed, whereby an IQ offset is introduced to reduce the correlation between the I and Q branch data. This modification reduces the crest factor of the forward link CDMA signal by $1.5 \sim 2.1$ dB in our simulations (for $K = 9$ and $K = 24$ test cases). Comparing with other existing CFR algorithms, the proposed algorithm requires a very simple change to the forward link CDMA structure and does not require additional computations.

CHAPTER VII

CONCLUSIONS

In this dissertation, we first studied the system performance when the transmitter is nonlinear. We then explored the optimal nonlinearity under the peak power constraint that maximizes the SNDR. We considered the power efficiency improvements for wireless transmissions. Two possible approaches: digital baseband predistortion linearization technique, and peak-to-average ratio reduction technique are investigated.

7.1 Contributions

Primary contributions of this dissertation are summarized here:

- We studied the system performance when the transmitter is nonlinear. We explored the optimal nonlinearity under the peak power constraint that maximizes the SNDR and extended the result to the fading channel case.
- We designed and integrated a high-speed predistortion testbed. We also carried out digital baseband predistortion linearization experiments and demonstrated the effectiveness of our proposed memory polynomials model and orthogonal polynomial basis.
- We proposed an adaptive digital predistortion linearization design that is especially suitable for the smaller, lower power wireless terminals. This low-cost, low-power predistortion architecture utilizes existing components of the wireless transceiver to fulfill the adaptive predistorter training functionality.
- We proposed an efficient dynamic selective mapping algorithm to reduce the PAR of the OFDM signal. DSLM can greatly reduce the computational requirement of the conventional SLM method without sacrificing the PAR reduction capability.
- We proposed IQ offset structure to reduce the PAR of the forward link CDMA signal by introducing a relative offset between the in-phase branch and the quadrature

branch of the system. Compared with existing PAR reduction algorithms, our algorithm is distortionless, offers good PAR reduction capability with very little system modifications and low computational complexity.

Following is the list of publications related to the work presented in this thesis.

Book chapter

B1. G. T. Zhou, H. Qian, and N. Chen, "Communication System Nonlinearities: Challenges and Some Solutions," in *Advances in Nonlinear Signal and Image Processing*, Eds.: S. Marshall and G. L. Sicuranza, Hindawi, 2005.

Journal papers

J1. G. T. Zhou, H. Qian, L. Ding and R. Raich, "On the baseband representation of a bandpass nonlinearity," *IEEE Transactions on Signal Processing*, Aug. 2005, to appear.

J2. H. Qian, C. Xiao, N. Chen, and G. T. Zhou, "Peak-to-average power ratio reduction for OFDM using dynamic selected mapping," July 2005, to be submitted.

J3. H. Qian, C. Zhao, and G. T. Zhou, "Low complexity crest factor reduction for forward link CDMA using IQ offset," *IEEE Communications Letters*, July 2005, submitted.

J4. N. Chen, G. T. Zhou, and H. Qian, "Peak-to-average power ratio reduction and power amplifier linearization for OFDM," *EURASIP Journal on Applied Signal Processing*, June 2005, submitted.

J5. R. Raich, H. Qian, and G. T. Zhou, "Optimization of SNDR for amplitude limited nonlinearities," *IEEE Transactions on Communications*, April 2005, accepted.

J6. R. Raich, H. Qian, and G. T. Zhou, "Orthogonal polynomials for power amplifier modeling and predistorter design," *IEEE Transactions on Vehicular Technology*, vol. 53, no. 5, pp. 1468-1479, Sept. 2004.

Conference papers

C1. H. Qian, C. Xiao, N. Chen, and G. Tong Zhou, "Dynamic Selected Mapping for OFDM," *Intl. Conference on Acoustics, Speech, and Signal Processing (ICASSP'2005)*, vol. 4, pp. 325-328, Philadelphia, PA, March 2005.

C2. H. Qian, R. Raich, and G. T. Zhou, "Optimization of SNDR in the presence of amplitude limited nonlinearity and multipath fading," *Proc. 38th IEEE Asilomar Conference on Signals, Systems, and Computers*, vol. 1, pp. 712-716, Pacific Grove, CA, Nov. 2004.

C3. H. Qian, L. Ding, G. T. Zhou, and J. S. Kenney, "Predistortion linearization measurement results for power amplifiers with memory effects," *Proc. IEEE Topical Workshop on Power Amplifiers for Wireless Communications*, San Diego, CA, Sept. 13-14, 2004, to appear.

C4. R. Raich, H. Qian, and G. T. Zhou, "Signal to noise and distortion ratio considerations for communication channels," *Proc. IEEE CAS Workshop/Symposium on Emerging Technologies: Frontiers of Mobile and Wireless Communication (MWC'04)*, vol. 1, pp. 93-96, Shanghai, China, May 2004.

C5. H. Qian, R. Raich, and G. T. Zhou, "On the benefits of deliberately introduced baseband nonlinearities in communication systems," *Proc. Intl. Conference on Acoustics, Speech, and Signal Processing (ICASSP'2004)*, vol. 2, pp. 905-908, Montreal, Canada, May 2004.

C6. L. Ding, H. Qian, N. Chen, and G. T. Zhou, "A memory polynomial predistorter implemented using TMS320C67xx," *Proc. TI Developer Conference 2004*, Houston, TX, Feb. 2004, to appear.

C7. R. Raich, H. Qian, and G. T. Zhou, "Digital baseband predistortion of nonlinear power amplifiers using orthogonal polynomials," *Proc. Intl. Conference on Acoustics, Speech, and Signal Processing (ICASSP'2003)*, vol. 6, pp. 689-692, Hong Kong, China, April 2003.

C8. H. Qian, and G. T. Zhou, "A neural network predistorter for nonlinear power amplifiers with memory," in *Proc.10th IEEE DSP Workshop (DSP'2002)*, pp. 312-316, Pine Mountain, GA, Oct. 2002.

Provisional Patent Applications

P1. H. Qian, C. Zhao, and G. T. Zhou, "Low complexity crest factor reduction for forward link CDMA using IQ offset," US provisional patent filed on July 6, 2005. (Invention disclosure GTRC ID No. 3543)

P2. H. Qian, C. Xiao, N. Chen, and G. T. Zhou, "Peak-to-average power ratio reduction for OFDM using dynamic selected mapping," US provisional patent filed March 18, 2005. (Invention disclosure GTRC ID No. 3426)

P3. H. Qian, G. T. Zhou, and L. Ding, "A Low Cost Predistortion Linearization Architecture for Portable Wireless Devices," US provisional patent filed Sept. 3, 2004. (Invention disclosure GTRC ID No. 3197)

7.2 Future Work

The work presented in this thesis can be extended to the following areas:

- Design new predistorter model for PAs with memory effects.
- Investigate PAR reduction algorithm with distortion.

7.2.1 New Predistorter Models with Memory Structures

In Chapter 3, we observe that for the large PA with memory effects, the memory polynomial model still cannot perfectly suppress the spectral regrowth at the PA output with limited delay length Q. With short delay length Q, the memory polynomial predistorter model only introduces short-term memory to the nonlinear model. For a large Q, the parameter estimation becomes computationally complex and is vulnerable to numerical instability. By including the long-term memory to the model, we may further improve the modeling accuracy and obtain better linearity.

We propose a new predistorter model that introduces additional terms that cover the long-term memory to the memory polynomial model:

$$y(n) = \sum_{k=1}^{K} \sum_{q=0}^{Q} a_{kq} \, |x(n-q)|^{2k} x(n-q) + \sum_{m=1}^{M} \beta_m \left[\sum_{l=1}^{L} \alpha^l \, |x(n-l)|^2 \right]^m x(n), \qquad (7.1)$$

where α is a forgetting factor, and L is the length of the past samples that contribute to the current output. α and L can be determined by the PA memory effects measurements. For example, if the time constant of the long-term memory is T s. We choose $\alpha = e^{-T_s/T}$, and $LT_s = 3T$ s, where T_s is the sampling interval. The first part of the proposed model is exactly the same as the memory polynomial model and it is used to capture the short-term memory. The second part is used to capture the long-term memory. The second part does not contain the current sample, nor the linear terms of past samples, since they have been included in the first part of the model. The term $\sum_{l=1}^{L} \alpha^l \, |x(n-l)|^2$ contains the energy of past signals.

The performance of (7.1) and other predistorter models that can capture both long-term and short-term memory effects will be further investigated.

7.2.2 Repeated Filtering and Clipping

PAR reduction algorithms without distortion in general demand high computational complexity. The IQ offset structure that we proposed in Chapter 6 requires very little computational overhead. However, its PAR reduction performance is bounded by about 2 dB. In specific applications, the PAR reduction of $4 \sim 6$ dB is required. PAR reduction with distortion, or combined PAR reduction with distortion and without distortion, are called for.

Deliberate clipping may effectively reduce the PAR, however, it introduces distortion as well. The spectral regrowth created by clipping is usually unacceptable. Conventional repeated clipping-and-filtering helps to reduce out-of-band radiation but also causes peak regrowth [55].

We propose a new repeated clipping-and-filtering algorithm with significant less peak regrowth. A preliminary simulation result is shown in Figure 7.1. In this simulation, we show the PSDs of the signals. The dash-dotted line in the bottom is the original CDMA

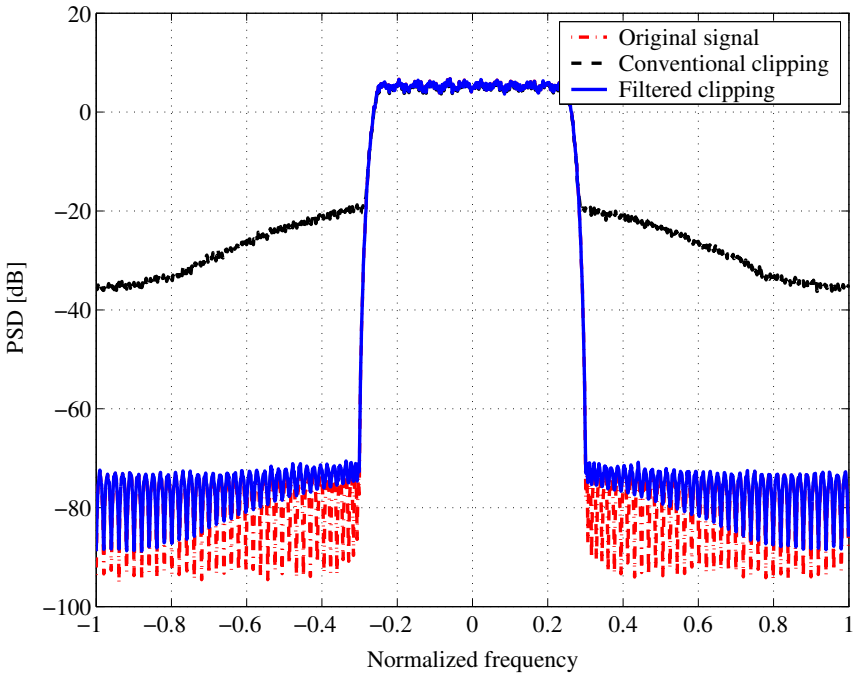

Figure 7.1: PSDs of the signals. The dash-dotted line: original CDMA signal; the dashed line: after clipping; the solid line: after the proposed repeated filtering-and-clipping.

signal. The dashed line is the signal after simple clipping. Strong spectral regrowth is observed. The solid line is the signal after the proposed repeated clipping-and-filtering. In this example, our proposed method was able to achieve PAR = 5.6 dB, ACPR = 78 dB, and $\rho = 0.986$. A nice trade-off between PAR, ACPR and the in-band distortion (ρ) was achieved.

The performance of the proposed repeated clipping-and-filtering PAR reduction algorithm and its extension to multi-band signals will be further investigated.

APPENDIX A

PROOF OF THEOREM 1

Proof. Similar to [84], we use functional derivatives to find the optimal nonlinearity.

Due to the constraint $g(\cdot) \leq 1$, we assume the following form for $g(\cdot)$:

$$\begin{cases} g(\gamma) < 1, & \gamma \in S, \\ g(\gamma) = 1, & \gamma \notin S, \end{cases} \tag{A.1}$$

where S is a subset of $[0, \infty)$.

Denote by $I(\cdot)$ the indicator function. Since $I(\gamma \notin S) + I(\gamma \in S) = 1$, we infer that for the $g(\cdot)$ in (A.1),

$$\begin{aligned} E[g^2(\gamma)] &= E[I(\gamma \notin S)g^2(\gamma)] + E[I(\gamma \in S)g^2(\gamma)] && \text{(A.2)} \\ &= E[I(\gamma \notin S)] + E[I(\gamma \in S)g^2(\gamma)] && \text{(A.3)} \\ &= C_o + E[I(\gamma \in S)g^2(\gamma)], && \text{(A.4)} \end{aligned}$$

where

$$C_o = E[I(\gamma \notin S)]. \tag{A.5}$$

Similarly,

$$E[\gamma g(\gamma)] = C_1 + E[I(\gamma \in S)\gamma g(\gamma)], \tag{A.6}$$

where

$$C_1 = E[\gamma I(\gamma \notin S)]. \tag{A.7}$$

It follows easily that $C_o \geq 0$, $C_1 \geq 0$.

Taking the functional derivative of (A.4) w.r.t. $g(\gamma_o)$, we obtain

$$\frac{\delta E[I(\gamma \in S)g^2(\gamma)]}{\delta g(\gamma_o)} = 2g(\gamma_o)p(\gamma_o), \tag{A.8}$$

for $\gamma_o \in S$, where $p(\gamma)$ the PDF of the random variable γ. Similarly, taking the functional derivative of (A.6) w.r.t. $g(\gamma_o)$, we obtain

$$\frac{\delta E[I(\gamma \in S)\gamma g(\gamma)]}{\delta g(\gamma_o)} = \int I(\gamma \in S)\gamma\delta(\gamma - \gamma_o)p(\gamma)d\gamma \tag{A.9}$$

$$= \gamma_o p(\gamma_o). \tag{A.10}$$

To maximize/minimize (2.38) w.r.t. $g(\cdot)$, we need

$$\frac{\delta \int E_{\beta(f)}[F(\text{SNDR}(\beta(f)))]\ df}{\delta g(\gamma_o)} = 0, \qquad \forall\ \gamma_o \in S. \tag{A.11}$$

Using the chain rule of partial derivatives, we obtain

$$\int E_{\beta(f)}[\frac{\partial F(\text{SNDR}(\beta(f)))}{\partial \text{SNDR}(\beta(f))}\frac{\delta \text{SNDR}(\beta(f))}{\delta g(\gamma_o)}]\ df = 0, \qquad \forall\ \gamma_o \in S. \tag{A.12}$$

Next, we substitute (2.27), (A.4), and (A.6) into (A.12), and simplify the left hand side of (A.12) with (A.8) and (A.10). We obtain

$$\begin{aligned} 2\gamma_o p(\gamma_o)E[\gamma g(\gamma)] \int E_{\beta(f)}[\frac{\partial F(\text{SNDR}(\beta(f)))}{\partial \text{SNDR}(\beta(f))}\frac{\tilde{\lambda}(\gamma)}{\tilde{\mu}(\gamma)}]\ df \\ -2g(\gamma_o)p(\gamma_o)E[\gamma g(\gamma)] \int E_{\beta(f)}[\frac{\partial F(\text{SNDR}(\beta(f)))}{\partial \text{SNDR}(\beta(f))}\frac{\tilde{\kappa}(\gamma)}{\tilde{\mu}(\gamma)}]\ df \end{aligned} = 0, \tag{A.13}$$

where

$$\tilde{\lambda}(\gamma) = E[g^2(\gamma)] + \frac{\sigma_v^2}{\beta^2(f)A^2}, \tag{A.14}$$

$$\tilde{\mu}(\gamma) = \Big(E[g^2(\gamma)] - (E[\gamma g(\gamma)])^2 + \frac{\sigma_v^2}{\beta^2(f)A^2}\Big)^2, \tag{A.15}$$

and

$$\tilde{\kappa}(\gamma) = E[\gamma g(\gamma)]. \tag{A.16}$$

Rearranging (A.13), we obtain

$$g(\gamma_o) = \frac{\gamma_o}{\eta}, \tag{A.17}$$

with

$$\eta = \frac{\int E_{\beta(f)}[\frac{\partial F(\text{SNDR}(\beta(f)))}{\partial \text{SNDR}(\beta(f))}\frac{\tilde{\kappa}(\gamma)}{\tilde{\mu}(\gamma)}]\ df}{\int E_{\beta(f)}[\frac{\partial F(\text{SNDR}(\beta(f)))}{\partial \text{SNDR}(\beta(f))}\frac{\tilde{\lambda}(\gamma)}{\tilde{\mu}(\gamma)}]\ df}. \tag{A.18}$$

Since (A.17) holds $\forall\ \gamma_o \in S$, the optimal nonlinearity must have the form

$$g(\gamma) = \begin{cases} \frac{\gamma}{\eta}, & \gamma \in S, \\ 1, & \gamma \notin S. \end{cases} \tag{A.19}$$

Please note that (A.19) is S-dependent. Given different S, (A.19) may result in different local maxima/minima.

Next, we will show that to optimize (2.38), S must be

$$S \quad = \quad [0, \eta]. \tag{A.20}$$

Comparing (A.1) with (A.19), we infer that $\gamma < \eta$ on S, or

$$S \subseteq S^\star, \tag{A.21}$$

where

$$S^\star = [0, \eta]. \tag{A.22}$$

Assume a set S who optimizes (2.38) satisfies

$$S \subset S^\star. \tag{A.23}$$

Over set $S^\star$, we may find an optimal nonlinearity that optimizes (2.38),

$$g^\star(\gamma) = \begin{cases} \frac{\gamma}{\eta^\star}, & \gamma \in S^\star, \\ 1, & \gamma \notin S^\star. \end{cases} \tag{A.24}$$

In other words, on set $S^\star$,

$$\text{SNDR}|_{g^\star} > \text{SNDR}|_g. \tag{A.25}$$

Function $g(\cdot)$ obtained with set S is not the overall optimizer of (2.38). The assumption (A.23) was not valid. We conclude that

$$S \quad = \quad [0, \eta]. \tag{A.26}$$

Substituting (A.26) into (A.19), we obtain that within the class of $g(\cdot)$ satisfying $0 \leq g(\cdot) \leq 1$, (2.39) is the optimizer and the threshold is determined by (2.40)-(2.46).

□

APPENDIX B

A GENERAL MARKOV MODEL FOR SIDE INFORMATION ANALYSIS

To analyze the exact probability distribution of occurrence of the index, we introduce a general Markov model. The state of the Markov model is chosen to be the maximum number of possible mappings that was assigned to an incoming OFDM block at the time when it is processed. When the output buffer underflows, the SLM processing unit is forced to generate an output even if the PAR threshold is not satisfied. The next block of data can try a maximum of L mappings. When the input underflows, the SLM processing unit is in the idle condition. The next block of data can try a maximum of LM mappings. The maximum number of possible mappings can be $L, L+1, \ldots, LM$. We infer that the number of states is $(L-1)M+1$.

The state transition matrix can be written as

$$\mathbf{P} = [P_{il}]_{((M-1)L+1)\times((M-1)L+1)}, \tag{B.1}$$

where $L \leq i, l \leq LM$, and P_{il} is the probability that $S = i$ conditioned on $S = l$ between two adjacent incoming blocks.

Next, we derive the closed-form expression of the state transition matrix. If at a certain time instant, the Markov chain starts at state l, $l \leq (M-1)L+1$. After finishing processing the current OFDM data, the Markov chain will end up with state $l+L-1, l+L-2, \ldots, L+1$, if the SLM processing unit finds a successful trial within $1, 2, \ldots, l-1$ mappings, respectively. Recall (5.8), the transition probability P_{il} is given by

$$P_{il} = Pr\{Z = l+L-i\} = a(1-a)^{l+L-i-1}, \qquad l \leq (M-1)L+1, \text{ and } i > L. \tag{B.2}$$

After finishing processing the current OFDM data, the Markov chain may also go to the state L if the SLM processing unit finds a successful trial at the lth mapping or the SLM

processing unit fails to find a successful trial after l mappings. The transition probability P_{il} is given by

$$P_{il} = Pr\{Z \geq l\} = (1-a)^{l-1}, \qquad l \leq (M-1)L+1, \text{ and } i = L. \tag{B.3}$$

If at a certain time instant, the Markov chain starts at state l, $l \geq (M-1)L+2$. After finishing processing the current OFDM data, the Markov chain may end up with state L, if the SLM processing unit finds a successful trial at the lth mapping or the SLM processing unit fails to find a successful trial after l mappings. The Markov chain may end up with state LM, if the SLM processing unit finds a successful trial within $1, 2, l-(M-1)L$ mappings, when the output buffer underflows. The Markov chain may also end up with any state between L and LM. The transition probability P_{il} is given by

$$\begin{aligned} P_{il} &= \begin{cases} Pr\{Z \geq l\}, & i = L, \text{ and } l \geq (M-1)L+2 \\ \sum_{d=1}^{l-(M-1)L} Pr\{Z = d\}, & i = ML, \text{ and } l \geq (M-1)L+2, \\ Pr\{Z = l+L-i\}, & L < i < ML \text{ and } l \geq (M-1)L+2, \end{cases} \\ &= \begin{cases} (1-a)^{l-1}, & i = L, \text{ and } l \geq (M-1)L+2 \\ \sum_{d=1}^{l-(M-1)L} a(1-a)^{d-1}, & i = ML, \text{ and } l \geq (M-1)L+2, \\ a(1-a)^{l+L-i-1}, & L < i < ML \text{ and } l \geq (M-1)L+2. \end{cases} \end{aligned} \tag{B.4}$$

Combining (B.2) - (B.4), we obtain the closed-form expression of transition probability matrix $\mathbf{P}$, where P_{il} can be expressed as:

$$P_{il} = \begin{cases} (1-a)^{l-1}, & i = L, \\ \sum_{d=1}^{l-(M-1)L} a(1-a)^{d-1}, & i = ML, \text{ and } l \geq (M-1)L+2, \\ a(1-a)^{l+L-i-1}, & \text{otherwise.} \end{cases} \tag{B.5}$$

By Ergodicity Theorem [19], we know that a unique steady state distribution exists, independent of the initial state. Denote $\boldsymbol{\pi} = [\pi_L, \pi_{L+1}, \ldots, \pi_{ML}]^T$ as the steady state vector of the Markov chain, and $\sum_{k=1}^{M} \pi_k = 1$. The element π_i represents the probability that the state $S = i$ occurs, $\pi_i = Pr\{S = i\}$. The steady state vector $\boldsymbol{\pi}$ is the eigen vector of the probability transition matrix $\mathbf{P}$ corresponding to the eigen value 1. The steady state vector $\boldsymbol{\pi}$ can be obtained by solving

$$\mathbf{P}\boldsymbol{\pi} = \boldsymbol{\pi}. \tag{B.6}$$

With the condition that the upcoming block of data can try a maximum of l mappings, the phase sequence index i may occur if the first successful trial is obtained after i mappings, for $i < l$, and the first successful trial is not obtained before the first $l-1$ mappings, for $i = l$. The conditional probability may be written as

$$\begin{aligned} p_{i|l} &= \begin{cases} Pr\{Z = i\}, & i < l, \\ Pr\{Z \geq i\}, & i \geq l, \end{cases} \\ &= \begin{cases} a(1-a)^{i-1}, & i < l, \\ (1-a)^i, & i \geq l. \end{cases} \end{aligned} \tag{B.7}$$

Then the phase sequence index i occurs with probability

$$\begin{aligned} p_i &= \sum_{l=L}^{l=ML} p_{i|l} Pr\{S = l\} \\ &= \begin{cases} Pr\{Z = i\}, & i < L, \\ Pr\{Z = i\} \times \sum_{d=i}^{ML} \pi_d + Pr\{Z > i\} \times \pi_i, & i \geq L, \end{cases} \\ &= \begin{cases} a(1-a)^{i-1}, & i < L, \\ a(1-a)^{i-1} \sum_{d=i}^{ML} \pi_d + (1-a)^i \pi_i, & i \geq L. \end{cases} \end{aligned} \tag{B.8}$$

Remark 1: The Markov chain in (B.5) can also be used to compute the probability of failure. With the condition that the upcoming block of data can try a maximum of l mappings, the probability of failure in finding a successful trial after lth mapping is given by $Pr\{Z > l\} = (1-a)^{l-1}$. Then the overall probability of failure is

$$R(\gamma) = \sum_{l=L}^{LM} (1-a)^{l-1} \pi_l. \tag{B.9}$$

Remark 2: To estimate the computational load, $E[Z]$ in (B.8) is a good estimate when the probability of failure is small. To compute the computational load, we need to know the number of mappings used for each OFDM block. Equation (B.8) also suggests the probability (p_i) of occurrence of the number of mappings (i) used for each OFDM block. The expected number of mappings used in the DSLM algorithm is given by

$$E[i] \;=\; \sum_{i=1}^{LM} i p_i, \tag{B.10}$$

where p_i is given in (B.8).

APPENDIX C

AN UPPER BOUND OF THE ENTROPY OF THE SIDE INFORMATION USING DSLM

If the DSLM algorithm has infinite buffer length, there is no output buffer underflow or input buffer underflow. The probability that index $I = i$ follows the Geometric distribution; i.e.,

$$p_i = a(1-a)^{i-1}, \tag{C.1}$$

where

$$a = (1 - e^{-\gamma})^N, \tag{C.2}$$

and $i = 1, 2, \ldots$. The entropy of the index I, $H_\infty(I)$, is given by (5.21).

For a practical implementation, the size of the phase table has to be finite. Assume that the DSLM has a finite buffer length with $L = 1$ and $M = M^\star < \infty$. The index i follows a truncated Geometric distribution,

$$p_i = \begin{cases} a(1-a)^{i-1}, & i < M, \\ (1-a)^{M-1}, & i = M. \end{cases} \tag{C.3}$$

For the above distribution, the entropy of the index is given by

$$\begin{aligned} H_{1,M^\star}(I) &= -\sum_{i=1}^{M^\star} p_i \log_2 p_i \\ &= -\sum_{i=1}^{M^\star} a(1-a)^{i-1} \log_2(a(1-a)^{i-1}) - (1-a)^{M^\star} \log_2(1-a)^{M^\star}. \end{aligned} \tag{C.4}$$

Now let us consider a DSLM with $L = 1$ and $M = M^\star + 1$. We know that

$$\begin{aligned} H_{1,M^\star+1}(I) &= -\sum_{i=1}^{M^\star} a(1-a)^{i-1} \log_2(a(1-a)^{i-1}) - a(1-a)^{M^\star} \log_2 a(1-a)^{M^\star} \\ &\quad -(1-a)^{M^\star+1} \log_2(1-a)^{M^\star+1}. \end{aligned} \tag{C.5}$$

Comparing (C.4) and (C.5), we have

$$\begin{aligned} H_{1,M^\star}(I) - H_{1,M^\star+1}(I) &= -(1-a)^{M^\star}\log_2(1-a)^{M^\star} + a(1-a)^{M^\star}\log_2 a(1-a)^{M^\star} \\ &\quad +(1-a)^{M^\star+1}\log_2(1-a)^{M^\star+1} \\ &= -\Big(a(1-a)^{M^\star}\log_2(1-a)^{M^\star} - a(1-a)^{M^\star}\log_2 a(1-a)^{M^\star}\Big) \\ &\quad -\Big((1-a)^{M^\star+1}\log_2(1-a)^{M^\star} - (1-a)^{M^\star+1}\log_2(1-a)^{M^\star+1}\Big) \\ &= a(1-a)^{M^\star}\log_2 a + (1-a)^{M^\star+1}\log_2(1-a). \end{aligned} \tag{C.6}$$

Recall that $a = (1-\exp(-\gamma))^N$, $0 < a,\ (1-a) < 1$, we infer that

$$H_{1,M^\star}(I) - H_{1,M^\star+1}(I) \ < \ 0, \tag{C.7}$$

or

$$H_{M^\star}(I) < H_{M^\star+1}(I). \tag{C.8}$$

The inequality in (C.8) tells us that the truncation in the probability distribution reduces the randomness of the variable, thus reduces the entropy.

The inequality in (C.8) can also be extend to the extreme case:

$$H_{1,M^\star}(I) < H_{1,M^\star+1}(I) < H_{1,M^\star+2}(I) < \ldots < H_\infty(I). \tag{C.9}$$

Now let us consider a general DSLM case with $L = L^\star$ and $M = M^\star$. From Appendix B, we know that the maximum number of possible mappings for a given OFDM block may change. We may consider the conditional entropy given the state information $S = s$.

$$H_{L^\star,M^\star}(I) = \sum_{s=L}^{LM} H_{L^\star,M^\star}(I|S)Pr(S=s) \tag{C.10}$$

$$= \sum_{s=L}^{LM} H_{1,S}(I)Pr(S=s) \tag{C.11}$$

$$< \sum_{s=L}^{LM} H_\infty(I)Pr(S=s) \ = \ H_\infty(I). \tag{C.12}$$

In other words, $H_\infty(I)$ in (5.21) is an upper bound for any DSLM with the same parameter a.

REFERENCES

[1] Agre, J. R., Clare, L. P., Pottie, G. J., and Romanov, N. P., "Development platform for self-organizing wireless sensor networks," in *Proceedings of SPIE, Unattended Ground Sensor Technologies and Applications*, vol. 3713, pp. 257 – 268, April 1999.

[2] Baudoin, G. and Jardin, P., "Adaptive polynomial pre-distortion for linearization of power amplifiers in wireless communications and WLAN," in *Proc. Intl. Conf. on Trends in Communications (EUROCON'2001)*, vol. 1, pp. 157–160, July 2001.

[3] Bauml, R. W., Fischer, R., and Huber, J. B., "Reducing the peak-to-average power ratio of multicarrier modulation by selected mapping," *Electronics Letters*, vol. 32, pp. 2056–2057, Oct. 1996.

[4] Baxley, R. J. and Zhou, G. T., "Assessing peak-to-average power ratios for communications applications." in *Proc. IEEE MILCOM Conference*, Monterey, CA, Nov. 2004 (to appear).

[5] Bello, P. A., "Characterization of randomly time-variant linear channels," *IEEE Transactions on Communications Systems*, vol. 11, pp. 360–393, Dec. 1963.

[6] Benedetto, S. and Biglieri, E., "Nonlinear equalization of digital satellite channels," *IEEE Journal on Selected Areas in Communications*, vol. SAC-1, pp. 57–62, Jan. 1983.

[7] Benedetto, S. and Biglieri, E., *Principles of Digital Transmission With Wireless Applications*. Kluwer Academic Publishers, July 1999.

[8] Benedetto, S., Biglieri, E., and Daffara, R., "Modeling and performance evaluation of nonlinear satellite links — a Volterra series approach," *IEEE Transactions on Aerospace and Electronic Systems*, vol. 15, pp. 494–507, July 1979.

[9] Boumaiza, S. and Ghannouchi, F. M., "Realistic power-amplifiers characterization with application to baseband digital predistortion for 3G base stations," *IEEE Transactions on Microwave Theory and Techniques*, vol. 50, pp. 3016 – 3021, Dec. 2002.

[10] Breiling, M., Muller-Weinfurtner, S. H., and Huber, J. B., "SLM peak-power reduction without explicit side information," *IEEE Communications Letters*, vol. 5, pp. 239–241, June 2001.

[11] Cavers, J. K., "Amplifier linearization using a digital predistorter with fast adaptation and low memory requirements," *IEEE Transactions on Vehicular Technology*, vol. 39, pp. 374–382, Nov. 1990.

[12] Ceylan, N., Mueller, J. E., Pittorino, T., and Weigel, R., "Mobile phone power amplifier linearity and efficiency enhancement using digital predistortion," in *33rd European Microwave Conference*, vol. 1, pp. 269 – 272, Oct. 2003.

[13] Chang, K., Bahl, I., and Nair, V., *RF and Microwave Circuits and Component Design for Wireless Systems*. New York, NY: John Wiley & Sons, 2002.

[14] Chen, N., Zhou, G. T., and Qian, H., "Peak-to-average power ratio reduction and power amplifier linearization for OFDM." submitted to *EURASIP Journal on Applied Signal Processing*, June 2005.

[15] Clark, C. J., Chrisikos, G., Muha, M. S., Moulthrop, A. A., and Silva, C. P., "Time-domain envelope measurement technique with application to wideband power amplifier modeling," *IEEE Transactions on Microwave Theory and Techniques*, vol. 46, pp. 2531–2540, Dec. 1998.

[16] Conexant Systems, Inc., "RF105 900 MHz Digital Spread Spectrum Transceiver Data Sheet," Sept. 1999.

[17] Conexant Systems, Inc., "RF106 900 MHz ISM Band Power Amplifier Data Sheet," August 2002.

[18] Copeland, G. C., "Crest factor reduction processor for wireless communications." United States Patent Application No. 20040052314 A1, March 2004.

[19] Cornfeld, I. P., Fomin, S. V., and Sinai, Y. G., *Ergodic theory*. New York and Berlin: Springer-Verlag, 1982.

[20] Cover, T. M. and Thomas, J. A., *Elements of Information Theory*. New York, NY: John Wiley and Sons, Inc., 1991.

[21] Cripps, S. C., *Advanced Techniques in RF Power Amplifier Design*. Norwood, MA: Artech House, 2002.

[22] D'Andrea, A. N., Lottici, V., and Reggiannini, R., "RF power amplifier linearization through amplitude phase predistortion," *IEEE Transactions on Communications*, vol. 44, pp. 1477–1484, Nov. 1996.

[23] Ding, L., Raich, R., and Zhou, G. T., "A Hammerstein predistortion linearization design based on the indirect learning architecture," in *Proc. IEEE Intl. Conference on Acoustics, Speech, and Signal Processing (ICASSP'02)*, vol. 3, (Orlando, FL), pp. 2689–2692, May 2002.

[24] Ding, L. and Zhou, G. T., "Effects of even-order nonlinear terms on power amplifier modeling and predistortion linearization," *IEEE Transactions on Vehicular Technology*, vol. 53, pp. 156–162, Jan. 2004.

[25] Ding, L., Zhou, G. T., Morgan, D. R., Ma, Z., Kenney, J. S., Kim, J., and Giardina, C. R., "A robust predistorter constructed using memory polynomials," *IEEE Transactions on Communications*, vol. 52, pp. 159–165, Jan. 2004.

[26] Doyle, J. and Broach, B., "Small gains in power efficiency now, bigger gains tomorrow," July 2002. www.eetimes.com.

[27] Eun, C. and Powers, E. J., "A predistorter design for a memory-less nonlinearity preceded by a dynamic linear system," in *Proc. Global Telecommunications Conference*, vol. 1, (Singapore), pp. 152–156, Nov. 1995.

[28] Eun, C. and Powers, E. J., "A new Volterra predistorter based on the indirect learning architechture," *IEEE Transactions on Signal Processing*, vol. 45, pp. 223–227, Jan. 1997.

[29] Fairchild Semiconductor International, "RMPA2451 2.4 – 2.5 GHz GaAs MMIC Power Amplifier Data Sheet," April 2004.

[30] Faulkner, M. and Johansson, M., "Spectral sensitivity of power amplifiers to quadrature modulator misalignment," *IEEE Transactions on Vehicular Technology*, vol. 41, pp. 516–525, Nov. 1992.

[31] Faulkner, M. and Johansson, M., "Adaptive linearization using predistortion - experimental results," *IEEE Transactions on Vehicular Technology*, vol. 43, pp. 323–332, May 1994.

[32] Georgiadis, A., "Gain, phase imbalance, and phase noise effects on error vector magnitude," *IEEE Transactions on Vehicular Technology*, vol. 53, pp. 443–449, March 2004.

[33] Hanzo, L., Munster, M., Choi, B. J., and Keller, T., *OFDM and MC-CDMA for Broadband Multi-User Communications, WLANs and Broadcasting*. West Sussex, England: John Wiley & Sons, 2003.

[34] Hau, G., Nishimura, T. B., and Iwata, N., "A linearized power amplifier MMIC for 3.5V battery operated wide-band CDMA handsets," in *IEEE Microwave Symposium Digest*, vol. 3, pp. 1503 – 1506, June 2000.

[35] Hau, G., Nishimura, T. B., and Iwata, N., "High efficiency, wide dynamic range variable gain and power amplifier MMICs for wide-band CDMA handsets," *IEEE Microwave and Wireless Components Letters*, vol. 11, pp. 13–15, Jan. 2001.

[36] Huang, X., Lu, J., Chuang, J., and Zheng, J., "Companding transform for the reduction of peak-to-average power ratio of OFDM signals," in *Proc. IEEE Vehicular Technology Conference*, vol. 2, pp. 835–839, May 2001.

[37] Jayalath, A. and Tellambura, C., "Reducing the peak-to-average power ratio of orthogonal frequency division multiplexing signal through bit or symbol interleaving," *Electronic Letters*, vol. 36, pp. 1161–1163, June 2000.

[38] Jayalath, A. and Tellambura, C., "A blind SLM receiver for PAR-reduced OFDM," in *Proc. IEEE 56th Vehicular Technology Conference*, vol. 1, pp. 219–222, Sept. 2002.

[39] Jones, A. E., Wilkinson, T. A., and Barton, S. K., "Block coding scheme for reduction of peak to mean envelope power ratio of multicarrier transmission schemes," *Electronics Letters*, vol. 30, pp. 2098 – 2099, Dec. 1994.

[40] Jung, W. J., Kim, W. R., Kim, K. M., and Lee, K. B., "Digital predistorter using multiple lookup tables," *Electronics Letters*, vol. 39, pp. 1386–1388, Sept. 2003.

[41] Keller, T. and Hanzo, L., "Adaptive multicarrier modulation: a convenient framework for time-frequency processing in wireless communications," *Proceedings of the IEEE*, vol. 88, pp. 611 – 640, May 2000.

[42] Kenington, P. B., *High-Linearity RF Amplifier Design*. Boston, MA: Artech House, 2000.

[43] Kenney, J. S., *The RF and Microwave Handbook*, ch. Nonlinear Microwave Measurement and Characterization. CRC Press, Jan. 2001.

[44] Kenney, J. S., Woo, W., Ding, L., Raich, R., Ku, H., and Zhou, G. T., "The impact of memory effects on predistortion linearization of RF power amplifiers," in *International Symposium on Microwave and Optical Technology*, (Montreal, Canada), pp. 189–193, June 2001.

[45] Kim, J. and Konstantinou, K., "Digital predistortion of wideband signals based on power amplifier model with memory," *Electronic Letters*, vol. 37, pp. 1417–1418, Nov. 2001.

[46] Kim, T. H., Kim, C. S., Lee, K. Y., Moon, J. H., Lee, J. C., Kim, J. H., Lee, B., and Kim, N. Y., "An advanced 2 watt high power amplifier for CDMA 900 MHz system," in *IEEE MTT-S International Microwave Symposium Digest*, vol. 1, pp. 437–440, June 2002.

[47] Krongold, B. S. and Jones, D. L., "PAR reduction in OFDM via active constellation extension," *IEEE Transactions on Broadcasting*, vol. 49, pp. 258–268, Sept. 2003.

[48] Kubo, T., Fudaba, N., Ishikawa, H., Hamada, H., Nagatam, K., Hayashi, H., Maniwa, T., and Oishi, Y., "A highly efficient adaptive digital predistortion amplifier for IMT-2000 base stations," in *Proc. IEEE Vehicular Technology Conference*, pp. 2206 – 2210, April 2003.

[49] Kusunoki, S., Yamamoto, K., Hatsugai, T., Nagaoka, H., Tagami, K., Tominaga, N., Osawa, K., Tanabe, K., Sakurai, S., and Iida, T., "Power-amplifier module with digital adaptive predistortion for cellular phones," *IEEE Transactions on Microwave Theory and Techniques*, vol. 50, pp. 2979–2986, Dec. 2002.

[50] Lau, V., "On the analysis of peak-to-average ratio (PAR) for IS95 and CDMA 2000," *IEEE Transactions on Vehcular Technology*, vol. 49, pp. 2174–2188, Nov. 2000.

[51] Lau, V., "Average of peak-to-average ratio (PAR) of IS95 and CDMA2000 systems – single carrier," *IEEE Communications Letters*, vol. 5, pp. 160–162, April 2001.

[52] Lee, J. S. and Miller, L. E., *CDMA Systems Engineering Handbook*. Artech House Publishers, 1998.

[53] Lee, J. S. and Miller, L. E., "Analysis of peak-to-average power ratio for IS-95 and third generation CDMA forward link waveforms," *IEEE Transactions on Vehcular Technology*, vol. 50, pp. 1004–1013, July 2001.

[54] Lee, K. C. and Gardner, P., "Comparison of different adaptation algorithms for adaptive digital predistortion based on edge standard," in *Proc. IEEE International Microwave Symposium Digest (MTT-S)*, vol. 2, pp. 1353 –1356, May 2001.

[55] Leung, S., Ju, S., and Bi, G., "Algorithm for repeated clipping and filtering in peak-to-average power reduction for OFDM," *Electronics Letters*, vol. 38, pp. 1726 – 1727, Dec. 2002.

[56] Li, X. and Cimini, L., "Effects of clipping and filtering on the performance of OFDM," *IEEE Communications Letters*, vol. 2, pp. 131–133, May 1998.

[57] Liu, T., Boumaiza, S., and Ghannouchi, F. M., "Dynamic behavioral modeling of 3G power amplifiers using real-valued time-delay neural networks," *IEEE Transactions on Microwave Theory and Techniques*, vol. 52, pp. 1025 – 1033, March 2004.

[58] Maas, S. A., *Nonlinear Microwave Circuits*. Piscataway, NJ: IEEE Press, 1997.

[59] Matero, J. and Kananen, K., "Dual band architechtures for mobile stations having transmitter linearization feedback." United States Patent No. 6,125,266, Sept. 26, 2000.

[60] Mathews, V. J. and Sicuranza, G. L., *Polynomial Signal Processing*. John Wiley & Sons, 2000.

[61] Muhonen, K. J., Kavehrad, M., and Krishnamoorthy, R., "Look-up table techniques for adaptive digital predistortion: a development and comparison," *IEEE Transactions on Vehicular Technology*, vol. 49, pp. 1995–2002, Sept. 2000.

[62] Muller, S. and Huber, J., "A novel peak power reduction scheme for OFDM," *Proc. IEEE International Symposium on Personal, Indoor and Mobile Radio Communications*, pp. 1090–1094, 1997.

[63] Nagata, Y., "Linear amplification technique for digital mobile communications," in *Proc. IEEE Vehicular Technology Conference*, vol. 1, (San Francisco, CA), pp. 159–164, May 1989.

[64] Naskas, N. and Papananos, Y., "An adaptive power amplifier lineariser based on a multilayer perceptron," in *Proc. IEEE Vehicular Technology Conference*, vol. 57, (Jeju, South Korea), pp. 1331–1334, April 2003.

[65] Naskas, N. and Papananos, Y., "A new non-iterative, adaptive baseband predistortion method for high power RF amplifiers," in *Proc. IEEE International Symposium on Circuits and Systems*, pp. 413 – 416, May 2003.

[66] Nesimoglu, T., Canagarajah, C. N., McGeehan, J. P., and Wilkinson, R. J., "A novel wideband active feedback amplifier linearization scheme suitable for handsets," in *IEEE Vehicular Technology Conference*, vol. 3, pp. 1712–1716, May 2000.

[67] Noblitt, K., "A comparison of bluetooth and IEEE 802.11," Dec. 2001.

[68] Ochiai, H. and Imai, H., "Performance analysis of deliberately clipped OFDM signals," *IEEE Journal on Selected Areas in Communications*, vol. 18, pp. 2270–2277, Nov. 2000.

[69] Ochiai, H. and Imai, H., "Performance of the deliberate clipping with adaptive symbol selection for strictly band-limited OFDM systems," *IEEE Transactions on Communications*, vol. 50, pp. 89–101, Jan. 2002.

[70] OMNEX Control Systems Inc., "Wireless I/O Interface Transmitter/Receiver Set RAD-ISM-900-...-UD Data Sheet," August 2003. http://www.omnexcontrols.com/files/Data_Sheets/RAD_ISM_900_UD.pdf.

[71] Papoulis, A. and Pillai, S. U., *Probability, Random Variables and Stochastic Processes*. McGraw-Hill, 4th ed., 2002.

[72] Proakis, J. G., *Digital Communications*. McGraw-Hill, 3rd ed., 1995.

[73] Qian, H., Raich, R., and Zhou, G. T., "On the benefits of deliberately introduced baseband nonlinearities in communication systems," in *Proc. Intl. Conference on Acoustics, Speech, and Signal Processing (ICASSP 2004)*, vol. 2, (Montreal, Canada), pp. 905–908, May 2004.

[74] Qian, H., Raich, R., and Zhou, G. T., "Optimization of SNDR in the presence of amplitude limited nonlinearity and multipath fading," in *Proc. 38th IEEE Asilomar Conference on Signals, Systems, and Computers*, vol. 1, (Pacific Grove, CA), pp. 712–716, Nov. 2004.

[75] Qian, H., Ding, L., Zhou, G. T., and Kenney, J. S., "Predistortion linearization measurement results for power amplifiers with memory effects," in *Proc. IEEE Topical Workshop on Power Amplifiers for Wireless Communications*, (San Diego, CA), Sept. 2004.

[76] Qian, H., Xiao, C., Chen, N., and Zhou, G. T., "Dynamic selected mapping for OFDM," in *Proc. Intl. Conference on Acoustics, Speech, and Signal Processing (ICASSP 2005)*, vol. 4, (Philadelphia, PA), pp. 325–328, March 2005.

[77] Qian, H., Xiao, C., Chen, N., and Zhou, G. T., "Peak-to-average power ratio reduction for OFDM using dynamic selected mapping." to be submitted, June 2005.

[78] Qian, H., Xiao, C., Chen, N., and Zhou, G. T., "Peak-to-average power ratio reduction for OFDM using dynamic selected mapping." US provisional patent, March 2005.

[79] Qian, H., Zhao, C., and Zhou, G. T., "Low complexity crest factor reduction for forward link CDMA using IQ offset." *IEEE Communications Letters*, submitted, July 2005.

[80] Qian, H., Zhao, C., and Zhou, G. T., "Low complexity crest factor reduction for forward link CDMA using IQ offset." US provisional patent, July 2005.

[81] Qian, H., Zhou, G. T., and Ding, L., "A low cost predistortion linearization architecture for portable wireless devices." US provisional patent, Sept. 2004.

[82] Raab, F. H., Asbeck, P., Cripps, S., Kenington, P. B., Popovic, Z. B., Pothecary, N., Sevic, J. F., and Sokal, N. O., "Power amplifiers and transmitters for RF and microwave," *IEEE Transactions on Microwave Theory and Techniques*, vol. 50, pp. 814–826, March 2002.

[83] Raich, R., Qian, H., and Zhou, G. T., "Orthogonal polynomials for power amplifier modeling and predistorter design," *IEEE Transactions on Vehicular Technology*, vol. 53, pp. 1468–1479, Sept. 2004.

[84] Raich, R., Qian, H., and Zhou, G. T., "Optimization of SNDR for amplitude limited nonlinearities." *IEEE Transactions on Communications*, to appear, April 2005.

[85] Raich, R. and Zhou, G. T., "On the modeling of memory nonlinear effects of power amplifiers for communication applications," in *Proc. the 10th IEEE DSP Workshop*, (Pine Mountain, GA), pp. 7–10, Oct. 2002.

[86] Raich, R. and Zhou, G. T., "Orthogonal polynomials for complex Gaussian processes," *IEEE Transactions on Signal Processing*, vol. 52, pp. 2788–2797, Oct. 2004.

[87] Razavi, B., *RF Microelectronics*. Upper Saddle River, NY: Prentice Hall PTR, 1997.

[88] Rinne, J. and Renfors, M., "The behavior of orthogonal frequency division multiplexing signals in an amplitude limiting channel," in *Proc. IEEE International Conference on Communications*, vol. 1, pp. 381–385, May 1994.

[89] Schetzen, M., *The Volterra and Wiener Theories of Nonlinear Systems*. Malabar, FL: Krieger Publishing Company, Inc., Jan. 1980.

[90] Shamai, S. and Bar-David, I., "The capacity of average and peak-power-limited quadrature Gaussian channels," *IEEE Transactions on Information Theory*, vol. 41, pp. 1060–1071, July 1995.

[91] Shanbhag, A. G. and Tiedemann, E. G., "Peak-to-average reduction via optimal Walsh code allocation in third generation CDMA systems," in *IEEE 6th International Symposium on Spread Spectrum Techniques and Applications*, vol. 2, pp. 560–564, Sept. 2000.

[92] Shi, Q., "OFDM in bandpass nonlinearity," *IEEE Transactions on Consumer Electronics*, vol. 42, pp. 253–258, Aug. 1996.

[93] Smith, J. G., "The information capacity of amplitude- and varianced-constrained scalar Gaussian channel," *Information and Control*, vol. 18, pp. 203–219, April 1971.

[94] Springer, A., Gerdenitsch, A., Li, Z., Stelzer, A., and Weigel, R., "Adaptive predistortion for amplifier linearization for UMTS terminals," in *IEEE Seventh International Symposium on Spread Spectrum Techniques and Applications*, vol. 1, pp. 78 – 82, Sept. 2002.

[95] Sundstrom, L., *Digital RF Power Amplifier Linearisers*. PhD thesis, Lund Univ., Lund, Sweden, 1995.

[96] Technical Specification Group Radio Access Network, 3rd Generation Partnership Project, Valbonne, France, *Base Station (BS) conformance testing (FDD)*, March 2003. 3GPP TS 25.141.

[97] Telecommunications Industry Association, Arlington, VA, *Mobile Station - Base Station Compatibility Standard for Dual-Mode Wideband Spread Spectrum Cellular Systems*, March 1999. ANSI/TIA/EIA-95-B-99.

[98] Telecommunications Industry Association, Arlington, VA, *Recommended Minimum Performance Standards for Base Stations Supporting Dual-Mode Wideband Spread Spectrum Cellular Mobile Stations*, Sept. 1999. ANSI/TIA/EIA-97-C-1999.

[99] Tellado, J., *Multicarrier Modulation With Low PAR – Applications to DSL and Wireless*. New York: Kluwer Academic Publishers, 2000.

[100] Tellado, J., Hoo, L. M. C., and Cioffi, J. M., "Maximum-likelihood detection of nonlinearly distorted multicarrier symbols by iterative decoding," *IEEE Transactions on Communications*, vol. 51, pp. 218–228, Feb. 2003.

[101] Texas Instrument Inc., "'C67x Floating-Point Benchmarks," March 2005. http://www.ti.com/sc/docs/products/dsp/c6000/67bench.htm.

[102] Universal Microwave Corp., "UMZ-575-A16 Voltage Controlled Osillator Data Sheet," Oct. 2001.

[103] University of Florida, "Wireless and mobile computing and networking at the University of Florida," July 2002. http://www.at.ufl.edu/p2p/ppt/Wireless_Mobile_July2002.ppt.

[104] Vaananen, O., Vankka, J., and Halonen, K., "Effect of clipping in wideband CDMA system and simple algorithm for peak windowing," in *Proc. World Wireless Congress*, (San Francisco, CA), pp. 614–619, May 2002.

[105] Vaananen, O., Vankka, J., Viero, T., and Halonen, K., "Reducing the crest factor of a CDMA downlink signal by adding unused channelization codes," *IEEE Communication Letters*, vol. 6, pp. 443–445, Oct. 2002.

[106] Vuolevi, J., Rahkonen, T., and Manninen, J., "Measurement technique for characterizing memory effects in RF power amplifiers," *IEEE Transaction on Microwave Theory and Techniques*, vol. 49, pp. 1383–1388, Aug. 2001.

[107] Wang, C., Hsu, M., and Ouyang, Y., "A low-complexity peak-to-average power ratio reduction technique for OFDM systems," *IEEE Global Telecommunications Conference*, vol. 4, pp. 2375–2379, 2003.

[108] Wang, X., Tjhung, T. T., and Wu, Y., "On the SER and spectral analyses of A-law companded multicarrier modulation," *IEEE Transactions on Vehicular Technology*, vol. 52, pp. 1408–1412, Sept. 2003.

[109] Wang, X., Tjhung, T., and Ng, C., "Reduction of peak-to-average power ratio of OFDM system using a companding technique," *IEEE Transactions on Broadcasting*, vol. 45, no. 3, pp. 303–307, 1999.

[110] Wright, A. S. and Durtler, W. G., "Experimental performance of an adaptive digital linearized power amplifier," *IEEE Transactions on Vehicular Technology*, vol. 41, pp. 395–400, Nov. 1992.

[111] Yang, D. and Yang, J., "System and method for digital memorized predistortion for wireless communication." United States Patent Application No. 2003/0207680, May 2002.

[112] Z-Communications, Inc., "V880ME08 Voltage Controlled Osillator Data Sheet," May 2004.

[113] Zavosh, F., Thomas, M., C. Thron, T. H., Artusi, D., Anderson, D., Ngo, D., and Runton, D., "Digital predistortion techniques for RF power amplifiers with CDMA applications," *Microwave Journal*, pp. 22–30, Oct. 1999.

[114] Zhou, G. T. and Kenney, J. S., "Predicting spectral regrowth of nonlinear power amplifiers," *IEEE Transaction on Communications*, vol. 50, pp. 718–722, May 2002.

[115] Zhou, G. T. and Peng, L., "Optimality condition for selected mapping in OFDM." *IEEE Transactions on Signal Processing*, revised, June 2005.

[116] Zhou, G. T., Qian, H., and Chen, N., *Advances in Nonlinear Signal and Image Processing*, ch. Communication System Nonlinearities: Challenges and Some Solutions. Hindawi, 2005. Chap. 6.

[117] Ziperovich, P., "Performance degradation of PRML channels due to nonlinear distortions," *IEEE Transactions on Magnetics*, vol. 27, pp. 4825–4827, Nov. 1991.

[118] Zolfaghari, A. and Razavi, B., "A low-power 2.4-GHz transmitter/receiver CMOS IC," *IEEE Journal of Solid-State Circuits*, vol. 38, pp. 176 – 183, Feb. 2003.

VITA

Hua Qian was born in Shanghai, China in 1976. He received the Bachelor and Master degrees in electrical engineering from Tsinghua University, Beijing, China in 1998 and 2000, respectively. He is currently working toward the Ph.D. degree in electrical and computer engineering at the Georgia Institute of Technology, Atlanta, Georgia, USA.

His general research interests are in the areas of signal processing and communications. Specific current interests include digital baseband predistortion linearization for power amplifiers with memory effects and peak-to-average power ratio reduction for wireless transmissions.